The Use of Ligand Field Molecular Mechanics and Related Tools in the Design of Novel Spin Crossover Complexes

By

Benjamin John Houghton

A thesis submitted in partial fulfilment of the requirements for the degree of Doctor of Philosophy in Chemistry

Department of Chemistry,

University of Warwick,

CV4 7AL

April 2015

Contents

Tables and Illustrations

Acknowledgments

Firstly I would like to acknowledge the EPSRC (through the DTA) and the University of Warwick as without their support this PhD would not have happened.

I would like to acknowledge the efforts of my supervisor Professor Robert Deeth who has guided me through the last three and a half years, offered invaluable support and more recently has assisted in proof reading this document.

I'd also like to acknowledge the Physical Society of Japan who has allowed me to reproduce the Tanabe-Sugano diagrams included within the work.

I would like to thank the Royal Society of Chemistry for allowing me to access the Cambridge Structural Database.

Finally I would like to thank Jennifer Motley and my family for their understanding and support during the writing process. It has been long and difficult and I couldn't have done it without them.

Declaration

This thesis is submitted to the University of Warwick in support of my application for the degree of Doctor of Philosophy. It has been composed by myself and has not been submitted in any previous application for any degree.

The work presented (including data generated and data analysis) was carried out by the author except in the cases outlined below:

- The training data generated by Handley and Deeth[1] for iron(II) amine donors was used in all training on these systems to allow for direct and meaningful comparisons.
- The Molecular Dynamics Runs in Chapter 5 were carried out by Robert J. Deeth (PhD supervisor) while all analysis was carried out by the author.
- DFT calculations on three mixed amine imine complexes, included as training data, were determined by Robert J. Deeth as indicated in the text.
- The unpublished Proton Scaled Metal Ligand Charge Scheme of Deeth is used in Chapter 5 as indicated in the text. The Gaussian NAO calculations (same section) were supplied by Deeth.

Parts of this thesis have been published by the author:

- R. J. Deeth, C. M. Handley and B. J. Houghton, Chapter 17: Theoretical Prediction of Spin-Crossover at the Molecular Level, Spin-Crossover Materials: Properties and Applications, Ed. Malcolm Halcrow, 2013.
- B. J. Houghton and R. J. Deeth, Spin-State Energetics of Fe(II) Complexes – The Continuing Voyage Through the Density Functional Minefield, European Journal of Inorganic Chemistry, Volume 2014, Issue 27, pages 4573–4580

- The Use of Drug Discovery Tools in the Study of Inorganic Problems – In Preparation

Abstract

The aim of the work presented in this thesis is to explore computational approaches to the modelling and discovery of spin crossover (SCO) transition metal complexes. Both 'ab initio' methods, based mainly on density functional theory, and empirical force fields based on ligand field molecular mechanics (LFMM) have been considered. It is shown that whilst a user can choose a functional and basis set combination through validation to experimental data which will yield accurate results for a series of related systems this combination is not necessarily transferable to other metal-ligand combinations.

The ability of density functional approaches to model remote substituent effects is explored. Using the iron(II) $^{R,R'}$pytacn complexes[2] as a case study it is shown that whilst density functional approaches predict the correct trend for these substituted pyridine complexes there are occasional outliers.

Traditional quantum approaches to the study of SCO, whilst accurate, are too time-consuming for the discovery of new complexes. Several LFMM parameter sets are optimised within this work. It is shown that this approach can accurately reproduce spin state energetics and geometries of iron(II) and cobalt(II) amines. A mixed donor type iron(II) amine/pyridine force field is also proposed.

Through the utilisation of the drug discovery tools of the Molecular Operating Environment high throughput screening of cobalt(II) tetramine complexes is carried out. It is shown that ligands derived from macrocyclic rings display the most promise. These complexes, which are predicted to adopt a sawhorse geometry, show promise as SCO candidates are proposed as potential synthetic targets.

This work illustrates the many exciting possibilities LFMM provides in the field transition metal computational chemistry allowing for theory to lead experiment rather than follow.

Abbreviations

AOM – Angular Overlap Model

BP86 – A combination of Becke's exchange and Perdew's correlation functionals

COSMO – Conductor-like Screening Model

DFT – Density Functional Theory

DommiMOE – d-Orbital Molecular Mechanics in MOE

FF – Force field

HF – Hartree Fock

HS – High Spin

IS – Intermediate Spin

KS – Kohn Sham

LFMD – Ligand Field Molecular Dynamics

LFMM – Ligand Field Molecular Mechanics

LFT – Ligand Field Theory

LS – Low Spin

MOE – The Molecular Operating Environment

OPBE – A density functional utilising Handy's OptX exchange and PBE correlation Functionals

PSML – Proton Scaled Metal Ligand (a charge scheme developed by Robert J. Deeth)

MM - Molecular Mechanics

RMSD – Root Mean Squared Deviation

SCF – Self Consistent Field

SCO – Spin Crossover

XC – Exchange-Correlation

Chapter 1: An Introduction to Spin Crossover

Spin crossover is a phenomenon by which certain transition metal complexes can change from one spin state to another through the application of a stimulus.[3,4] Various stimuli have been reported to induce spin crossover such as changes in temperature or pressure, the use of a strong magnetic field or irradiation through use of a laser.[3] The latter can result in a state which is metastable at low temperature; this effect is described as light induced excited spin-state trapping (LIESST).[3] The requirement to be held at low temperature currently hinders practical exploitation of this effect.[4]

Spin crossover complexes have been the focus of a great deal of interest in recent years due to their potential for use as molecular materials with potential applications including, but not limited to, memory storage devices and displays.[3,4] The potential for use in displays exploits the fact that a change in spin-state is often associated with a change in the colour of a complex with one group going so far as to produce a prototype display.[3,5] This colorimetric change has shown promise for use in molecular sensors.[6,7] For instance, Young et al published results of a study in which the iron(II) based diaminotriazine complex, $[FeL_2]^{2+}$ (L = 6-([2,2'-bipyridin]-6-yl)-1,3,5-triazine-2,4-diamine, shown in Figure 1.1), shows promise.[8,9] Through hydrogen bonded self-assembly of the complex and barbiturates the iron(II) centre undergoes a transition from a purple Boltzmann distribution of high and low spin centres to a colourless solution of high spin centres.[8,9] This colour change was not instantaneous but was noted to be significant after one hour and complete after fifteen.[9]

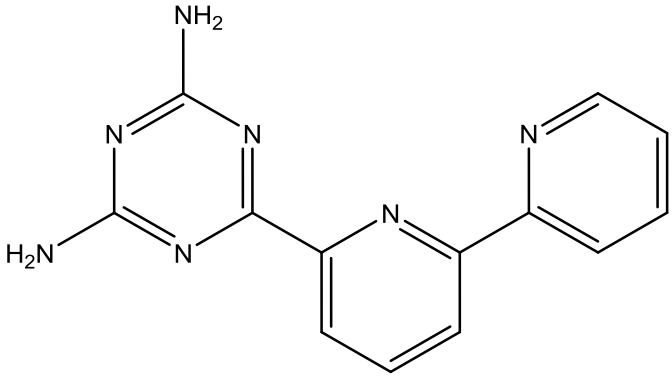

Figure 1.1; The ligand shown by Young et al to display promise in barbiturate sensing.[8,9]

The most commonly-studied spin crossover species are based upon a pseudo-octahedral iron(II) core with six nitrogen donors.[3] Octahedral d^6 species can be either high spin ($^5T_{2g}$) or low spin ($^1A_{1g}$) with four and zero unpaired electrons respectively.[10] The first iron(II) complexes to show a reversible change of magnetic moment with temperature were $Fe(phen)_2(NCE)_2$ (E = S, Se; phen = 1,10-phenanthrolene, Figure 1.2).[3,11] However, the data were initially misinterpreted as being due to dimer formation.[3,11] It took three years until the temperature dependent magnetic moment was correctly interpreted as spin crossover.[3,12]

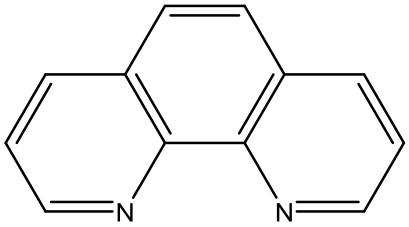

Figure 1.2; The 1,10-phenanthrolene ligand upon which the first iron(II) SCO complex was based.[11]

Whilst progress has been made since the initial discovery above, its rate has been slow.[3] It is clear from the recent book edited by Halcrow that the majority of SCO species are based on an iron(II)-N_6 coordination sphere. This is due to the fact that spin crossover is a very

delicate and experimentally challenging phenomenon.[3] This chapter will focus on some of the major areas of SCO research, split into iron(II) mononuclear complexes both in solution and the solid state and SCO complexes containing other metal ions.

Fe(II) Monomeric Species

Iron(II) is d^6 as such it could in theory adopt one of three spin states. However, in octahedral symmetry, only the high and low spin states are observed. A simple theoretical explanation of the energetics of these complexes is given by ligand field theory (LFT). In LFT (and its parent crystal field theory) the only explicit orbitals are the d functions. As such, in octahedral symmetry the ground spin-state is determined purely through balancing the spin pairing energy and the energy required to promote an electron from the t_{2g} orbitals to the e_g orbitals, Δ_{oct}, with each electron occupying the t_{2g} orbitals experiencing a stabilising effect equivalent to 2/5 Δ_{oct} whilst those in the e_g orbitals are destabilised by 3/5 Δ_{oct}. For d^6 species (such as those based on iron(II) centres forming the initial focus of this thesis) the balance of these components can be simply rationalised. A high-spin d^6 system will have a stabilisation energy of -2/5 Δ_{oct}. The stabilisation energy of the intermediate-spin species is -7/5 Δ_{oct} + p (where p denotes the spin pairing energy) and that of the low-spin species is -12/5 Δ_{oct} + 2p. When Δ_{oct} = p, the energy of the high and low-spin species are the same and this is known as the spin-crossover point and is consistent with the information described by the Tanabe-Sugano diagram, Figure 1.4.

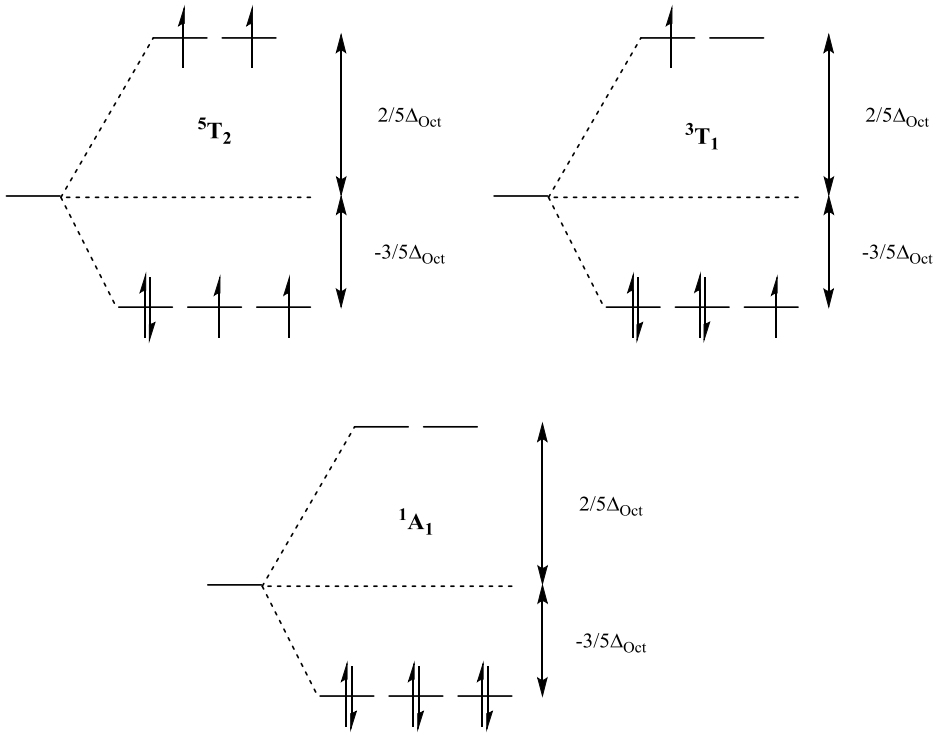

Figure 1.3; The possible three d-electron configurations of an octahedral d^6 complex. Clockwise these are high spin ($^5T_2$), intermediate spin ($^3T_1$) and low spin ($^1A_1$). In the case of octahedral iron(II) the intermediate spin state is inaccessible.

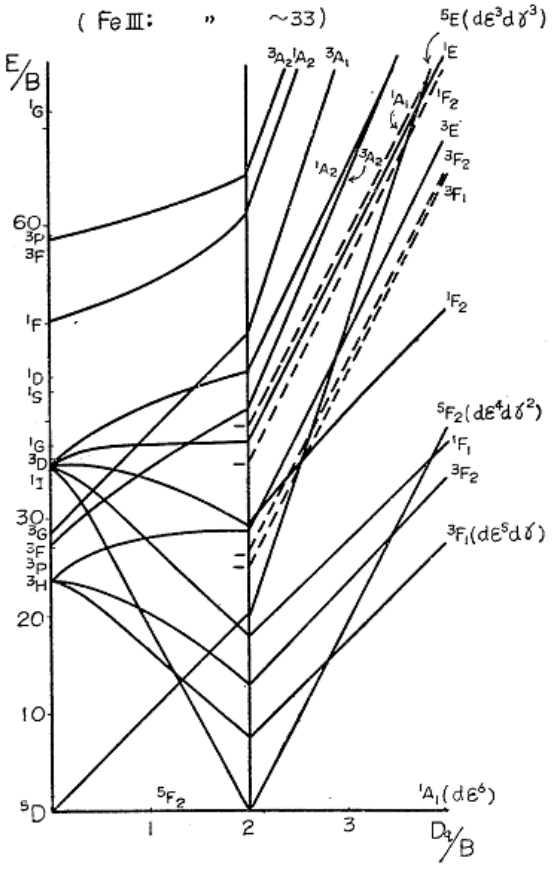

Figure 1.4; The Tanabe-Sugano diagram for d^6 species.[13] (Note the $^3T_1$ and $^5T_2$ states are referred to by the older $^3F_1$ and $^5F_2$ levels respectively, also Fe(III) is an old reference to Fe(II)). Figure reproduced with permission of The Physical Society of Japan.

However, a contradiction exists in this pairing energy model when compared with that in the Tanabe-Sugano diagram since in the former when Δ_{oct} = p the energy of the intermediate-spin state also converges to the spin-crossover point, something which is not seen in the classic diagram. This contraction stems from the fact that a description of the spin pairing energy in this way is not sufficient, and this interaction is better described as a loss of favourable exchange upon pairing rather than the gain of an unfavourable pairing energy. When expressed in terms of exchange (X) these equations become;

$$-\frac{2}{5}\Delta_{oct} - 10X \qquad \textbf{HS} \qquad \text{Equation 1.1}$$

$$-\frac{7}{5}\Delta_{oct} - 7X \qquad \textbf{IS} \qquad \text{Equation 1.2}$$

$$-\frac{12}{5}\Delta_{\mathrm{oct}} - 6X \qquad \textbf{LS} \qquad \text{Equation 1.3}$$

At the extremes of Δ_{oct}, where Δ_{oct} is zero or infinite, the ground spin-state becomes low or high-spin respectively, with no value of Δ_{oct} favouring the intermediate spin-state. The crossing point of the high-spin and low-spin states in equations 1.1 and 1.3 is when the exchange energy is equal to two times Δ_{oct}. However, at this value of the exchange the intermediate-state lies higher in energy by an energy equivalent to one lot of exchange, X. This is therefore consistent with the Tanabe-Sugano diagram.

When considering isolated systems, for instance an infinitely dilute solution, the fraction of a sample in the HS state, χ_{HS}, at temperature T is given by Equation 1.4;[14]

$$\chi_{HS}(T) = \left[1 + \exp(\frac{\Delta G_{HL}}{k_B T})\right]^{-1} \qquad \text{Equation 1.4}$$

Where ΔG_{HL}, the difference in Gibbs free energy of the HS and LS states, is given by Equation 1.5.[14]

$$\Delta G_{HL} = \Delta H_{HL} - T\Delta S_{HL} \qquad \text{Equation 1.5}$$

ΔH_{HL} denotes the difference in enthalpy between the high and low states, while ΔS_{HL} denotes the entropic difference.[14] The temperature at which half of the sample is in the HS form is therefore given by Equation 1.6.[14]

$$T_{1/2} = {}^{\Delta H_{HL}}/_{\Delta S_{HL}} \qquad \text{Equation 1.6}$$

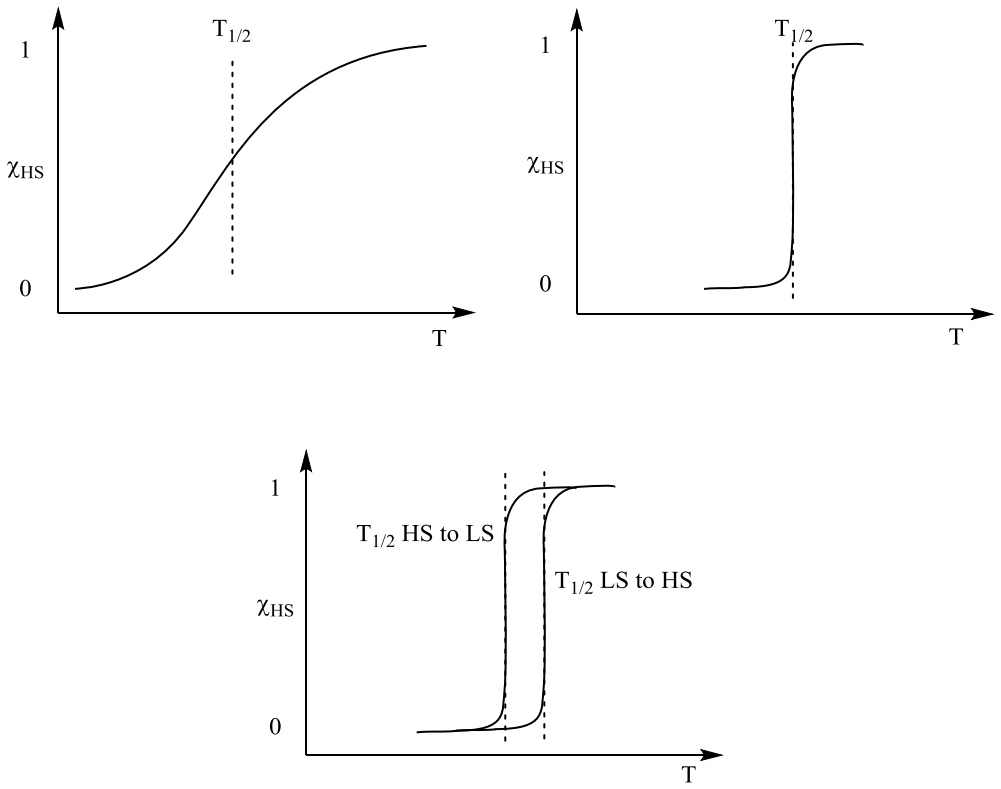

Figure 1.5; Three typical spin transition curves expressed as the fraction of the sample which is HS as a function of temperature. Top left: a gradual spin transition.[15] Top right: an abrupt spin transition of a bulk sample.[15] Bottom centre: an example of hysteresis were the transition occurs at a different temperature upon heating when compared to cooling.[15]

While equations 1.4-1.6 illustrate the determination of $T_{1/2}$ they do not accurately account for the nature of the transition about this temperature.[14] SCO transitions by and large fall into three categories, gradual, abrupt and abrupt with hysteresis as illustrated by Figure 1.5. Gradual spin transitions are typical of a sample in solution. Bulk phase materials can display either abrupt or gradual transitions dependent on the extent of cooperatively in the sample.[16] Hysteresis, which is characterised by the transition from low spin to high spin occurring at a different temperature to the reverse process, is typical of strongly cooperative systems.[10] This bistability is a highly desirable property for applications of SCO in electronic devices.[10]

SCO complexes which exhibit gradual transitions resulting from Boltzmann distribution over all vibronic levels of the high and low spin states.[10] This results from spin crossover centres acting in an isolated manner without the inter-complex interactions seen in the solid state and discussed later in the chapter.[10] A typical example is $[Fe(tacn)_2]^{2+}$, (tacn = 1,4,7-Triazacyclononane) which displays a gradual transition with a $T_{1/2}$ = 335 K.[17-19]

The complex $[Fe(btz)_2(NCS)_2]$ (btz = 2,2‘-bi-4,5-dihydrothiazine, Figure 1.6) is an example of a gradual bulk phase transition.[20] $[Fe(btz)_2(NCS)_2]$ displays an incomplete spin transition in the scan region of 90 – 300 K and centred around 225 K.[16,20] This transition is incomplete at both the low and high temperature ends of the scan range.[16,20]

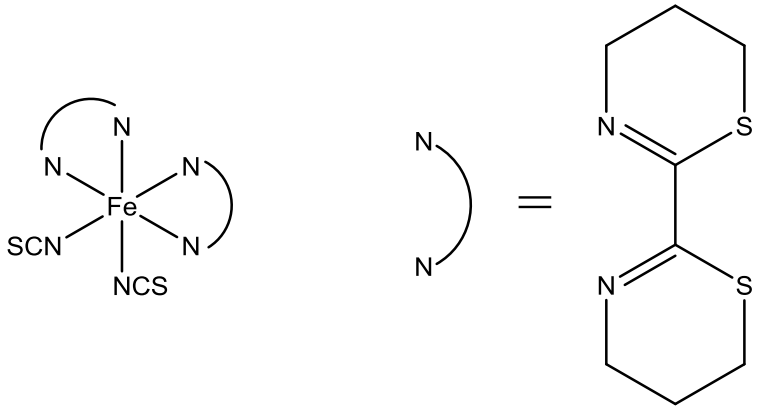

Figure 1.6; $[Fe(btz)_2(NCS)_2]$ on the left and the btz ligand on the right.[20]

SCO in iron(II)-N_6 complexes is accompanied by 0.2 Å increase in iron-nitrogen bond length.[16] This increase in a complexes volume results in an increase in internal pressure within the sample, as such a transition in one centre encourages other complexes to transition.[16,21,22] This leads to an abrupt transition in the recorded temperature dependant magnetic moment.[22]

The observation of an abrupt transition without hysteresis is possible upon recording the temperature dependant magnetic moment of a solid SCO sample.[3] One example is *trans*-

[Fe(4-*p*-methylphenyl-3,5-bis(pyridin-2-yl)-1,2,4-triazole)$_2$(NCS)$_2$], Figure 1.7, which displays an abrupt transition with a $T_{1/2}$ of 231 K.[23] This spin transition is sensitive to the geometry at the metal which in turn is a function of the methyl substituent on the phenyl ring.[23] A meta-methyl group results in a complex with trans-thiocyanate ligands which is HS across the temperature range studied.[23]

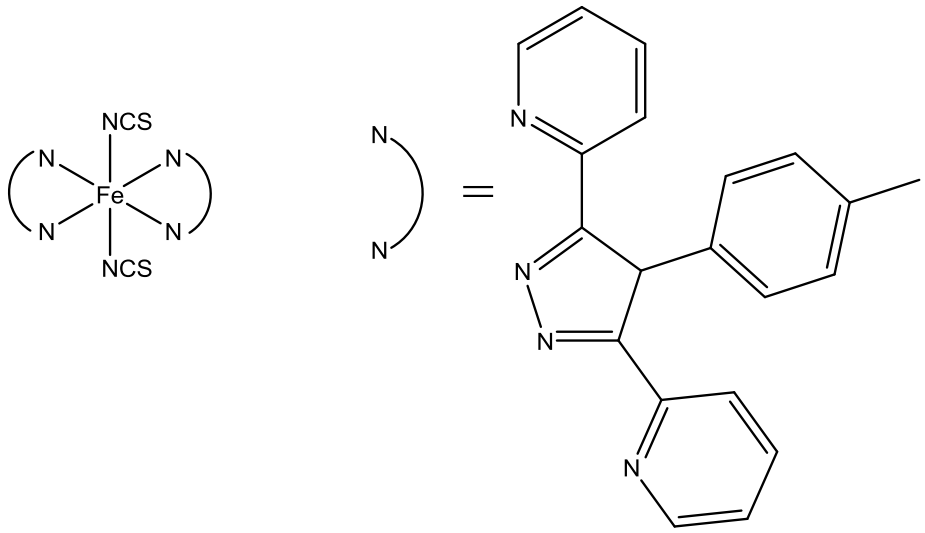

Figure 1.7; a representation of trans-[Fe(4-p-methylphenyl-3,5-bis(pyridin-2-yl)-1,2,4-triazole)$_2$(NCS)$_2$] on the left and the 4-p-methylphenyl-3,5-bis(pyridin-2-yl)-1,2,4-triazole ligand on the right.[23]

The related complex [Fe(dpp)$_2$(NCS)$_2$].pyridine (dpp = dipyrido[3,2-a:2'3'-c]phenazine illustrated in Figure 1.8) displays an abrupt transition with a hysteresis loop of 40 K.[24] The transition upon heating occurs at 163 K whilst upon cooling the transition occurs at 123 K.[24] While the magnetic moment of the HS form of 5.2 Bohr magnetons (μ_B) approaches the spin only magnetic moment of 5.7 μ_B the low spin form at 86 K has a magnetic moment of 1.6 μ_B, possibly the result of contamination with iron(III).[24] The presence of iron(III) (6 mol%) was confirmed through the use of Mossbauer spectroscopy.[24] The structure of the bulk phase involving π-stacking of the ligands into columns and van der

Waals interactions between columns are thought to be the route of the strong hysteresis behaviour of this dpp complex.[24]

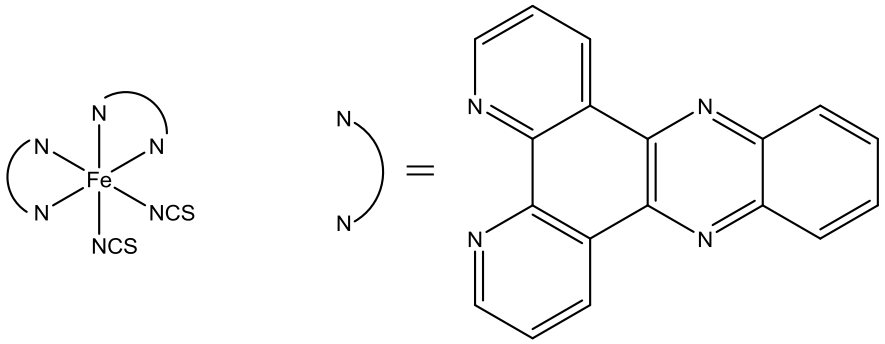

Figure 1.8; [Fe(dpp)$_2$(NCS)$_2$] on the left and the dpp ligand on the right.[24]

To date the widest hysteresis reported is that of [Fe(4-(3,5-dimethyl-1H-pyrazol-1-yl)-2-(pyridin-2-yl)-6-methylpyrimidine)$_2$](BF$_4$)$_2$ for which one of the anhydrous phases displays a 130 K wide hysteresis.[25] Current understanding of the origin of hysteresis indicates that it involves a combination of substantial structural rearrangement on change of spin state as well as interactions between individual spin crossover centres.[26]

Hysteresis spanning room temperature is a goal for real applications.[10] Few examples currently exist but one such system, [FeL(imidazole)$_2$] Figure 1.9, was first synthesised by Müller et al who reported a hysteresis width of 4 K.[27] However, the composition of this complex was uncertain since elemental analysis suggested there were just 1.8 imidazole ligands per iron centre.[28] This prompted Weber et al to repeat the synthesis and claim the correct stoichiometry of 2 imidazoles.[28] They reported that upon heating, the complex transitioned from low to high spin at 314 K and upon cooling a transition from high to low spin occurred at 244 K.[28] The reported 70 K wide hysteresis results from a hydrogen bond network, the extent of which directly impacts upon the width of the hysteresis loop but given the conflicting reports this result remains uncertain.[27,28]

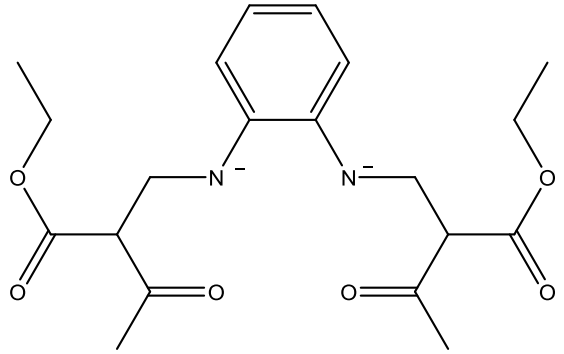

Figure 1.9; The ligand utilised by Müller in the synthesis of the [FeL(Him)$_2$] SCO complex.[27]

Whilst the majority of iron(II) SCO research has focussed on iron complexes with an N_6 coordination sphere, these are not the only systems for which the iron(II) centre displays SCO.[29] A key example is the complex depicted in Figure 1.10 which is the first with an N_4O_2 core.[30,31] This two-step transition is the first species for which the changes in spin state directly result from structural phase transitions.[31]

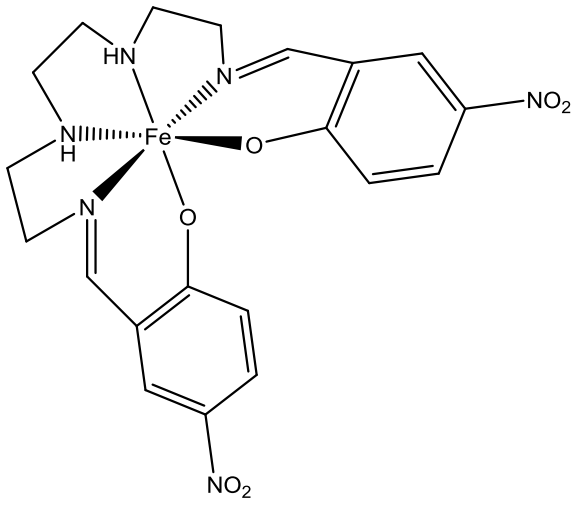

Figure 1.10; The first iron(II) SCO complex with an N_4O_2 core.[30,31]

Spin crossover is such a subtle phenomenon that choice of counter ion or solvent can alter the spin state from high to low spin in both solution and the solid state.[10]

The choice of counter ion has been shown to dictate SCO in the solid state.[32] The magnetic moment of the perchlorate salt [Fe(2,2'-bi-2-imidazoline)$_3$](ClO_4)$_2$ (ligand illustrated in Figure 1.11) which is HS above 140 K drops abruptly to 0.59 B.M. upon cooling to 93 K.[32] However, the BPh_4^- salt of the same complex is HS across the 93-293 K temperature range.[32]

The authors hypothesise that changing the anion from BPh_4^- to perchlorate results in "an alteration in the ligand field by hydrogen bonding between the NH groups and the perchlorate anions".[32]

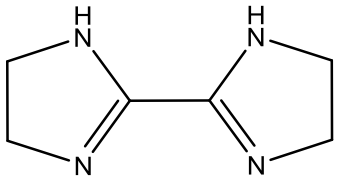

Figure 1.11; The ligand 2,2'-bi-2-imidazoline for which SCO in the solid state is dictated by choice of counter ion.[32]

Sensitivity to anions in the solution state and its potential applications in chemosensing has been the focus of work by Ni and Shores[6,7] (previous work had been carried out on the coupling of anion recognition and iron(II) centres without focus on changes in spin state[33]). Arguably the most interesting example is [Fe(2,2′-bi-1,4,5,6-tetrahydropyrimidine)$_3$](BPh_4)$_2$ (ligand shown in Figure 1.12) which allows for anion association through hydrogen bonding.[6] Addition of halide salts of Bu_4N^+ (at 233 K) reduces the magnetic susceptibility of the solution from a HS to (close to) a LS state for salts of bromide and iodide.[6]

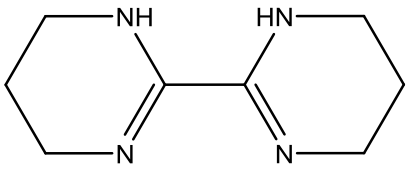

Figure 1.12; A pictorial representation of the 2,2'-bi-1,4,5,6-tetrahydropyrimidine ligand.[6]

Changes in solvent have been shown to induce a change in spin state, both in solution and in the solid state.[34,35] The Halcrow group studied the effect of solvent on the complex $[Fe(3\text{-bpp})_2]^{2+}$ (3-bpp = 2,6-di(pyrazol-3-yl)pyridine, Figure 1.13) and found the LS state to be stabilised by solvents which facilitate hydrogen bonding.[34] This effect was found to be greatest in D_2O with $T_{1/2}$ increasing as a function of the mole fraction of D_2O in $(CD_3)_2CO$.[34] The structurally similar 1-bpp complex (HS) which lacks the ability to form hydrogen bonds shows no dependence on solvent as evidenced by a lack of variation in the ^1H isotopic shifts upon solvent change.[34]

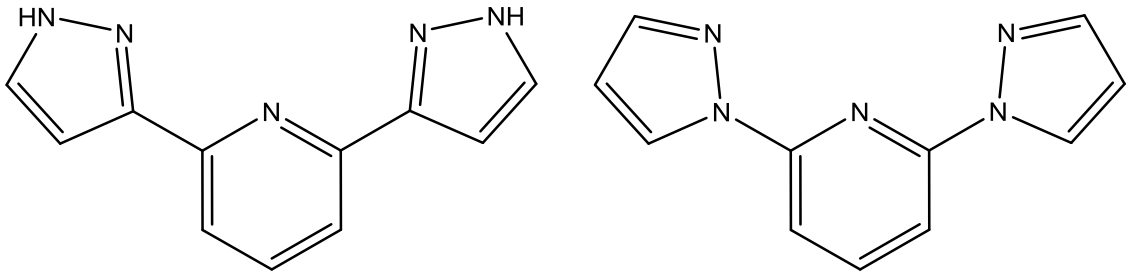

Figure 1.13; The iron(II) complexes of the 3-bpp ligand on the left and 1-bpp ligand on the right were studied by the Halcrow group in a range of solvents.[34]

In the solid state, a solvent-free sample of [Fe(tris(2-pyridylmethyl)amine)$(NCS)_2$)] undergoes an incomplete spin transition upon cooling.[36] However, upon exposure to methanol vapour a noticeable colour change from yellow to red occurs (indicative of a change in spin state).[36] Temperature dependent magnetic susceptibility measurements on the species with absorbed methanol show a complete spin transition from low to high spin

as well as indicating an initial HS-HS to HS-LS intermediate transition followed by full conversion to a LS-LS state as indicated by the curves inflection around 260 K.[36] The presence of two distinct iron centres was confirmed by crystallography.[36] This methanol-absorbed sample consists of two alternating layers, one with and one without methanol.[36] The sorption of methanol shortens inter-iron distances in this molecular layer increasing communication between centres.[36] At 120 K both iron centres are low spin. At room temperature the methanol-absorbed layer is HS and upon heating to 350 K, both centres are HS as indicated by crystallography.[36] This illustrates the clear impact of solvent on spin crossover in the solid state.

Spin crossover complexes are not limited to just one metal centre. Examples are known ranging from dinuclear complexes,[37] 2x2 grids,[38] Fe_5 clusters,[39] cages (nanoballs) containing six iron centres[40] through to polymeric systems.[41] Halcrow notes that whilst such systems guarantee interaction between metal centres they do not guarantee strong cooperativity with the largest hysteresis reported in molecular crystals and not polymers.[15,26] Cooperativity, which results in abrupt transitions and hysteresis, stems from changes in lattice energy upon spin state switching.[15,26] Lattice energy results from a "sum of all interactions and steric contacts in the crystal lattice" rather than simply whether the centres are linked covalently.[15]

Metals other than iron(II)

The spin crossover phenomenon is not limited to iron(II) in fact any metal centre with 2-8 d-electrons could exhibit more than one possible spin state. In this section a few choice examples will be used to illustrate spin crossover in a range of metal centres.

d^4 metal centres

The first reported d^4 SCO system was that of Mn(III) tris(1-(2-azolyl)-2-azabuten-4-yl)amine, Figure 1.14.[42] The recorded magnetic moment of Mn(III) tris(1-(2-azolyl)-2-azabuten-4-yl)amine reflects a shift from a ^5E_g state to a $^3T_{1g}$ state upon cooling to 40-50K.[42] When considering manganese(III) the ground state is of intermediate and not low spin.[43] The d4 Tanabe-Sugano diagram reflects this, indicating that for no value of the ligand field splitting parameter is the ground state a singlet.[13]

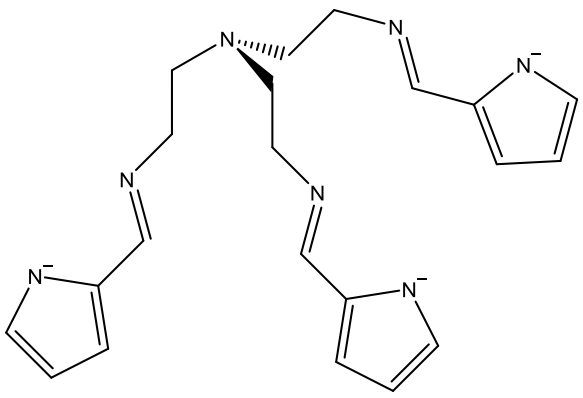

Figure 1.14; The tris(1-(2-azolyl)-2-azabuten-4-yl)amine used in the first Mn(III) SCO complex.

The relative rarity of d^4 SCO species may be a result of the gain in ligand field stabilisation energy (LFSE) upon switching from the ^5E to $^3T_1$ being insufficient to offset the loss of

exchange and an increase in unfavourable Coulombic interactions.[43,44]

The Morgan group has synthesised a series of SCO complexes based upon Schiff bases.[44] These Schiff bases with a $N_4(O^-)_2$ core show an interesting requirement on the oxygens being *trans* in order to display a temperature dependence in the magnetic moment.[44] This was observed through a comparison of two similar ligands, one in which the shorter ligand backbone results in a *cis* geometry and one where a longer backbone results in a *trans* metal geometry.[44] SCO from high to intermediate spin in the *trans* species is accompanied by an equatorial elongation (0.08 Å for the Mn-imine bonds and 0.11 Å in the Mn-amine bonds) consistent with promotion to the antibonding $d_{x^2-y^2}$ orbital.[44]

d^5 – Iron(III)

Iron(III) SCO systems, like their iron(II) counterparts, have been extensively studied.[45] In 1931 Cambi reported the first example of SCO in tris N,N-dialkyldithiocarbamate iron(III) complexes, Figure 1.15.[46,47] Typically, SCO complexes derived from iron(III) dithiocarbamates display gradual spin transitions in both the condensed and solution states.[45]

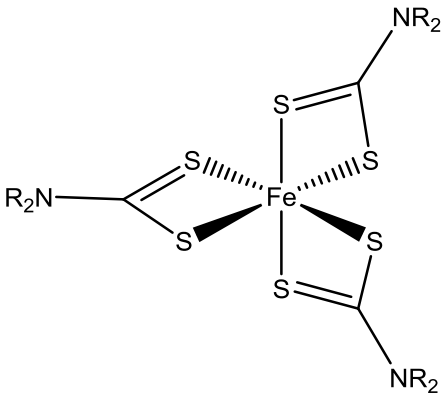

Figure 1.15; The general structure of iron(III) dithiocarbamates where R denotes any alkyl group.[46,47]

SCO has also been displayed in iron(III) complexes with non-innocent ligands such as is the case with the *o*-aminophenol derived ligand shown in Figure 1.16.[48] In contrast an innocent ligand allows for the identification of the metal oxidation state.[49] This complex is reported to be the first iron SCO complex derived from bidentate ligands with a nitrogen and oxygen donors.[48] The low spin state (below 130 K) displays a lower than expected effective magnetic moment of around 1 Bohr magnetons as a result of interactions with the ligand radicals.[48]

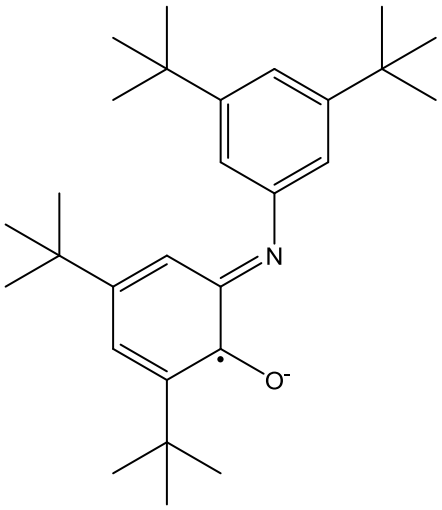

Figure 1.16; The non-innocent o-aminophenol derived ligand which was shown to facilitate SCO by Chaudhuri et al.[48]

d^7 – Co(II)

Research into cobalt(II) SCO has primarily focussed around imine systems.[50,51] The first cobalt(II) SCO complex took the form of bis-(2,6-pyridindialdihydrazone) cobalt(II) iodide, a complex with a tridentate terimine ligand, for which the magnetic moment, studied as a function of temperature, was found to vary from 1.90 to 3.69 Bohr magnetons over the 80 - 373 K temperature range.[52] More recent examples include the extensively studied bis-2,2':6'2''-terpyridine cobalt(II) complex and its derivatives.[50,51]

The complex tris-2,2'-bipyridine cobalt(II) illustrates how environment can impact upon SCO. Whilst tris-2,2'-bipyridine cobalt(II) is, in isolation, high spin its confinement in zeolite pores encourages spin crossover.[53] At low temperature the sample exhibits a magnetic moment of 1.9 Bohr magnetons consistent with a low spin sample and elevating the temperature raises the magnetic moment.[54] However, the spin transition remains incomplete even at 500 K.[54] The spin transition curve is gradual and independent of the percentage occupancy of the zeolite pores showing that cooperativity between metal centres is absent.[54] This introduction of spin crossover is thought not to originate from simple pressure effects but rather from the fact that encapsulation encourages the complex to adopt a more idealised octahedron rather than the D_3 distortion seen in the free complex.[54,55]

d^8 – Ni(II)

Spin transitions in nickel(II) are often associated with geometric changes.[29] An important example is the room temperature, light induced spin transition of the nickel (II) complex formed from a porphyrin ring with a branching azopyridine group (Figure 1.17).[56] Upon irradiation of the low spin sample with 500 nm light, the azopyridine group acts as a fifth ligand resulting in a 75% yield (in DMSO) of the paramagnetic five coordinate nickel complex.[56] The reverse process occurs on irradiation with 435 nm light in 97 % yield (in DMSO).[56] This process (in acetonitrile) is repeatable, showing no signs of degradation after 10,000 cycles in air (the sample has a half-life of 27 hours).[56]

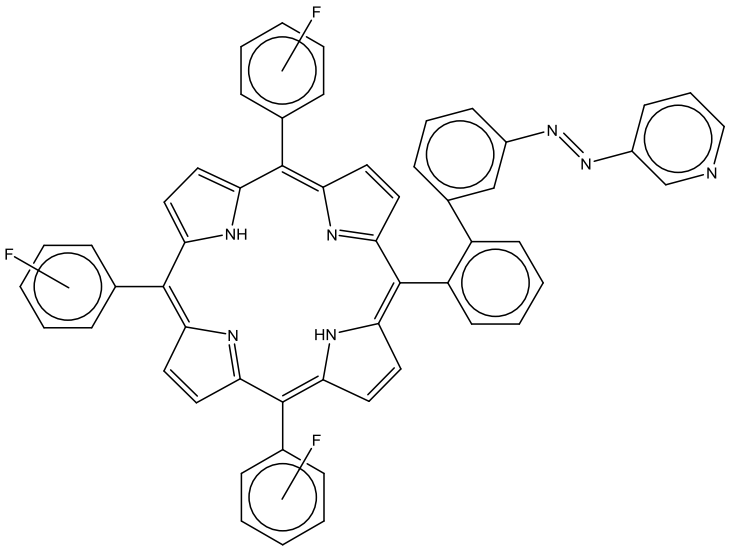

Figure 1.17; The porphyrin ring based ligand used to facilitate room temperature spin state bistability.[29,56]

Chapter 2: Theoretical Approaches to Spin Crossover.

Density Functional Theory – A theoretical background

Various theoretical approaches have been applied to spin crossover complexes including Density Functional Theory (DFT) as well as wavefunction based approaches such as CASPT2 (an approach which combines the Complete Active Space wavefunction method with second order perturbation theory and will be discussed later in this chapter).[57-62] The idea that a knowledge of the electron density in turn results in a knowledge of all other properties of a system has been around for close to a century. The details of Density Functional Theory have been extensively discussed elsewhere.[63,64] The following is a brief description of the background to DFT which is based largely on that given by Koch and Holthausen in A Chemist's Guide to Density Functional Theory.[65]

The seminal work of Hohenberg and Kohn of 1964 presents much of the theoretical groundwork on which current DFT is based.[66] These are commonly described as the Hohenberg-Kohn (HK) theorems. The first HK theorem states that "the external potential is (to within a constant) a unique functional of the electron density; since, in turn, the external potential fixes the Hamiltonian we see that the full many particle ground state is a unique functional of the electron density".[†66] The second HK theorem establishes the use of the variational principle in the determination of the ground state of a system from DFT.[66] Since an in depth look at the derivation can be found in many good textbooks the present discussion will be limited to the above statement.

[†]Not a direct quote since words have been used in the place of symbols.

$$E_0 = \min_{\rho \to N}(F[\rho] + \int \rho(\vec{r})\, V_{Ne} d\vec{r}) \qquad \textbf{Equation 2.1}$$

Since $F[\rho] + \int \rho(\vec{r})\, V_{Ne} d\vec{r}$ returns the energy associated with a given density, its minimisation as in Equation 2.1 returns the ground state energy (E_0). $F[\rho]$ describes the universal functional of the electron density, ρ, containing the system independent functionals accounting for the kinetic energy and electron-electron interactions (classical Coulombic, self-interaction, exchange and correlation). The second term in Equation 2.1 describes the potential energy resulting from the nuclei-electron interaction. $\rho(\vec{r})$ denotes the probability of finding electrons within the volume element $d\vec{r}$ and V_{Ne} is the potential due to nuclei-electron interaction which acts upon it. It remains important to state that whilst the Hohenberg-Kohn theorems provide a proof of concept they provide no route to the functionals required for connecting the electron density and the ground state properties in practice.

In fact the only aspect of the universal functional for which we do know the form is the classical Coulomb interaction, the non-classical elements remain unknown. However, the following year came the Kohn-Sham approach on which all DFT in this thesis is based. The major breakthrough was that whilst we do not know the form of the universal functional needed we can calculate most of the kinetic energy well through the use of a non-interacting reference system. This reference system describes uncharged fermions and is built up from one electron functions more commonly known as orbitals. The remainder of the kinetic energy is then grouped with the non-classical interactions which, while unknown, are small by comparison. This collection of unknown terms is what is more commonly known as the exchange-correlation energy and the quest for functionals which accurately describe it form the basis of much of modern density functional theory.

The Local Density Approximation

The local density approximation (LDA) assumes that the exchange-correlation energy (E_{XC}) of a system can be expressed in terms of a uniform electron gas. Such that;

$$E_{XC}[\rho] = \int \rho(\vec{r})\, \varepsilon_{XC}\big(\rho(\vec{r})\big) d\vec{r} \qquad \textbf{Equation 2.2}$$

In which $\varepsilon_{XC}\big(\rho(\vec{r})\big)$ denotes the exchange-correlation energy associated with an electron in a uniform electron gas. The exchange contribution is that given by Dirac (Equation 2.3) and the correlation energy results from analytical interpolation schemes. Among the most commonly utilised LDA correlation functionals are those developed by Vosko, Wilk and Nusair.[67]

$$\varepsilon_x^{LDA} = -\frac{3}{4}\sqrt[3]{\frac{3\rho(\vec{r})}{\pi}} \qquad \textbf{Equation 2.3}$$

The Generalised Gradient Approximation

Following the limited success of the LDA improvements had to be made. To account for the fact that the true electron density of a system is not a homogeneous electron gas it follows that the any realistic description of the XC energy should represent this. This inhomogeneity could be accounted for, in part, through the inclusion of the gradient of the electron density. This inclusion makes what is known as the gradient expansion approximation.

This expansion performed worse than initially hoped. This is primarily a result of the fact that the resulting holes display none of the attractive traits found within the LDA. Holes

describe how an electron reduces the probability of finding other electrons in its vicinity. Holes fall in to two categories. The Coulomb hole is a result the electrostatic interactions between electrons and is independent of electron spin while the Fermi hole is a result of "the antisymmetry of the wavefunction".[65] The correlation hole should integrate over all space to zero and the Fermi hole to negative one. Within this expansion these properties were not preserved. The solution to this was to strictly enforce these conditions upon the holes by truncating them, such that they integrate to the desired values. The second failing was that despite the fact that the LDA exchange hole correctly takes a negative sign at all points in space, the hole which results from the gradient expansion approximation doesn't strictly adhere to this rule. To solve this problem the hole is simply set to zero at these points in space.

Within the generalised gradient approximation (GGA) it is common to split the XC energy into exchange and correlation terms and to treat the functionals separately. Through the GGA the exchange energy is written in the form given by Equation 2.4.

$$E_X^{GGA} = E_X^{LDA} - \sum_\sigma \int F(s_\sigma)\rho_\sigma^{4/3}(\vec{r})\, d\vec{r} \qquad \textbf{Equation 2.4}$$

s_σ signifies the reduced density gradient and is described by Equation 2.5. The exchange functional, *F*, can take a range of functional forms. These can be broadly categorised as those with firm theoretical grounding (e.g. PBE[68,69]) and those with empirical parameters (e.g. Becke's 1988 functional[70]).

$$s_\sigma(\vec{r}) = \frac{|\nabla\rho_\sigma(\vec{r})|}{\rho_\sigma^{4/3}(\vec{r})} \qquad \textbf{Equation 2.5}$$

Performance of Functionals for Spin Crossover Research

At the time of Harvey's review in 2004 it was already noted that large differences occurred between different density functionals.[71] Pure functionals (those which are purely based on DFT and do not include any Hartree-Fock exact exchange) are known to overstabilise the low-spin state whilst hybrid functionals (discussed shortly) systematically overstabilise the high-spin state due to their inclusion of a portion of Hartree-Fock exact exchange.[59] A study by Lawson Daku et al. in 2005, set out to compare the effect of using different density functionals in the study of iron(II) tris(2,2'-bipyridine).[72] From their results, it was readily apparent that large differences occur between the calculated spin state splittings both on changes in functional and basis set.[72] Their paper concludes that the functionals RPBE and B3LYP* give the most accurate results for this complex.[72] It has been suggested by Deeth and Fey that this over stabilisation of the low-spin state could also in theory be compensated for through the use of a constant correction,[73] however to the best of the author's knowledge a correction of this form has not been used since by any groups.

Swart et al. have primarily focussed their studies around the use of the OPBE functional which combines Handy's OPTX description of exchange and Perdew, Burke and Ernzerhof's electron correlation terms and have noted its successes.[57-59,68,74,75] The OPTX exchange term is a refitting[74,75] of Becke's 1986 exchange functional (which in addition to Dirac exchange includes a term dependent on the gradient of the density)[76].

The OPBE functional, initially chosen as it predicted the correct ground state in a cost effective manner,[57] was later validated against CASPT2 for three complexes, $Fe(H_2O)_6^{2+}$, $Fe(NH_3)_6^{2+}$ and $Fe(bpy)_3^{2+}$ with a mean absolute deviations (MAD) of 1.0 kcal mol^{-1} (with a TZP basis set will be discussed in greater detail in a following section).[59] These

deviations are close to an order of magnitude smaller than the next most accurate functional PBE0 with a MAD of 9.1 kcal mol^{-1}.[59] OPBE was also shown to predict the correct ground state for a series of challenging complexes.[59]

In 2009 Swart et al asserted that their newly formed SSB-D functional provided all the benefits of OPBE for spin-state energetics whilst adding benefits such as hydrogen bonding and π-π stacking which improved performance for biologically important interactions.[77]

More recently Swart et al have used a multi-method approach which combined DFT with a polarisable force field and hybrid Quantum Mechanical/Molecular Mechanics (QM/MM) calculations.[60] The use of this multiscale approach allowed the determination of the temperature dependence of the spin crossover behaviour of Fe(II)(trispyrazolylborate)$_2$ with a predicted transition temperature in the region of 290 K, in close agreement to the experimentally determined value of 285-290 K.[60]

Neese rejects the OPBE functional and concludes that only the double-hybrid functional B2PLYP, along with "large and flexible basis sets" (basis set effects will be discussed in a following section), is able to provide good results for spin crossover complexes.[61] However, the justification for why OPBE fails is that it favours the high-spin state of the complex $[Fe^{IV}O(NH_3)_5]^{2+}$ when a supposedly similar complex $[Fe^{IV}(O)(TMC)(CH_3N)]^{2+}$ (TMC = tetramethylcyclam) has an intermediate spin ground state (Figure 2.1).[61] In addition for another complex $[Fe(N_2H_4)(N_HS_4)]^0$ ($N_HS_4^{2-}$ = 2,2'-bis(2-mercaptophenylthio)diethylamine dianion) OPBE "incorrectly" predicts a low spin ground state.[61] However, on closer inspection of the supporting information accompanying this study it appears that the geometries used for the $[Fe(L)(N_HS_4)]^0$ ($N_HS_4^{2-}$ = 2,2 0 –bis(2-

mercaptophenylthio)diethylamine dianion) family of complexes are not those seen in the crystal structures, Figure 2.2.[61] Therefore, the reader is left wondering if Neese's claims on the inaccuracy of OPBE are valid since if the calculation were to be carried out on the crystallographically observed geometry of the complex would it still incorrectly predict the complex to have a low spin ground state? We will return to the topic of the OPBE functional's reliability in the following chapter.

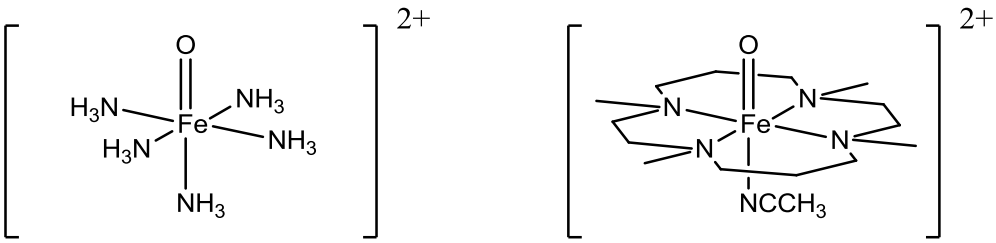

Figure 2.1; Left is the model complex used in the Neese group's study whilst on the right is the complex from which the experimental results were obtained.[61]

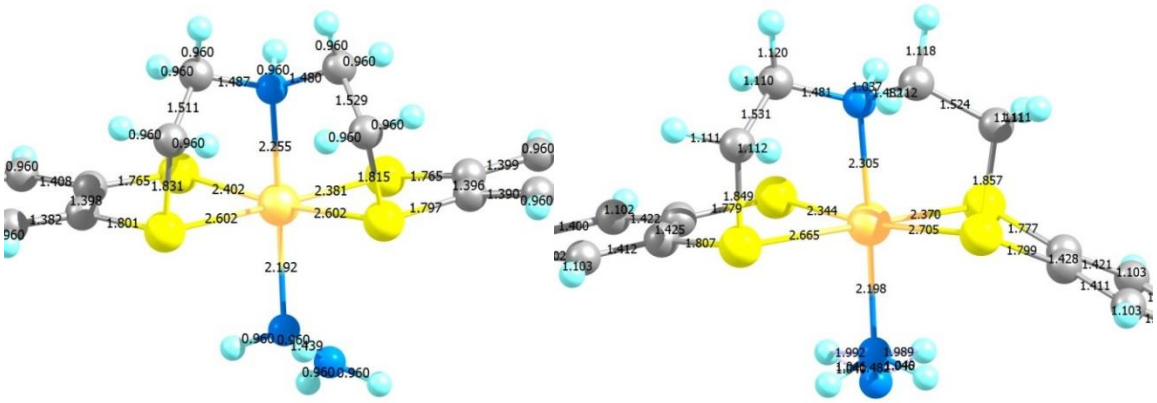

Figure 2.2; A comparison of the structure of high spin $[Fe(N_2H_4)(N_HS_4)]^0$ given by X-ray diffraction on the left and that used by Neese in his calculations on the right.[61,78]

Hybrid Methods

Hybrid functionals such as B3LYP, which add in a weighted amount of Hartree-Fock (HF) exchange to the calculation, have drawn substantial interest.[71] The justification behind hybrid functionals, conceptualised in terms of holes, is as follows; the holes resulting from exchange-correlation functionals, based in the LDA and GGA schemes, are by their construction localised and as such provide a good model for capturing left-right correlation. They fail in instances where the hole is expected to be entirely delocalised for instance when the antisymmetry of the wave function is taken independently. This nonclassical exchange term can be calculated exactly (for a non-interacting system) and in hybrid methods a portion of this is mixed in with the exchange and correlation as calculated using an LDA based approach. In Becke's methodology this resulted in 20% exact exchange being included as this produced the best results with respect to their chosen training set.[79]

Reiher et al. have suggested that for SCO research the optimal amount of HF exact exchange is in the region of 8 to 16% rather than the 20% included in standard B3LYP.[80] This is simply the result of the fact that percentages within this region predict the correct spin state for the systems studied, Figure 2.3.[80] The conclusion is reached that 15% exact exchange (B3LYP*) will offer a reasonable balance between the need for accurate spin state splittings and good performance for other systems.[80]

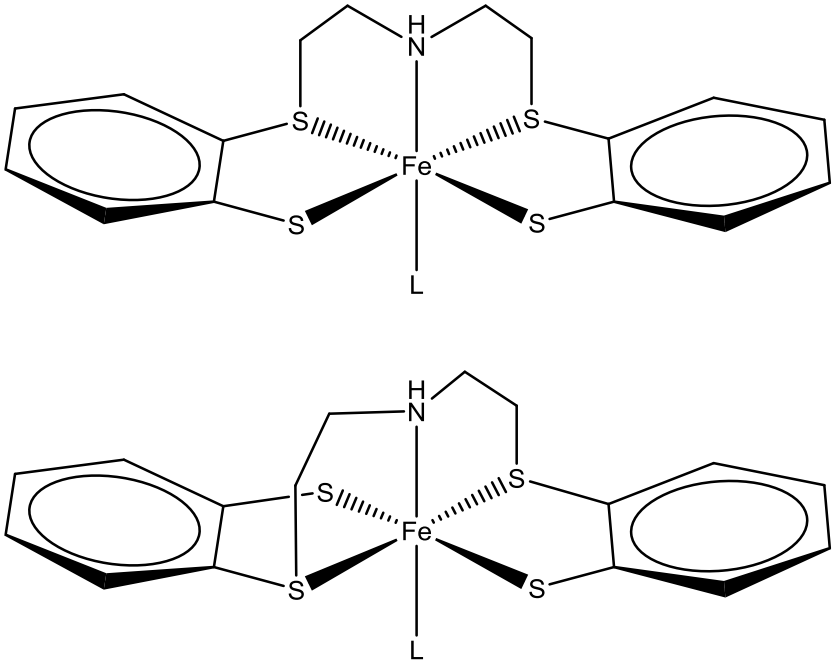

Figure 2.3; The complexes used in Reiher's reparameterisation of B3LYP. For L = NH_3 and N2H4 a cis-geometry is adopted while for L = CO, NO^+, PH_3 and PMe_3 a trans-geometry is adopted.

Other groups have supported the use of functionals with 10% exchange as in B3LYP**[81] and TPSSh[82]. While the Pierloot group found that no one value of exact exchange suits all purposes with closely related complexes often requiring different amounts in order to achieve reliable results.[62] For instance it was found that "the optimal exact-exchange contribution varies between 25% for $Fe(H_2O)_6^{2+}$ and $Fe(NH_3)_6^{2+}$ and 10% for $Fe(bpy)_3^{2+}$."[62]

Basis Set Effects

As described earlier in this chapter, KS theory is based on describing the electrons in terms of non-interacting fermions which, when taken together, have the same density as the true interacting system; this describes the Kohn-Sham molecular orbitals. However, solving the Kohn-Sham equations in this manner is not a simple task resulting from the fact that the KS functional is a coupled integro-differential problem. Like earlier wavefunction based approaches the molecular orbitals are instead described in terms of a linear combination of atomic orbitals. If infinite terms are used this linear combination can express every KS MO exactly. These atomic orbitals are more commonly termed basis functions. The form they take as well as how many to use to describe a given atomic orbital forms a topic of great interest to researchers.

The difference between basis sets lies within their functional form, with the most common types known as Gaussian Type Orbitals (GTO) (with contracted Gaussians consisting of a linear combination of Gaussian functions) and Slater Type Orbitals (STO). While Gaussian type basis sets have long been the most common form, STOs include the cusp at $r \rightarrow 0$ were GTOs have a gradient of zero. STOs also more accurately model the exponential decay of orbitals. These factors together indicate that STOs should be a more natural choice. However, with the many centred integrals difficult to compute with STOs, many have resorted to contracted Gaussians to exploit GTOs ease of computation whilst improving upon some of its pitfalls.

Swart assessed the importance of basis sets in calculation of spin-state energetics and found that Slater-type orbital basis sets show much more rapid convergence compared with Gaussian-type orbital basis sets.[58] In order for accurate results to be achieved using a GTO

basis set, a basis set such as Dunning's correlation consistent basis sets were required.[58] However, these are very computationally demanding.[58]

High Level Approaches

In principle, highly accurate results can be obtained through ab initio wavefunction methods such as CASPT2 which combines second order perturbation theory with a "complete active space (CAS) self-consistent field".[62,83] Perturbation theory is based upon the assumption that the problem only differs slightly from an already known (calculated) result and so the application of a perturbation to this result enhances it.[84] Such results are often used as a tool for benchmarking quantum mechanical methods and numerous examples of this exist in the literature.[59,62,85] It is noted, however, that in the search for accurate results from the CASPT2 method, the calculations easily become very computationally demanding and as such are impractical for use as a routine computational tool.[62] Pierloot acknowledges, however, that since DFT gives structures of a relatively high quality these could be used in conjunction with single point energies using CASPT2.[62]

Time consuming coupled cluster methods can also be of use in the study of transition metals.[86] However, as has been reviewed by Kepp, to recover enough static correlation explicit triples need to be included which increases computational cost.[86]

Ultimately as Neese has pointed out "there appears to be no reason to have uncritical trust in either the results of DFT methods or the results of wavefunction-based ab initio methods."[87]

Modelling Spin Transitions of Bulk Lattices

Various theoretical approaches have been used to model the spin transitions of complexes in the solid state.[88] Cooperativity in the solid state adds an additional level of complexity to these studies which is not seen in isolated molecules.

A recent example is the use of the mechanoelastic model in the study of the spin crossover phenomenon in a two dimensional sample upon heating and cooling[89] (the model was initially developed for the HS to LS transition).[90] Within the mechanoelastic model the volumetric change of a complex on SCO induces a force within the springs connecting it to its nearest neighbours resulting in displacements which propagate throughout the system. Inherent to this is a clear dependence on spring constants.[89] A weak constant results in a smooth transition with only slight hysteresis.[89] Upon increasing the force constant the transition becomes more abrupt and the hysteresis broadens.[89]

What is the alternative?

While quantum mechanics may be accurate enough for computing spin state energetics, even DFT calculations are computationally expensive and so the calculation of compounds en masse is impractical.[91] The alternative is to use faster, empirical methods, like molecular mechanics, although conventional molecular mechanics is not appropriate for transition metal systems.[91] In response Deeth notes that "since we cannot make DFT faster we must make molecular mechanics smarter."[91] The solution, Ligand Field Molecular Mechanics (LFMM) will form the basis of the next chapter.

Chapter 3: An Introduction to Ligand Field Molecular Mechanics

Introduction

Density Functional Theory (DFT) has formed the backbone of inorganic computational chemistry for more than a decade. While such quantum mechanical (QM) calculations have proven to show high levels of accuracy, they are not without their limitations.[86] It has been shown in the literature, and will be further elaborated in Chapter 4, that such techniques may require skill and judgement from the user in order to select the most appropriate theoretical approach.[86]

QM calculations are limited by their speed. As such, DFT proves to be inappropriate for users wishing to carryout high throughput screening or molecular dynamics. For organic systems classical methods such as molecular mechanics (MM) have been developed.[63] However, traditional molecular mechanics does not provide a general method for dealing with d-electron effects. Such effects are crucial to the structure and bonding of many transition metal complexes. As such, a new theoretical approach which includes explicit d-electron effects is required.[92]

Ligand Field Molecular Mechanics (LFMM) was designed to fulfil the need for a fast and reliable approach to calculating structures and properties of transition metal complexes.[93] Combining its two namesakes, ligand field theory and molecular mechanics, LFMM works to provide DFT levels of accuracy at MM prices and has proven to be a highly useful tool for the study of systems ranging from spin-crossover in transition metal complexes[94] to bioinorganic chemistry.[95]

Molecular Mechanics

Molecular mechanics in its simplest form expresses the potential energy of a molecule in purely classical terms.[63] Given as a sum of terms describing bond stretching, E_s, angle bending, E_b, torsional twisting, E_t and non-bonding interactions, E_{nb}, (Equation 3.1) these potential energy terms, in conjunction with their associated empirical parameters, form a force field (FF).[63,96,97]

$$E_{tot} = \sum E_s + \sum E_b + \sum E_t + \sum E_{nb} \qquad \textbf{Equation 3.1}$$

Force fields vary based upon their expansion of the above terms with some also involving further terms[63,96,97] such as the stretch-bend term implemented in the Merck Molecular Force Field[98] (an adaptation of which is implemented in LFMM[96]).

Transition metal systems pose a real challenge for force field developers. This challenge can be broken down into two basic components; that of molecular mechanics' reliance on a single reference angle for a given three atoms chain and MM's inability to appropriately take into account d-electron effects.[97] In common molecular mechanics, each bond angle is represented by a single reference value.[97] In organic chemistry this is not a problem as, broadly speaking, carbon adopts one of three basic geometries, either tetrahedral, trigonal planar or linear, with each associated with only one A-C-A angle.[97] However, most metal complexes cannot be described this simply.[97] For instance a complex adopting an octahedral geometry requires two unique A-M-A angles whilst the bipyramidal geometry contains three unique A-M-A angles (Figure 3.1) .[97]

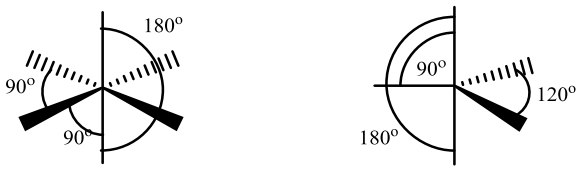

Figure 3.1; Left the octahedral geometry with two unique A-M-A angles and right a trigonal bipyramidal geometry with three unique angles.[97]

LFMM – The methodology

LFMM combines its namesakes in order to describe a system; this is achieved by splitting the system into two overlapping regions, the ligand region and the coordination region.[96] Any parameters not covered by the chosen MM force field are instead described by LFMM terms.[96] These parameters, as well as the split into two regions, are outlined in Figure 3.2 below.[96]

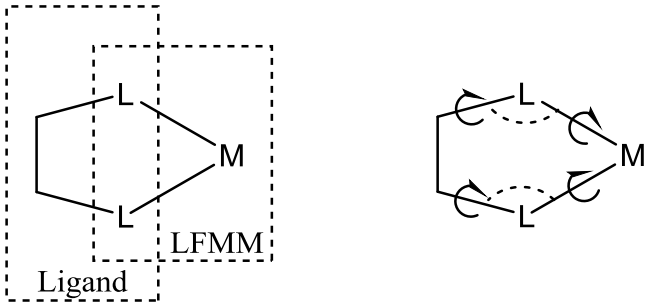

Figure 3.2; The ligand and LFMM regions and the angle and torsional terms spanning it.[96]

Metal ligand bond lengths are described in terms of a Morse function, in which *D* is the dissociation energy, r_0 describes a bondlength associated with the energy minimum, *r* is the bond length for which the energy is to be determined and α describes the curvature of the dissociation curve.[96]

$$E_{Morse} = D(1 - e^{a(r-r_0)})^2 - D \qquad \textbf{Equation 3.2}$$

Cu(II) Amines

The first published example of the use of LFMM (at the time termed d-orbital molecular mechanics for inorganics or DOMMINO) was in the study of a series of four and six coordinate copper (II) saturated amine complexes.[93] This old implementation of LFMM calculated d-electron stabilisation energies based upon the Ligand Field model.[93] It was shown that after parameterisation LFMM correctly predicts a planar geometry for four coordinate species as well as a tetragonally elongated octahedral structure for six coordinate species given a regular six coordinate starting structure.[93] This preference for tetragonal elongation results from the energy gain predicted by the Ligand Field stabilisation energy (Figure 3.3).[93] The uniqueness of this approach was in the fact that one set of parameters can deal with the long axial and short equatorial bonds of a typical Jahn-Teller distorted copper(II) complex.[93]

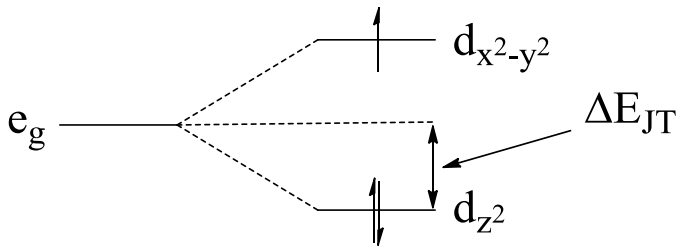

Figure 3.3; The effect of tetragonal elongation on the e_g orbitals of an octahedral species.[93]

The Angular Overlap Model

LFMM employs an angular overlap model approach to the inclusion of d-electron affects.[96] As such it is important we stop for a brief discussion of its theoretical basis.

The angular overlap model (AOM)[99] is based around the idea that it is possible to describe the ligand field potential as a sum of localised contributions from M-L bonds.[97] This is in contrast to crystal field theory and its successor ligand field theory which sought to describe the total ligand potential in terms of global symmetry.[97] The AOM therefore breaks down the complex into a set of diatomic interactions each with their own σ and π contributions.[97] These contributions in turn are the basis for the AOM parameters e_σ, $e_{\pi x}$ and $e_{\pi y}$.[97] It becomes possible to describe each of the metal d-orbital energies as a function of these parameters with the amount a given d-orbital's energy is affected by a ligand dictated by the square of the orbital overlap between the metal d-orbital and the appropriate ligand orbital.[97] This is termed S^2.[97] When S^2 is 1 the full amount of d orbital destabilisation occurs with the opposite true when S^2 is 0 as shown by the Wolfberg-Helmholtz approximation equation (Equation 3.3)[97,100] in which K is given by Equation 3.4 and its components "the diagonal matrix elements H_M and H_L represent the valence state ionization energies of the metal and ligand orbitals, respectively, in the complex".[100]

$$e \approx KS^2 \qquad \textbf{Equation 3.3}$$

$$S^2 \approx H_L^2/(H_M - H_L) \qquad \textbf{Equation 3.4}$$

The sign of these e parameters is dictated by the bonding or antibonding nature of the metal ligand interactions.[97,100] Since metal d orbitals are known to be primarily antibonding with respect to σ interactions e_σ is positive. [97,100] However $e_{\pi x}$ and $e_{\pi y}$ can take on a positive

or negative sign dependant on whether the interaction between the metal d orbitals and the ligand orbitals is antibonding or bonding in nature. [97,100]

One example is the relation between the relative orientation of a ligands σ orbital and the amount the d_{z^2} orbital is destabilised. [97] If a ligand points directly at the large lobe of the d_{z^2} orbital then the maximum amount of destabilisation (e_σ) occurs, whilst the same ligand perpendicular to the z axis interacts with the torus of the d_{z^2} orbital with this incurring a destabilisation of 0.25 e_σ. [97] The exact amount a given d orbital is affected by an AOM parameter is dictated by the F factor.[97] The F factor is a simple trigonometric function of the ligands position with respect to the complexes internal coordinates as shown in Figure 3.4.[97] For instance the effect of a ligand on the d_{z^2} orbital can be shown in terms of F^2 as indicated by Equation 3.3 and Figure 3.5.[97]

$$E(d_{z^2}) = F_\sigma^2(d_{z^2})e_\sigma = \frac{1}{16}(1 + 3\cos(2\theta))^2 e_\sigma \qquad \textbf{Equation 3.3}$$

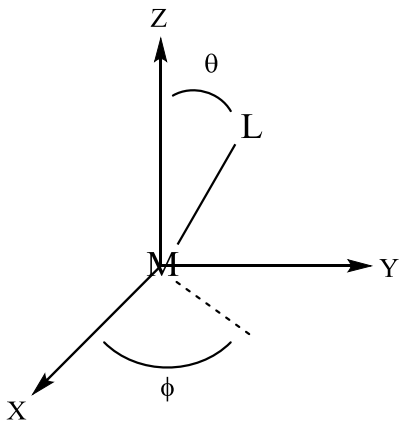

Figure 3.4; The definitions of the angles employed in determining the magnitude of F^2.[97]

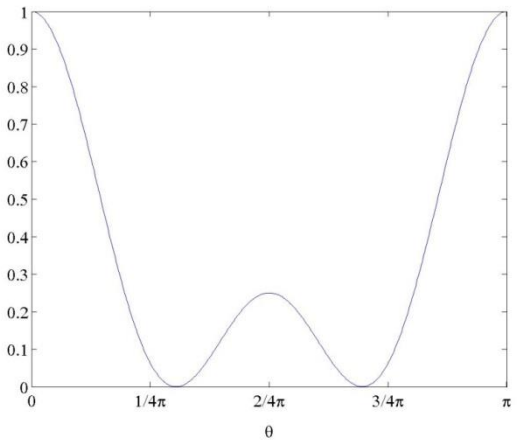

Figure 3.5: The effect of a ligand's orientation with respect to the z axis in destabilising the d_{z^2} orbital as a proportion of e_σ[97]. The y-axis represents $F_\sigma^2(d_{z^2})$ as shown in Equation 3.3.

Within LFMM the angular overlap parameters, e_λ, are described in terms of Equation 3.4 in which *r* describes the metal-ligand bond length and the *a* parameters are determined empirically.[101] It is important to note that not all of the terms in Equation 3.4 are utilised for a given *e* parameter. Instead only a single term is used for each e_σ, e_π and e_{ds}. The distance dependence for $e_\sigma$and e_π is assumed to be between r^{-5} and r^{-6},[100] and the distance dependence in this study will be chosen to either r^{-5} or r^{-6}. The ds-mixing term is in this work assumed to vary as r^{-6} and as such only the a_6 parameter is non zero in the expansion of e_{ds} as per Equation 3.4.

$$e_\lambda = a_0 + a_1 r^{-1} + a_2 r^{-2} + a_3 r^{-3} + a_4 r^{-4} + a_5 r^{-5} + a_6 r^{-6} \quad \textbf{Equation 3.4}$$

Previous applications of the angular overlap model express the *e* parameters in wavenumbers and this convention is retained in LFMM.[101] As described later the implementation in the molecular operating environment utilises kcal mol^{-1} which requires a conversion. Within LFMM the electrostatic interactions between electrons is treated

through use of a spin pairing term, e_{pair}, based on Equation 3.4.[96] The use of this term, which is used only for low spin complexes, is entirely pragmatic. In general two terms will be utilised, the distance independent a_0 term and a single distance dependent a_n term. The choice of distance dependence is finds no physical grounding. In fact none of the parameters retain their true physical meaning. All parameters result from fitting to structural and energetic data. If spectroscopically meaningful parameters are required they should be determined at the outset with the remaining parameters fitted around these.

The last LFMM term to be discussed is the 1,3-ligand-ligand repulsion.[101] Ligand-ligand repulsion is simply implemented as a repulsive A_{LL}/r^n term.[101] Here n will always be taken as 6.

Implementation in the Molecular Operating Environment with the test case $[MCl_4]^{2-}$

In 2005 LFMM was implemented into the Molecular Operating Environment (MOE).[96] Complexes of the type $[MCl_4]^{2-}$ were chosen to validate its implementation.[96] Dependent on the metal, these four coordinate species adopt either a tetrahedral high-spin geometry, as is the case for cobalt and nickel, or square planar low spin geometry in the case of palladium.[96] The geometry at these metal centres is dictated by balancing the angular component of the LFSE and the ligand-ligand repulsion.[96] In cases where a tetrahedral geometry is observed it is the ligand-ligand repulsion term which dominates whilst in the case of a square planar geometry it is the LFSE which wins out.[96]

LFMM was able to predict a tetrahedral geometry for high spin $[CoCl_4]^{2-}$ and $[NiCl_4]^{2-}$ whilst the hypothetical low spin $[NiCl_4]^{2-}$ complex was predicted to adopt a square planar

geometry.[96] The geometry at the HS nickel centre is not truly tetrahedral rather a small Jahn-Teller distortion occurs lowering the symmetry to D_{2d} (Figure 3.6).[96] The opposite distortion, a flattening, was observed in the d^9 $[CuCl_4]^{2-}$ complex (Figure 3.6).[96]

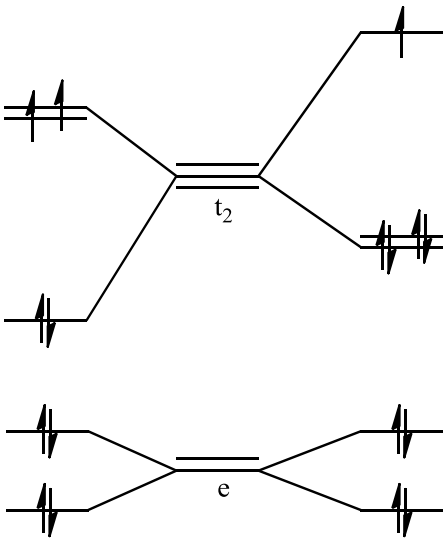

Figure 3.6; The effect of distortion on the metal d-orbitals of tetrahedral species, on the left $[NiCl_4]^{2-}$, a d^8 species displaying a D_{2d} distortion and on the right the d-orbitals of compressed $[CuCl_4]^{2-}$.[96]

In order to adequately reproduce Jahn-Teller distortions in six coordinate copper(II) systems it has been shown that the user is required to use a bespoke force field.[102] This stems from the fact that the force field previously employed contains inherent compromises in order to perform adequately for 4, 5 and 6 coordinate species.[102] As expected a bespoke LFMM force field reproduced well the available experimental data, with an average rms deviation in Cu-N distances of 0.03 Å and an rms deviation in Jahn-Teller distortions of 0.08 Å.[102] However, the energies obtained from this LFMM approach and DFT (RPBE) differ by up to 5 kcal mol^{-1}.[102] Unfortunately, since a complete description of the environmental effects inherent in the solid state is unavailable it was not possible to show which approach yields more accurate results.[102]

Ruthenium Arenes

Metals with π-bonded ligands form are an incredibly interesting and useful class of compounds finding applications in numerous catalytic processes.[103] Ruthenium half-sandwich complexes (Figure 3.8) are also candidates for anti-cancer drugs and it is for this reason they attracted the attention of the Deeth group.[103] After all, the computational study of the interactions of these complexes with DNA and other large biomolecules would come at much too high a computational cost if studies were carried out using the high level techniques discussed previously.[103]

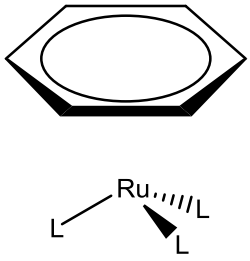

Figure 3.8; A representation of the ruthenium arene complexes studied by Brodbeck and Deeth.[103]

These ruthenium half-sandwich complexes form an interesting challenge for LFMM as the force field needs to be capable of handling both Werner-type coordination and metal-carbon interactions simultaneously.[103] The challenge of handling the coordination of the η^6-arene ligand was approached through the use of a dummy atom in the rings centre coordinated to the ruthenium.[103] Forces acting upon this dummy atom are then transferred out to the carbon atoms of the ring.[103] KS-DFT results were used in the determination of the AOM parameters allowing the group to show that the arene ligand behaves as a strong π donor and a weak σ donor.[103] The force field was constructed through keeping the AOM parameters fixed while varying the remaining LFMM parameters.[103]

Automated Parameter Optimisation

Commonly FF fitting techniques work to minimise a single penalty function[104-106] for instance a weighted sum of square errors of a number of different properties of the system, Eq 3.4,[107] with χ^2 the function to be minimised, ω_i^2 the weighting attributed to a property (e.g. relative energy), y_i^0 its reference value and y_i the calculated value.[107] Various approaches to the minimisation of χ^2 exist.[63] The simplest approach varies parameters one at a time in order to reduce χ^2 while more complex schemes include its derivatives with respect to variation in parameters.[63]

$$\chi^2 = \sum_i^N \omega_i^2 (y_i - y_i^0) \qquad \textbf{Equation 3.4}$$

Weighting introduces problems as these are user defined.[1] Since weightings can be varied the solutions are not unique.[1] The user needs to understand the nature of the error to ensure they are fairly balanced.[1] One method of removing this user introduced weakness is the use of a multi-objective optimisation algorithm (MOOA) previously used only once for force field fitting.[108] MOOAs do not result in a single solution but rather result in a set of solutions each of which is Pareto-optimal i.e. it is superior to all other solutions in at least one objective.[109]

A class of MOOA uses genetic algorithms which take their inspiration the biology of evolution. However, despite their potential, Handley and Deeth describe how these multi-objective evolutionary algorithms (MOEA) for FF fitting have not yet been widely utilised.[1] Handley and Deeth using their recently developed PROTEUS (Pareto OpTimal EvolUtionary System) script have shown that through the use of a MOEA it is possible to optimise a given set of LFMM parameters through fitting to a training database.[1] The

Scientific Vector Language (SVL) script for this routine is based upon NSGA-II (where NSGA refers to a Natural Selection Genetic Algorithm) developed by Deb et al.[110] PROTEUS operates through DommiMOE in order to optimise the LFMM parameters for a given ligand type or types.[1]

Within PROTEUS a parameter set is optimised with respect to two objectives, the RMSD of predicted values of ΔE_{HL} (as defined in Figure 3.09 as the difference in energy between the high and low spin geometries of a given complex) and a geometric term derived from the deviations in metal-ligand and ligand-ligand distances (deviations are measured against the training data).[1] New parameters are generated, ranked and improved upon following a simple series of steps.[1,110]

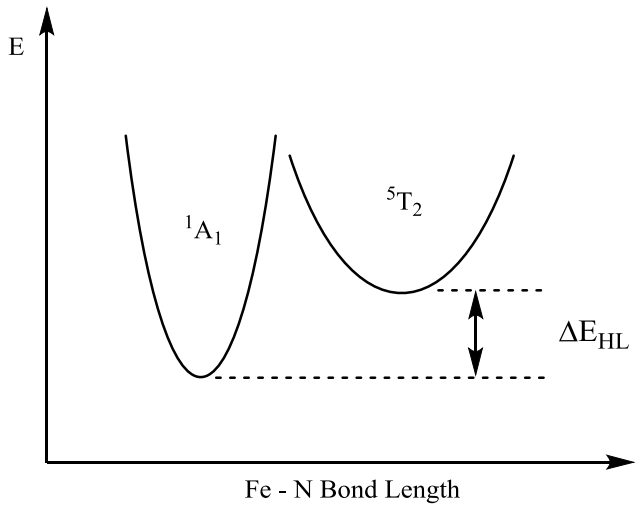

Figure 3.09; A depiction of ΔE_{HL}, the difference in energy between the high and low spin forms of a metal complex.[1]

Firstly, a starting set of parameters is input by the user and the bounds within which the parameters can vary are set.[1,110] A series of bit strings are generated, in PROTEUS the size of this is, as a default, 10 times the number of parameters to be optimised (10N).[1,110] Each bit string is 30N long; i.e. each parameter is described by 30 bits.[1,110] The composition of a

bit string is randomly determined upon its generation.[1,110] From the bit strings (chromosomes) an initial population of parameter sets is generated by decoding these bit strings into real parameters.[1,110] These parameters are assigned a Pareto rank according to their fitness with respect to the two objectives defined above.[1,110] The first new set of parameters is now ready to be generated.[1,110] Firstly, potential parents are selected from the population and for each potential parent two other members of the population are randomly selected.[1,110] The set of three are sorted by their Pareto rank.[1,110] The two potential parents with the lowest rank are chosen to mate.[1,110] If potential parents have the same rank then the solutions with the lowest density are chosen.[1,110] With density defined as a function of the distance to its nearest neighbours.[1,110]

Mating occurs by cutting the chromosome at a random point along the string, cutting the partner at the same point and joining the start of one string with the end of the other and vice versa.[1,110] The children then have a chance of being mutated based upon a predetermined term.[1,110] If mutation occurs, the bit string is altered at a random point along it.[1,110] This is process repeated until the desired number of children have been formed.[1,110] The children are then ranked alongside the parents and the population reduced back to size of the parents through removing the weakest members of the population.[1,110] This process is repeated until the predefined number of generations has been reached.[1,110]

In summary, a parameter set is taken and from it a random population of parameter sets are generated.[1,110] Through successive generations, diversity and strength is encouraged.[1,110] This ultimately leading to a Pareto optimal set of solutions.[1,110] This process is illustrated as three idealised generations in Figure 3.10 (in reality many more generations are needed).[1,110]

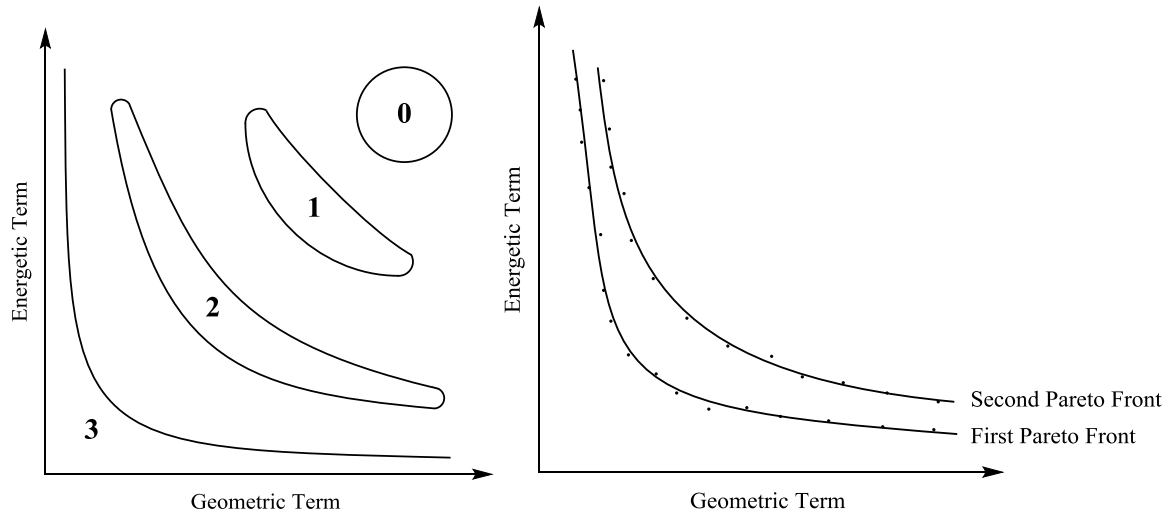

Figure 3.10; On the left a pictorial representation of the improvement of parameters in the objectives over time, illustrated as three idealised generations. On the right the distinction between the lowest ranked Pareto fronts.[1,110]

Spin Crossover

LFMM has most recently been applied to the prediction of novel spin crossover complexes.[94] Deeth et al in 2010 showed that LFMM could be trained to reproduce the spin states of four iron (II) amine systems, Figure 3.11, which span the SCO divide.[94]

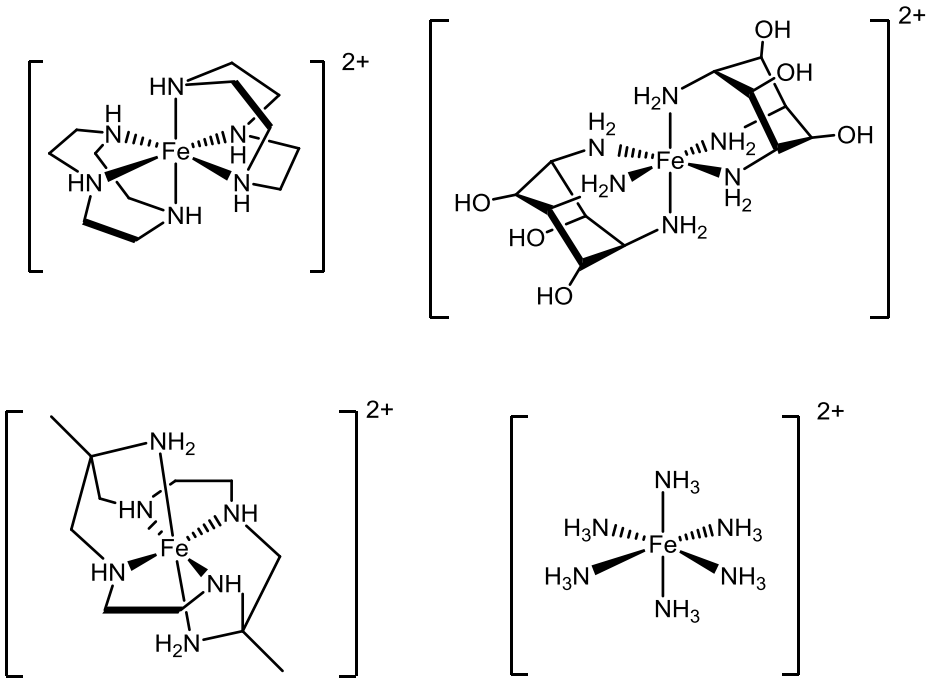

Figure 3.11; A depiction of the training set used in the initial iron(II) SCO force field.[94]

The use of PROTOEUS to optimise the LFMM parameters was seen to dramatically reduce the error in all objectives, a 75% reduction in the energy error to 0.2 kcal mol^{-1} and 90% in the geometry error down to 0.026 Å (the energy errors are calculated as root mean squared deviations from the calculated DFT energies whilst the geometry error is given as the RMSD in the Fe-N and N-N distances).[1] The results of this study will be commented upon further in Chapter 5.

Alternate Approaches in the Literature

Solutions other than LFMM do exist to describe the inclusion of metals into traditional molecular mechanics.

VALBOND, a force field approach based on its namesake valence bond theory has been shown to offer a means of studying transition metals.[111-114] It is based on the description of bond angles in terms of their hybridisation.[111-114] Meuwly et al have more recently expanded upon VALBOND such that it is now capable of handling trans effects, VALBOND-TRANS.[115]

The Comba group has had a great deal of success in the modelling of transition metal complexes using molecular mechanics in their MOMEC package.[116] The groups approach required the use of different parameters for axial and equatorial bonds with bond angles at the metal a product of ligand-ligand repulsion.[116] This lacks the elegance of the LFMMs single parameter approach.[116]

Carlson and Zapata have also utilised an AOM type description of d electron effects within their molecular mechanics based methodology.[117] With more recent implementations including that in AMOEBA by Xiang and Ponder[118] as well as Cirera, Babin and Paesani's use of a "hybrid Monte Carlo/molecular dynamics method" within DL_POLY to study the SCO phenomenon in metal organic frameworks.[119] This approach correctly predicts an abrupt transition but this transition is 100 K higher than the experimental value.[119]

Comba et al have taken to including LFMM into their MOMEC program; whilst this work is unpublished, communications with Comba have indicated that whilst they use different

functional forms for some of the LFMM terms they currently believe their results to be comparable with the DommiMOE implementation of the Deeth group. This is similar to the ongoing work of the Jensen group in Bergen, Norway who are in the process of implementing LFMM into Tinker.

Concluding Remarks

It has been shown through use of a range of examples that, given a broad training database of either experimental results or computational calculations, it is possible to reproduce the geometries and energetics of these complexes as well as predict those of new complexes. The integration of the AOM into MM has been proven to overcome the shortfalls of molecular mechanics in the treatment of transition metal complexes and the all-important d electron effects.

Chapter 4: Traversing the Density Functional Minefield

An Introduction

The topic of which functional to choose and which corrective factors to add is a common topic of discussion in the literature.[86] This chapter aims to clarify this topic, enabling future users to make more informed computational choices.

Does One Functional Suit All Problems?

While the approaches of others have been summarised in Chapter 2 it is important to test the validity of a chosen approach and not simply accept the often contradictory approaches of others.

Post SCF energetic calculations (ADF (version 2012.01[120] calculates the energy for 75 different functionals through the use of the keywords METAGGA and HARTREEFOCK) on a given system are computationally cheap calculations to run. The ADF documentation describes how post-SCF calculations allow for a reasonable approximation of the bonding energies obtained from a series of functionals. This is verified in table 4.1 in which the difference between the energetics obtained from the OPBE geometry optimisation (TZP with small frozen cores) and those obtained post-SCF (OPBE SCF, TZP with no frozen cores) are small at least for the following five SCO complexes (Figure 4.1): **1** a simplified Morgan type complex,[44] as described in Chapter 1, **2** $[Fe(1,4,7\text{-triazacyclononane})_2]^{2+}$,[17-19,121] **3** $Mn(Cp)_2$ (Cp^- = cyclopentadienyl),[122] **4** a Cambi type iron(III) dithiocarbamate species[46,47] and **5** Mn(III) tris(1-(2-azolyl)-2-azabuten-4-yl)amine with the ligands depicted

in Figure 4.1.[42] The OPBE functional performs adequately for both the iron(II) and iron(III) species predicting ΔE_{HL} values of 2.08 and 0.61 kcal mol^{-1} respectively. OPBE predicts a HS ground state for **1** and **5** despite their SCO character. While a ΔE_{HL} of 6.8 kcal mol^{-1} for complex **3** is predicted to be too positive to display SCO (ΔE_{HL} values between 0-6 kcal mol^{-1} are expected for SCO to be displayed).[61] These complexes highlight the problem of functional choice for SCO research. Functional choice is highly system dependent and a functional which is suitable for the study of a series of related systems such as iron(II) amines is not necessarily suitable for the study of another metal-ligand series. Functional validation is required for each new problem or else no value can be placed on the results.

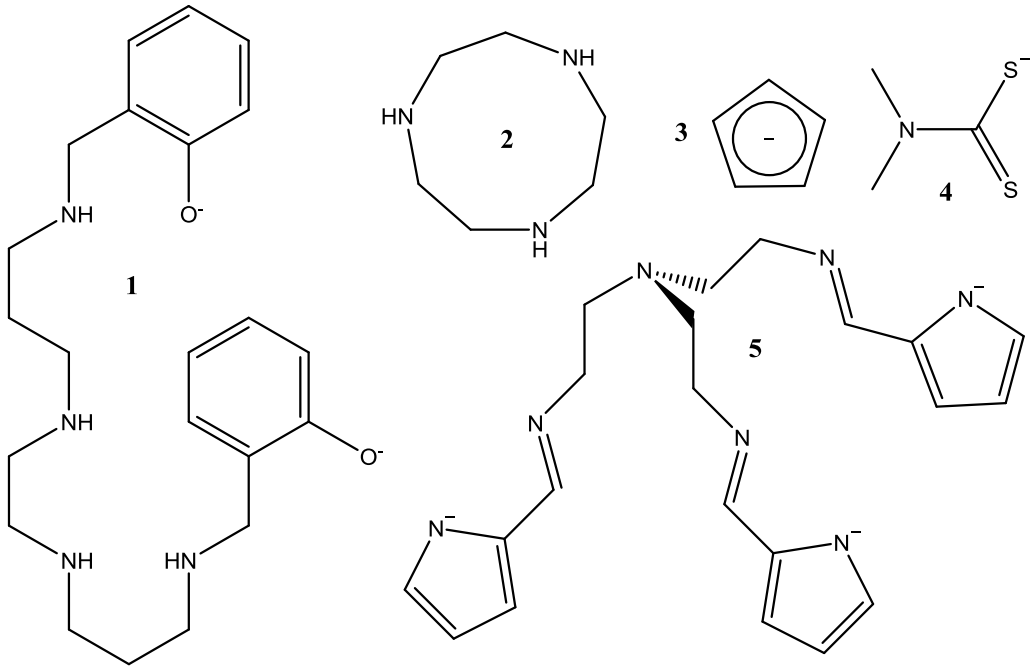

Figure 4.1; The ligands associated with the five SCO complexes studied.

Table 4.1; The calculated spin state splittings as calculated for five SCO complexes through POST-SCF calculations on OPBE optimised geometries. References for all 75 functionals are included in Appendix 1.

1 – MnO_2N_4[44]	
Functional	**ΔE_{HI}**
OPBE Opt	-3.79
SOGGA11	6.62
PKZB	5.74
BOP	5.54
revPBE	5.10
PKZBx-KCIScor	4.77
TPSSh	4.56
RPBE	3.34
KCIS-modified	2.94
B97-D	0.65
SSB-D	0.43
Becke88x+BR89c	0.39
B3LYP-D	-0.85
B3LYP*(VWN5)	-0.98
Operdew	-2.03
M06-L	-2.42
*	-2.61
OPBE	-3.04
BLAP3	-3.69
Becke00	-4.07
BmTau1	-4.70
OLYP	-5.23
mPBE1KCIS	-5.49

2 – DETTOL	
Functional	**ΔE_{HL}**
OPBE Opt	1.24
mPBEKCIS	15.45
VS98	15.28
XLYP	14.98
BOP	13.36
KCIS-modified	12.48
revPBE	10.97
TPSSh	10.82
RPBE	8.48
B97-D	6.35
Becke88x+BR89c	5.13
BLAP3	4.52
Operdew	3.39
B3LYP*(VWN5)	2.76
BmTau1	2.74
B3LYP-D	2.10
OPBE	2.08
*	0.85
Becke00	0.31
OLYP	-0.48
SSB-D	-2.63
tau-HCTH	-3.27
M06-L	-3.59

3 – MnCp2	
Functional	**ΔE_{HL}**
OPBE Opt	6.16
revPBE	10.80
BLYP	9.74
BOP	8.98
RPBE	8.60
PKZB	8.20
XLYP	7.91
PKZBx-KCIScor	7.27
OPBE	6.78
Operdew	5.91
KCIS-modified	4.83
TPSSh	4.80
OLYP	-0.20
Becke88x+BR89c	-2.55
B97-D	-2.80
*	-4.51
tau-HCTH	-6.21
BLAP3	-6.99
HCTH/93	-7.36
HCTH/147	-7.71
HCTH/407	-8.11
HCTH/120	-8.31
BmTau1	-8.87

4 – Dithiocarbamates	
Functional	**ΔE_{HL}**
OPBE Opt	0.93
XLYP	5.63
revPBE	5.33
PKZBx-KCIScor	5.02
PKZB	4.44
RPBE	3.62
KCIS-modified	2.77
OPBE	0.61
Operdew	0.25
TPSSh	-0.30
BLAP3	-3.16
OLYP	-3.61
BmTau1	-4.35
B3LYP*(VWN5)	-6.12
Becke88x+BR89c	-6.13
*	-7.38
SSB-D	-7.49
mPBE1KCIS	-8.06
tau-HCTH	-8.67
B97-D	-9.03
HCTH/93	-10.65
HCTH/147	-10.83
HCTH/407	-11.37

5 – MnPyrolTren	
Functional	**ΔE_{HI}**
OPBE Opt	-3.07
BOP	3.71
revPBE	2.89
PKZB	2.40
PKZBx-KCIScor	1.95
RPBE	1.37
KCIS-modified	0.32
TPSSh	0.18
VS98	-2.07
B97-D	-2.52
SSB-D	-2.52
Becke88x+BR89c	-2.59
Operdew	-3.38
OPBE	-4.04
B3LYP*(VWN5)	-4.82
BLAP3	-4.83
B3LYP-D	-5.59
BmTau1	-5.77
OLYP	-5.90
Becke00	-6.57
*	-6.61
mPBE1KCIS	-8.91
tau-HCTH	-9.20

* tau-HCTH-hybrid[68]

How can calculations of spin-state energetics be improved?

Commonly utilised corrections to density functional calculations include solvation, zero-point energies and dispersion. The effects of these corrections can be seen for a series of iron complexes in Tables 4.2 and 4.3. The **Co**nductor-like **S**creening **Mo**del (COSMO)[123] is utilised to capture condensed phase effects.[124] Zero point energy corrections lift the calculated energy off the bottom of the potential energy well to the first vibronic level. The calculated ΔH_{HL} (ΔE_{HL} + ZPE) is the difference in energy of the lowest vibronic level of the high and low spin states as illustrated in Figure 4.2 below. While it is appreciated that the true ground state is determined by ΔG and not simply ΔH,[125] we choose here to neglect entropic effects when computing spin state energetics in line with the work of others.[59,61]

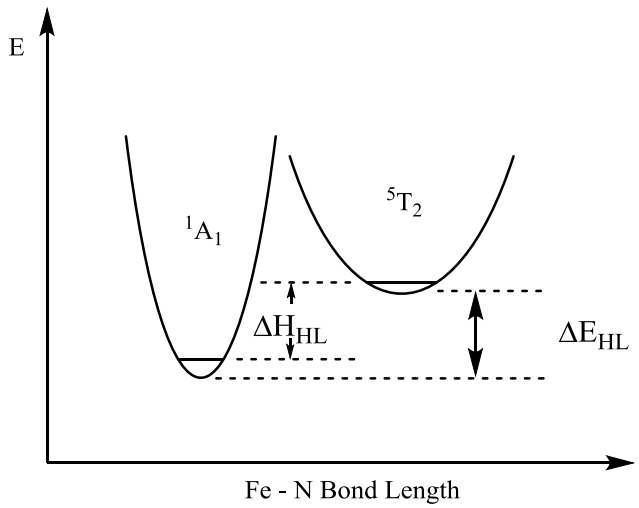

Figure 4.2; A definition of spin state splitting (ΔE_{HL}) and the zero point energy correction.

Choice of DFT methodology is critically important. The BP86 functional[70,126] with a small basis set will be used for the structural prediction of the complexes in Figure 4.3. The Def2-SVP basis set[127] was chosen (the RI approximation[128] was utilised with an Def2-SVP/J auxiliary basis set). Calculations using BP86 were carried out in ORCA[129] versions 2.9.1 and 3.0.1. Table 4.2 indicates that this methodology is appropriate in the prediction of

experimental structures. Despite the choice of additional terms, dispersion or solvation, the structure remains constant (taking the iron-nitrogen bonds as representative of the structure at large). Whilst the differences in iron-nitrogen bond lengths resulting from different additive effects are negligible, the inclusion of solvation comes at little additional cost so is included in subsequent geometry optimisations for completeness.

This approach is not without issues. For instance, the crystal structure of LS PAZXAP[130] (**8**) displays axial bonds up to 0.029 Å longer than the shortest equatorial bond (average equatorial bond 2.007 Å, axial 2.030 Å with an estimated error of ±0.003) whilst the DFT calculation reports all the Fe-N bonds to be equal in length. However, the differences are relatively small and given possible crystal packing effects we assume that the DFT and experimental bond lengths are not significantly different.

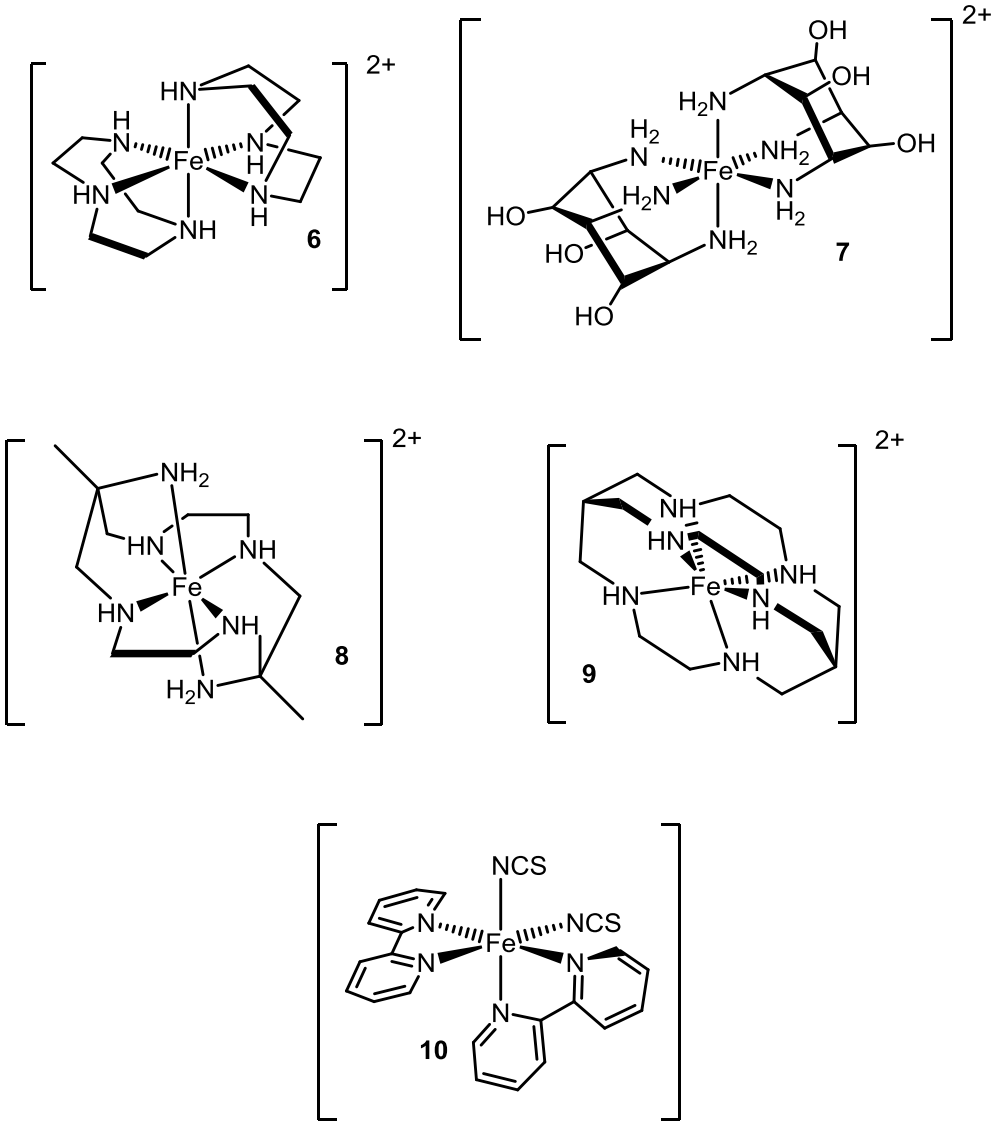

*Figure 4.3; The five iron(II) hexamine complexes studied for which the ground states span the SCO divide. The five compounds are DETTOL (**6**), PURYIK (**7**), PAZXAP (**8**), Fe399 (**9**) and FEBPYC (**10**).*

Table 4.2; A comparison of the effects of inclusion of dispersion and solvation on the calculated iron nitrogen bond lengths (Å) of four iron(II) amines which span the SCO divide.

		Experimental	Gas Phase	Dispersion	Solvation	Dispersion and Solvation
DETTOL (6)	HS	-	2.25	2.22	2.23	2.20
	LS	2.03[121]	2.04	2.02	2.03	2.01
PURYIK (7)	HS	2.21[131]	2.24	2.20	2.22	2.19
	LS	-	2.03	2.02	2.02	2.01
PAZXAP (8)	HS	-	2.20	2.18	2.18	2.17
	LS	2.02[130]	2.03	2.02	2.02	2.01
Fe399 (9)	HS	-	2.24	2.22	2.22	2.21
	LS	-	2.04	2.02	2.03	2.02
FEBPYC (10)	HS					
	Fe-NCS	2.09[132] 2.05[133]	1.98	1.97	2.04	2.02
	Fe-NPYD	2.17[132] 2.17[133]	2.23	2.20	2.21	2.19
	LS					
	Fe-NCS	2.01[132] 1.95[133]	1.92	1.95	1.92	1.91
	Fe-NPYD	2.03[132] 1.97[133]	1.94	1.93	1.95	1.94

BP86 predicts the incorrect spin state for PURYIK (Table 4.3). The trend is not linear requiring just a simple correction (Figure 4.4). After shifting the energetics by the 16 kcal mol^{-1} needed to shift DETTOL to slightly LS, the complexes PURYIK and Fe399[134] will remain out of order. It is therefore concluded that whilst BP86 with a small basis set produces reliable structures, the energetics are not adequate. However, the effects of solvation, dispersion and ZPE corrections on the calculated values of ΔE_{HL} are as reported by others.[86] Both dispersion and solvation favour the low spin state by on average 6.4 kcal mol^{-1} and 2.6 kcal mol^{-1} respectively whilst ZPE corrections favour the high spin state by on average 2.5 kcal mol^{-1}.

Table 4.3; The values of ΔE_{HL} (kcal mol^{-1}) as calculated using the BP86 functional, Def2-SVP basis set and Def2-SVP/J auxiliary basis set in conjunction with various corrections in.

	DETTOL	PURYIK	FE399	PAZXAP
No effects	12.37	13.89	13.47	17.94
Dispersion	19.82	21.77	19.58	22.04
Solvation	16.11	17.07	14.67	20.00
Dispersion + Solvation	22.46	23.56	22.96	22.11
No effects + ZPE	10.22	11.32	10.98	15.20
Dispersion + ZPE	16.27	18.68	17.16	18.72
Solvation + ZPE	13.73	14.12	12.80	16.90
Dispersion + Solvation + ZPE	20.33	18.99	21.03	19.43

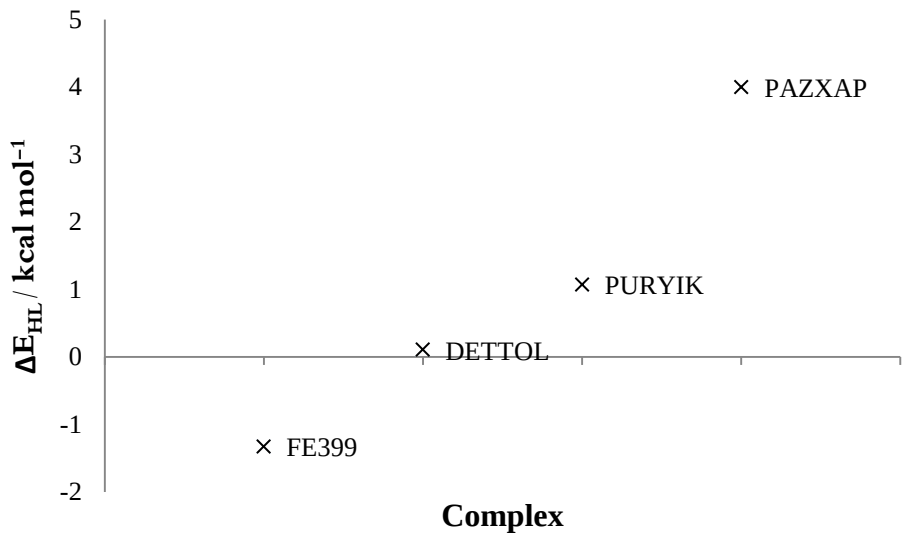

Figure 4.4; The spin state splittings (ΔE_{HL}) of the four complexes studied using the BP86 functional, Def2-SVP basis set and Def2-SVP/J auxiliary basis set in conjunction with the COSMO solvation model scaled by 16 kcal mol^{-1} to ensure DETTOL is SCO.

Any functional that is chosen to study SCO should of course predict the correct ground state. Table 4.1 indicates that OPBE[74,75] predicts the correct ground state for DETTOL. This is in line with the thinking of Swart et al[57,59] that OPBE is a suitable functional for the study of SCO in iron(II) hexamines.

Table 4.4; The basis set dependence of ΔE_{HL} when using slater type basis sets ADF (Version 2012.01[120] and OPBE with COSMO(water).

	SZ	DZ	DZP	TZP	TZ2P
PAZXAP	-107.83	12.64	12.11	9.45	9.24
Fe399	-125.79	6.75	3.87	1.08	0.89
DETTOL	-117.77	8.04	5.68	2.20	2.18
PURYIK	-123.52	4.97	2.83	-0.74	-0.56

The basis set dependence of OPBE with COSMO(water) for calculating ΔE_{HL} using ADF is given in Table 4.4. Small single zeta and double zeta basis sets prove to be unreliable for the calculation of ΔE_{HL}. However, either of the two triple zeta basis sets provides the correct ground state and so can be considered suitable for use. Inclusion of a second set of polarisation functionals as in TZ2P does not lead to increased accuracy and so is not recommended. The functional OPBE with a TZP basis set and COSMO(water) is therefore an appropriate methodology for the calculation of ΔE_{HL} in line with the work of Swart. [57,59] Since ZPE corrections are not highly functional dependent the BP86 ZPE values could be utilised.[135] At 2.15 kcal mol^{-1} for DETTOL this brings the calculated ΔE_{HL} for DETTOL down from 2.20 kcal mol^{-1} (TZP basis with solvation) to 0.05 kcal mol^{-1} which still favours the low spin state. However, the method is probably only accurate to within a few kcal mol^{-1} so the prediction of a low spin state is of limited significance.

Grimme has provided the means of including dispersion in DFT calculations, with the aim of improving them.[136] Dispersion is added to the standard Kohn-Sham energy as shown in Equation 4.1, with the dispersion energy taking the form as shown in Equation 4.2, where s_6 is a global scaling factor, N_{at} is the number of atoms, C_6^{ij} is the dispersion coefficient for atom pair *ij* while R_{ij} is an interatomic distance and f_{dmp} is a damping function the effect of which is illustrated in Figure 4.5.[136]

$$E_{DFT-D} = E_{KS-DFT} + E_{disp} \qquad \text{Eqn. 4.1}$$

$$E_{disp} = -s_6 \sum_{i=1}^{Nat-1} \sum_{j=i+1}^{Nat} \frac{C_6^{ij}}{R_{ij}^6} f_{dmp}(R_{ij}) \qquad \text{Eqn. 4.2}$$

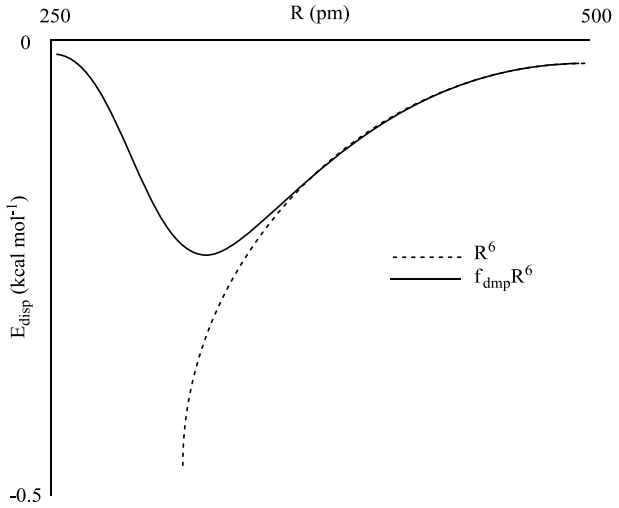

Figure 4.5. The effect of the damping function on dispersion contributions to calculated interaction potentials.[136]

The parameters in Equation 4.2 are functional dependent. Grimme initially reported the tuning of his dispersion scheme to two functionals, BLYP and PBE. The function dependent s_6 term was determined for each functional through fitting to a set of 29 pairs of atoms, small molecules and DNA bases for which the "true" binding energy is known theoretically and/or experimentally.[136] This scheme was later modified and the list of

functionals for which dispersion is calibrated expanded to include BP86, TPSS, and B3LYP as well as proposing a new functional B97-D which is explicitly parameterised for dispersion.[137] This new functional was reported to be incredibly accurate for the complexes studied, even approaching CCSD(T) levels of accuracy.[137] To date, OPBE has not been tuned for Grimme dispersion (any implementation) so we decided to explore the effect of its addition.

Using the s22 training set[138] (as Grimme used in his D3 implementation[139]) an optimal s_6 parameter (for use within the Grimme 2006 implementation, here calculated within ADF 2012.01 using the TZP basis set) was determined for OPBE through minimising the mean absolute deviation. The s22 training set comprises 22 small molecule dimers for which accurate interaction energetics were determined using a highly accurate high level wavefunction based approach.[138] An optimal s_6 of 1.75 was determined for OPBE (Table 4.5 and Figure 4.6). This is markedly higher than for the other functionals as determined by the Grimme group (a range of 0.75 – 1.25 is reported by Grimme[137]).

Table 4.5; The effect of varying s_6 on calculated binding energetics in kcal mol^{-1} for OPBE.

	ΔE_{ref}^{138}	ΔE_{nodisp}	S_6			
			1	1.5	1.75	2
1	-3.17	-0.21	-1.6	-2.29	-2.63	-2.98
2	-5.02	-2.18	-2.95	-3.33	-3.53	-3.72
3	-18.61	-12.05	-14.58	-15.82	-16.45	-17.09
4	-15.96	-9.06	-11.72	-13.05	-13.72	-14.37
5	-20.65	-12.25	-15.58	-17.25	-18.08	-18.91
6	-16.71	-9.42	-13.39	-15.38	-16.37	-17.37
7	-16.37	-8.18	-12.42	-14.54	-15.59	-16.65
8	-0.53	0.75	-0.10	-0.51	-0.70	-0.92
9	-1.51	2.20	0.05	-1.01	-1.56	-2.08
10	-1.50	1.89	-0.29	-1.39	-1.93	-2.47
11	-2.73	7.00	1.27	-1.58	-3.01	-4.43
12	-4.42	6.38	0.18	-2.93	-4.48	-6.03
13	-10.12	5.29	-3.73	-8.23	-10.48	-12.73
14	-5.22	9.63	1.11	-3.17	-5.30	-7.42
15	-12.23	10.39	-2.84	-9.45	-12.74	-16.05
16	-1.53	-0.37	-1.37	-1.87	-2.11	-2.37
17	-3.28	0.52	-1.82	-3.00	-3.58	-4.16
18	-2.35	1.25	-1.03	-2.16	-2.74	-3.3
19	-4.46	-0.18	-3.28	-4.82	-5.60	-6.37
20	-2.74	2.83	-0.82	-2.64	-3.55	-4.47
21	-5.73	1.96	-3.33	-5.99	-7.31	-8.64
22	-7.05	1.39	-2.70	-4.74	-5.76	-6.78
	MAD	7.25	3.22	1.30	0.83	1.39

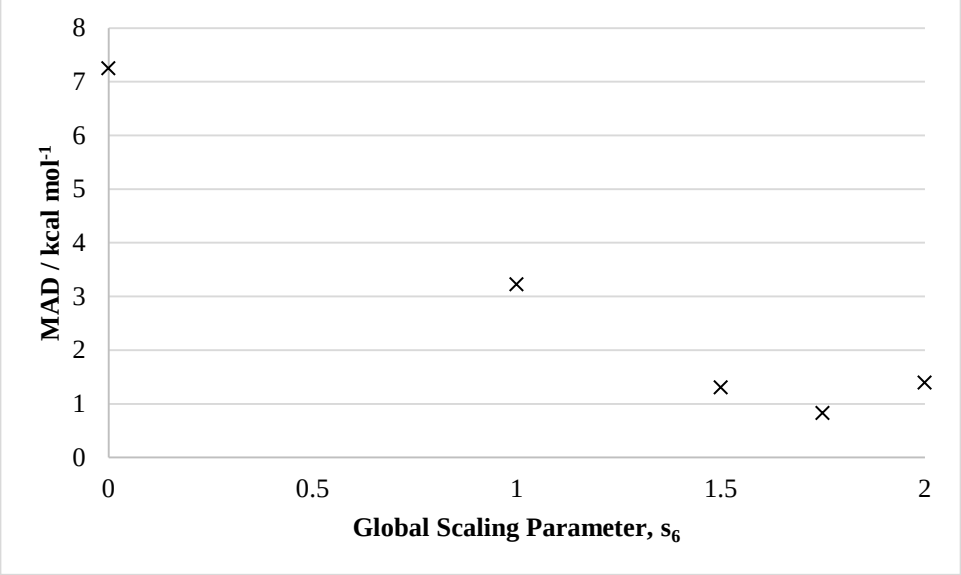

Figure 4.6: A plot of MAD as a function of the s_6 parameter.

Whilst it may be expected that the inclusion of additional terms such as dispersion should "improve" the quality of DFT calculations, for SCO using the OPBE functional, this is simply not the case as shown in Table 4.6. This is likely a result of the fact that OPBE succeeds for iron amines not as a result of its theoretical grounding but rather as a result of cancelation of errors. All density functionals treat exchange correlation in an approximate manner since its true form is unknown. As such any attempt at improvement may simply remove the cancellation of errors which made a functional successful in the first instance.

Table 4.6; The effect dispersion has on the value of ΔE_{HL} (as obtained from single point energy calculations using the TZP basis set) for DETTOL. The structures used are those obtained using the BP86 functional, SVP basis set and COSMO solvation model as above. S denotes solvation while D denotes dispersion. Default dispersion refers to a global scaling factor of 1 which is the default value for an unparameterised functional.

Method	ΔH_{HL}/ kcal mol^{-1}
OPBE (TZP) + S	2.20
OPBE (TZP) + S + Default D	8.50
OPBE (TZP) + S + D (s_6 = 1.75)	13.23

$^{R,R'}$Pytacn Complexes an Application of Density Functional Theory to Spin Crossover Problems

The study of Prat et. al. provides an interesting challenge for density functional approaches.[2] The $^{R,R'}$Pytacn complexes ($^{R,R'}$Pytacn = 1-[(4-R-6-R-2-pyridyl)methyl]-4,7-dimethyl-1,4,7-triazacyclononane), Figure 4.7, display a clear relationship between substitution at the ortho and para positions and magnetic moment. Complexes are denoted by the shorthand R,R'.

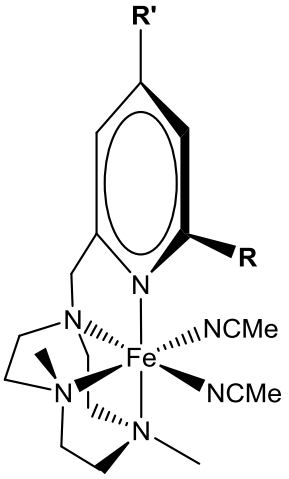

Figure 4.7; The $^{R,R'}$Pytacn complexes studied.

Substitution at the R' position with the electron withdrawing NO_2 group results in a low spin complex whilst substitution with the electron donating NMe_2 group results in an increased population of the high spin state as evidenced by the trend in reported magnetic moments.

H,NO_2 (0) < H,CO_2Et (0.78) < H,Me (1.24) ≈ H,H (1.26) < H,Cl (1.71) < H,OMe (2.09) < H,NMe_2 (2.62).

Substitution at the R position results in high spin species with magnetic moments ranging from 4.63 for F,H and 4.95 for Me,H.

Table 4.7; For the eleven complexes studied in the paper of Prat et.al.[2] the calculated iron-pyridine, average iron-amine and iron-acetonitrile bond lengths are reported as well as the calculated spin state splitting ΔE_{HL}.

	H,NMe_2	H,NO_2	H,OMe	H,CO_2Et	H,H	H,Cl	H,Me	Me,Me	F,H	Cl,H	Me,H
σ_p[140]	-0.83	0.78	-0.27	0.45	0	0.23	-0.17	-0.17	0	0	0
μ_{eff}^2 / B.M.	2.62	0	2.09	0.78	1.26	1.71	1.24	4.75	4.63	4.87	4.95
Fe-N (pyr) / Å	2.13	2.14	2.16	2.17	2.17	2.17	2.16	2.23	2.22	2.25	2.22
Fe-$NCCH_3$ / Å	2.12	2.12	2.10	2.12	2.10	2.10	2.10	2.14	2.10	2.11	2.10
Fe-N (amine) / Å	2.28	2.26	2.25	2.26	2.27	2.26	2.27	2.26	2.26	2.26	2.28
Fe-N (pyr) / Å	1.98	1.94	1.97	1.96	1.96	1.96	1.97	2.07	2.02	2.08	2.06
Fe-$NCCH_3$ / Å	1.87	1.89	1.87	1.88	1.87	1.88	1.87	1.88	1.88	1.88	1.87
Fe-N (amine) / Å	2.06	2.05	2.05	2.05	2.05	2.05	2.05	2.06	2.05	2.05	2.06
Fe-N (pyr) / Å	-0.16	-0.20	-0.19	-0.21	-0.20	-0.21	-0.19	-0.16	-0.20	-0.17	-0.17
Fe-$NCCH_3$ / Å	-0.25	-0.23	-0.23	-0.24	-0.23	-0.23	-0.23	-0.27	-0.22	-0.23	-0.23
Fe-N (amine) / Å	-0.22	-0.21	-0.20	-0.21	-0.21	-0.21	-0.21	-0.19	-0.21	-0.21	-0.21
Energy / kcal mol^{-1}	-23.40	-25.64	-24.23	-23.81	-24.67	-24.30	-24.33	-20.53	-21.67	-18.05	-19.83

Using the BP86 functional, def2-SVP basis set, def2-SVP/J auxiliary basis set and the COSMO solvation model for acetonitrile, the geometries and energetics were calculated for the pytacn species.

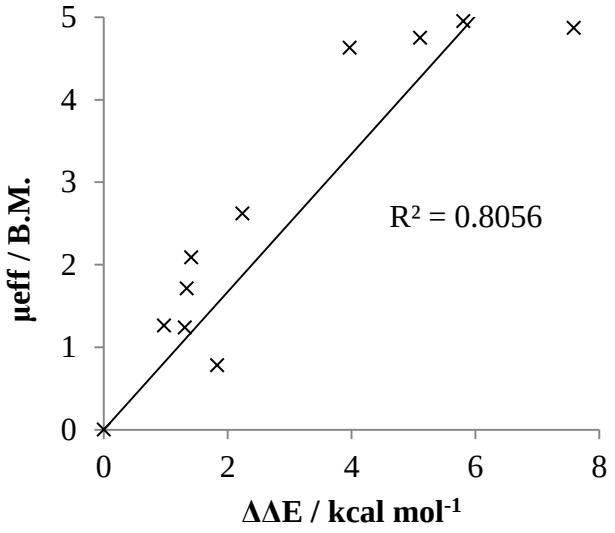

Figure 4.8; The correlation between computed spin state splittings relative to the para-NO_2 species and the reported magnetic moments of the complexes in deuterated acetonitrile (CD_3CN).[2]

A comparison of changes in spin state splitting $\Delta\Delta E_{HL}$ and reported magnetic moments are shown in Figure 4.8. While the pytacn species substituted by NO_2 and NMe_2 at the R' position are correctly predicted at either end of the LS spectrum the trends are not the same with the para-CO_2Et species the outlier in the series.

Experiment: $NO_2 < CO_2Et < Me \approx H < Cl < OMe < NMe_2$

BP86: $NO_2 < H < Me \approx Cl < OMe < CO_2Et < NMe_2$

However, the correlation (Figure 4.8) appears strong. This illustrates that even simple protocols can give qualitatively accurate results.

Conclusions

The overall success of density functional approaches to spin crossover must to some extent result from a cancellation of errors.[86] Therefore outliers appear to be inevitable. The CASPT2 or related high level approaches could, in theory, result in a more reliable agreement. However, such approaches lie outside the reach of most non specialists and so are outside the reach of those chemists who wish to use it as a routine tool for the study of real chemical problems. Therefore, in the remainder of this study density functional approaches will be deemed sufficient for the study of SCO if they can be validated for the systems of interest.

Chapter 5; The Use of Force Field Based Methods for the Study of Transition Metal Complexes

Introduction

As outlined in Chapter 3, a multi-objective evolutionary algorithm approach has been developed and tested for the spin state energetics of Fe(II) amine complexes.[1] This preliminary study was restricted to simple amine donors and did not include electrostatic interactions. Given the ultimate goal is to be able to simulate SCO materials in the solid state where inter-molecular interactions play a critical role in cooperativity, we needed to extend the treatment both to the inclusion of electrostatics and new ligand types, especially unsaturated N donors. To gain experience with the PROTEUS software, attempts were made to reproduce the original results reported by Handley and Deeth. However, it became apparent that simply repeating the procedures used by Handley did not yield the same results. A thorough debugging unearthed multiple errors in the PROTEUS code. The major errors are summarised below.

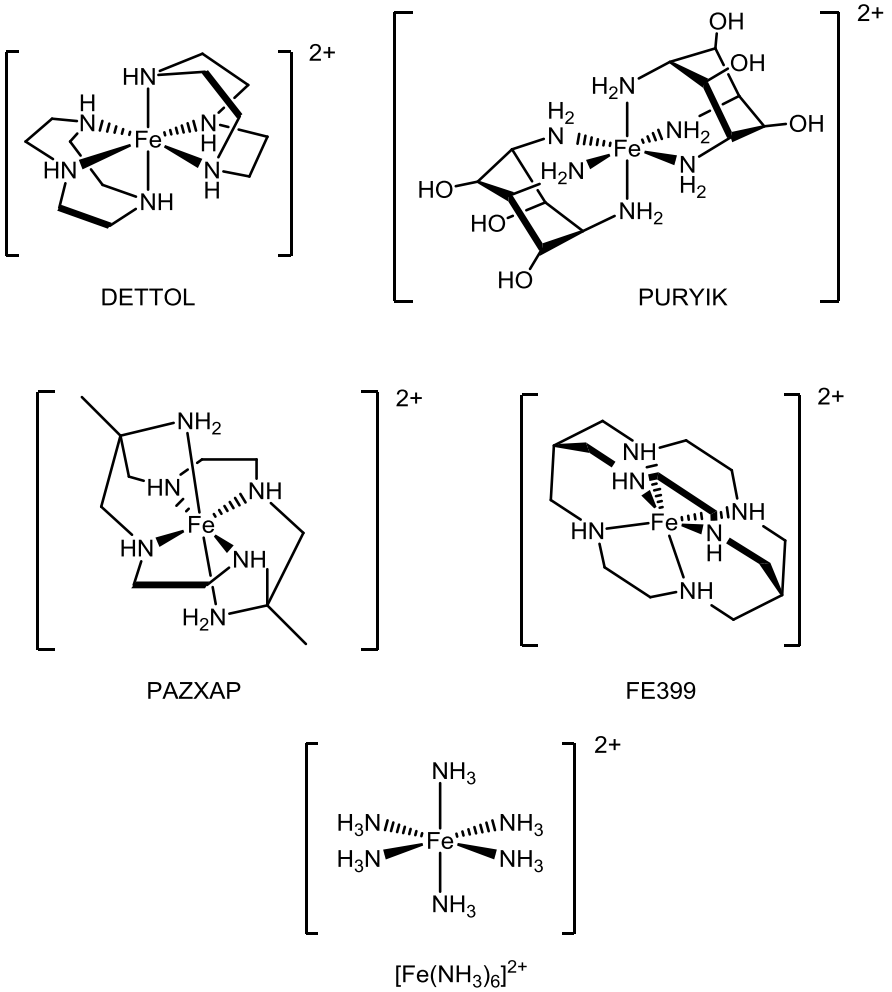

Figure 5.1; The five iron(II) hexamine complexes used as training data in the parameterisation of iron(II) amine bonds for LFMM along with their references.

The first and most stark error was that the published version of PROTEUS (the parameter optimisation tool described in Chapter 3) only treated part of the geometric objective (the ligand-ligand term and not the metal-ligand term) of the final structure in a training set as each time the error was calculated it overwrote previous error calculations. As such, the previous study reported an erroneous structural error. The 0.2 kcal mol^{-1} reported RMSD in calculated values of ΔE_{HL} (for the complexes in Figure 5.1) was correct but the true cost in the structures was masked. This was corrected to ensure proper counting of the structural contributions from all complexes by changing the section of code which calculates geometric errors from:

```
pen_config = add sqr (bonds1 - bonds0); // Add the square of the errors
if args.use_ll_dist then //If the ligand-ligand distances are to be included
  pen_config = add sqr (dist1 - dist0);
endif;
```

to:

```
pen_config = pen_config + add sqr (bonds1 - bonds0);
if args.use_ll_dist then
  pen_config = pen_config + add sqr (dist1 - dist0);
endif;
```

where the pen_config variable tracks the structural penalty function, bonds1 and bonds0 represent the LFMM and DFT metal-ligand bond lengths respectively and dist1 and dist0 the LFMM and DFT ligand-ligand distances. Thus, when the above code is looped it now accumulates the geometric errors for a given parameter set as opposed to just overwriting them.

The calculation of the RMSD error also needed correcting from:

```
pen_config = pen_config/N_test;
pen_config = pen_config/6;
pen_config = sqrt pen_config;
```

to:

```
local lig_number;
lig_number = 6;
if args.use_ll_dist then
```

```
  lig_number = lig_number + 15;
endif;
pen_config = pen_config / (N_test * lig_number);
pen_config = sqrt pen_config;
```

The original Handley version only counted the six metal ligand bonds neglecting the fifteen ligand-ligand distances. Finally, the spin pairing term was mistreated. This was not apparent in single ligand cases as it only affected instances involving more than one ligand type. The code was modified appropriately. PROTEUS was further modified to allow each parameter to be varied within defined windows (e.g. ± 10%) rather than having windows set for whole families of parameters. This allows for increased user control.

Taking a previous parameter set as a starting point (0.25 kcal mol^{-1} energetic RMSD and 0.066 Å structural RMSD), two 50 generation optimisation runs allowed reproduction of parameters of similar quality. The final Pareto front is shown in Figure 5.2. Since the original parameters produced by Handley and Deeth were unsound with regards to structures (causing issues particularly for PAZXAP) it is proposed now that a more suitable parameter set may in fact be those given in Table 5.1 for which the energetic RMSD is 0.90 kcal mol^{-1} and the structural RMSD is 0.059 Å, any further improvements in geometry result in unacceptable increases in the energetic RMSD.

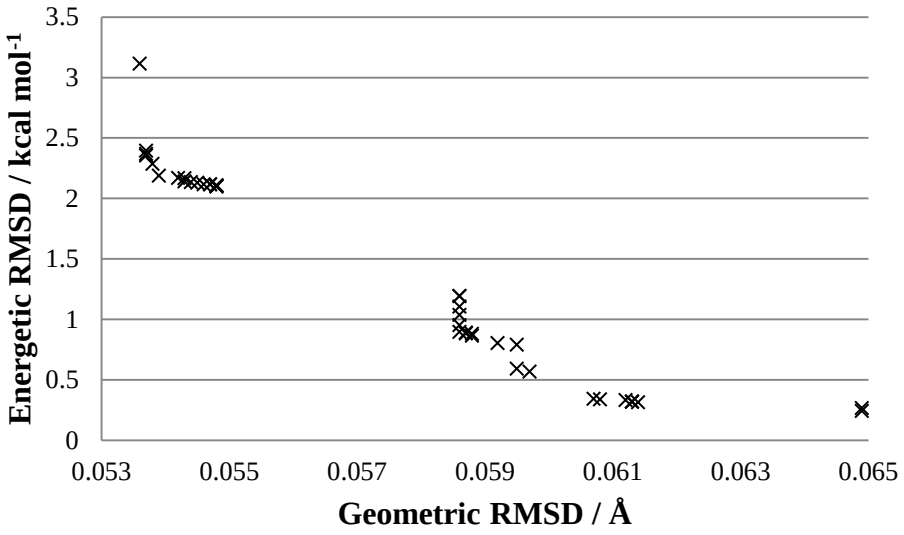

Figure 5.2; Final Pareto front of the second 50 generation optimisation run with each point marks a Pareto optimal parameter set from which the parameters in Table 5.1 were taken.

Table 5.1; The proposed parameter set derived from the optimisation run of Figure 5.2 for which the energetic RMSD is 0.90 kcal mol^{-1} and the structural RMSD is 0.059 Å. The values are reported in their full length as obtained from the parameter optimisation. Their sensitivity to variation will be explored in the next section.

Parameter		Units	Value
Morse	r_0	Å	2.17
	D	kcal mol^{-1}	54.9
	α		1.13
Ligand-Ligand Repulsion	A_{LL}	kcal mol^{-1} Å^6	3,950
AOM	e_σ (a_6)	cm^{-1} Å^6	416,000
	e_{ds} (a_6)	cm^{-1} Å^6	148,000
Spin pairing	a_0	kcal mol^{-1}	14.9
	a_5	kcal mol^{-1} Å^5	-61.4

Computational Details

Unless otherwise stated structures in this chapter were optimised using the BP86 functional,[70,126] the RI approximation, the def2-SVP basis set[127] and the COSMO solvation model[123] (water) within the ORCA package. The RI approximation[128] was utilised and so the def2-SVP/J auxiliary basis set was used. Initially Version 2.9.1 of the ORCA code was used followed by Version 3.0.1.[129] Since no difference is expected in the structures predicted by these implementations distinctions will not be made in the body of the text. Energetics were determined through single point calculations within ADF 2012.01[120] using the OPBE functional,[74,141] TZP basis set[142] with small frozen cores,[143] COSMO[123] (water, dielectric constant = 78.39, radius = 1.93 Å). To assist with efficient convergence, SCF sub keys of mixing and level shifting were set to 0.1 and 0.3 respectively compared to default values of 0.3 and 0. Ligand Field Molecular Mechanics calculations were carried using DommiMOE[101] within Molecular Operating Environment 2010.10[144] and 2011.10.[145]

Force Field Sensitivity Testing

It is important to test the sensitivity of parameters to variation. Table 5.2 records the effect of 10% variations on each of the LFMM parameters derived from PROTEUS as in Table 5.2.

Table 5.2; The effects of a ten percent variation in each parameter on the energetic and geometric penalty functions. It is important to note that whilst the numbers are reported to an appropriate number of significant figures the underlying variations were based on the raw parameter values from the parameter optimisation run.

Parameter		Units	Value (PROTEUS)	Variation Applied	Test Value	Energetic RMSD / kcal mol^{-1}	Geometric RMSD / Å
Morse	r_0	Å	2.17	0.22	2.39	36.6	0.318
					1.96	1.31E+09	1.295
	D	kcal mol^{-1}	54.9	5.5	60.4	1.7	0.058
					49.5	4.5	0.061
	α		1.13	0.11	1.24	3.0	0.061
					1.01	1.31E+09	0.612
Ligand-Ligand Repulsion	A_{LL}	kcal mol^{-1} Å^6	3,95	400	4,340	3.3	0.064
					3,550	6.3	0.059
AOM	e_σ (a_6)	cm^{-1} Å^6	416,000	42,000	457,000	14.3	0.064
					374,000	84.3	1.979
	e_{ds} (a_6)	cm^{-1} Å^6	148,000	15,000	163,000	1.0	0.059
					134,000	3.3	0.055
Spin pairing	a_0	kcal mol^{-1}	14.9	1.5	16.4	8.8	0.059
					13.4	9.2	0.059
	a_5	kcal mol^{-1} Å^5	-61.4	-6.1	-67.6	2.5	0.059
					-55.3	2.3	0.059

It is clear from Table 5.2 that the structural accuracy of the parameter set is generally less sensitive to variation than the energetic accuracy. For twelve of the sixteen parameter sets generated structural accuracy is maintained. However, the energetic error shows substantial

increases on variation for all except one of the parameter sets. This could be at the heart of why it is far easier to obtain structural accuracy than energetic.

The effect of variations upon energetics and structures should always be kept in mind when setting the windows in which parameters are allowed to vary. Changing r_0 or α can have catastrophic effects on the energetics so these parameters need to be tightly controlled. Limits on variation must be set with this in mind. r_0 is very sensitive to variation and so smaller bounds should be set on this than the ligand-ligand repulsion term.

A ten percent increase in the d-s mixing parameter leads to only a minor increase in the energetic RMSD from 0.9 to 1.0 kcal mol^{-1} whilst the structural RMSD remains constant at 0.059 Å. This behaviour is as expected since previous work suggests that the ds-mixing term can generate switching behaviour, for example tetragonally elongated and compressed octahedra in copper(II) complexes.[102] The relatively small change considered here is not sufficient to cause any large variation.

Molecular Dynamics in LFMM

To conclude our look at the performance of LFMM in the study of SCO in iron(II) amines it is important to ascertain what, if any, value can be placed on the results of a molecular dynamics (MD) simulation carried out using Ligand Field Molecular Dynamics (LFMD). Whilst the LFMM parameters were obtained using DFT data which is at 0K, the force field has been trained such that it should understand the energetic effects associated with structural changes. The LFMD runs here were carried out by Robert J. Deeth but all analysis and DFT calculations were carried out by the author. The simple graphs below (Figures 5.3-6) illustrate a series of energies recorded over the last 10 ps of a 200 ps LFMD run (using the parameters given in Table 5.3) at 360 K on the DETTOL complex described earlier compared to single point DFT calculations (OPBE, TZP, COSMO (eps = 78.39 and radius = 1.39)).

Table 5.3; The force field parameters used by Robert J. Deeth for the LFMD run are those found in the paper of Deeth et al 2010[94] and are given in this table.

Parameter		Units	Value
Morse	r_0	Å	2.15
	D	kcal mol^{-1}	58.3
	α		1.32
Ligand-Ligand Repulsion	A_{LL}	kcal mol^{-1} Å^6	3,940
AOM	e_σ (a_6)	cm^{-1} Å^6	413,000
	e_{ds} (a_6)	cm^{-1} Å^6	126,000
Spin pairing	a_0	kcal mol^{-1}	14.5
	a_4	kcal mol^{-1} Å^4	-44.0

The results at 360 K show clear differences between the LFMM energetics and those obtained from single point DFT calculations (OPBE, TZP). Whilst the energetics appear from the superposed plots to follow the same general trend the corresponding R^2 is just 0.51 and 0.58 for the low and high spin states respectively. Another run this time at 220 K had comparable results with a LS R^2 of 0.56 and a HS R^2 of 0.58.

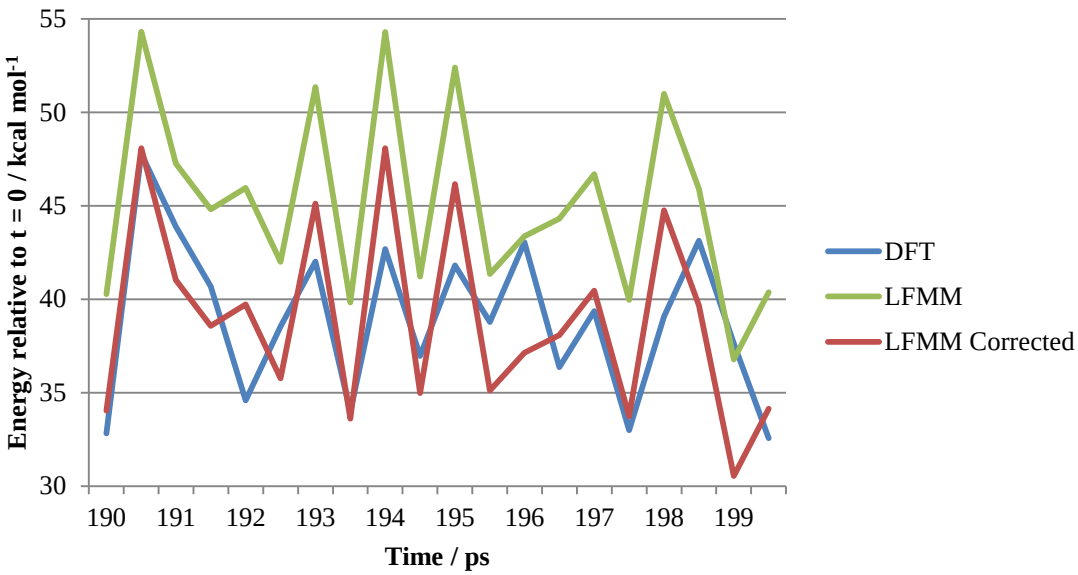

Figure 5.3; The recorded energies relative to t=0 of the last 10 ps of the LS structure at 360 K. The "correction" is a transposition by 6.23 kcal mol^{-1} (the average of the last 10 ps DFT energetics, included purely for illustration).

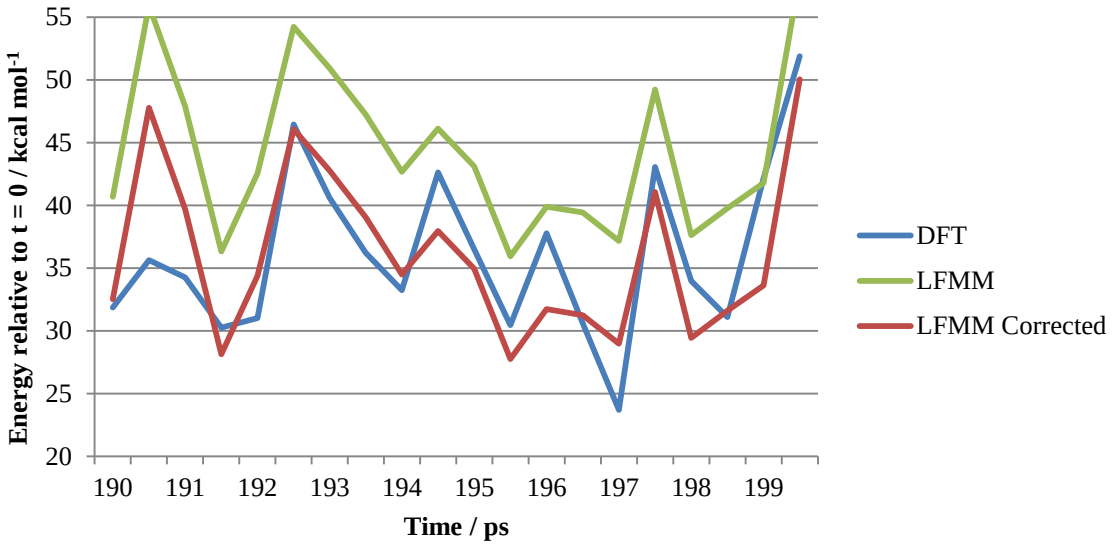

Figure 5.4; The recorded energies relative to t=0 of the last 10 ps of the HS structure at 360 K. The "correction" is a transposition by 8.17 kcal mol^{-1} (the average of the last 10 seconds DFT energetics, included purely for illustration).

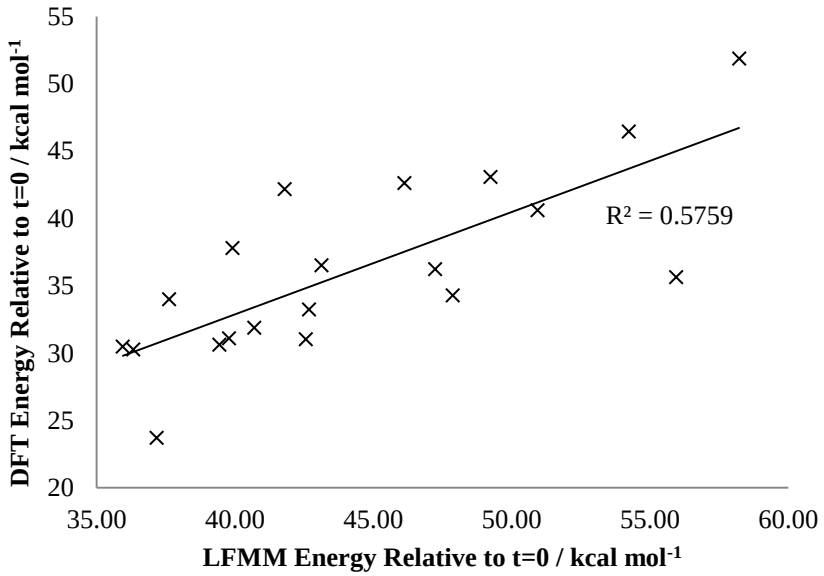

Figure 5.5; A plot of DFT energies (relative to the energy at t=0) and the LFMM energy (relative to the energy at t=0) at the same geometry as obtained from the last 10ps of the high spin LFMD run at 360K.

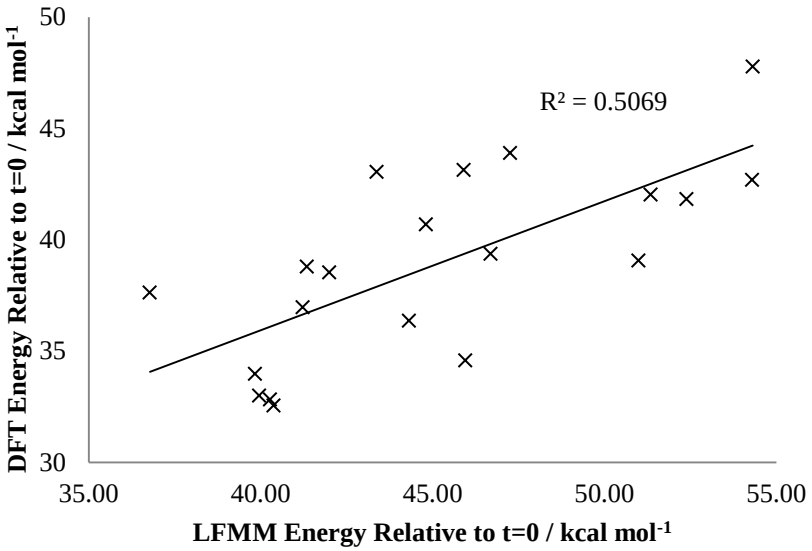

Figure 5.6; A plot of DFT energies (relative to the energy at t=0) and the LFMM energy (relative to the energy at t=0) at the same geometry as obtained from the last 10ps of the low spin LFMD run at 360K.

This force field was trained to spin state splittings of complexes in local minima at 0 K. A more accurate representation of LFMD's ability would therefore be in its ability to track changes in ΔE_{HL} as a function of temperature, Table 5.6. This was achieved by taking the difference in the average energy of the low and high spin states over the last 10 ps of the LFMD run, Table 5.4. LFMD predicts spin crossover within the region of 220-360 K as the sign of ΔE_{HL} changes from positive to negative indicating a HS ground state. DFT (SPE on LFMD structures) on the other hand destabilises the low spin state but does not favour the HS state. Experimentally $T_{1/2}$ = 335 K.[17-19] This simple DFT methodology does not reproduce experiment. It is possible that the geometrical changes during MD are even further away from the DFT PE surface. As such the DFT energies become increasingly unreliable. LFMD being tuned to the local minima thus gets the average behaviour as a function of temperature correct while DFT (using LFMM structures) gets it wrong. The test would be to perform DFT MD but this is outside the scope of this work.

Table 5.4; Spin state splittings for DETTOL averaged over the last 10 ps of a 200 ps run.

	ΔE_{HL} / kcal mol^{-1}		Error in ΔE_{HL}
T / K	LFMD	DFT	/ kcal mol^{-1}
360	-0.36	0.21	-0.57
220	1.76	2.13	-0.37

The construction of a mixed amine/imine force field for Fe(II)

Introduction

To date LFMM force fields for SCO applications have centred on a single ligand type i.e. iron(II) amines. However, the majority of iron(II) spin crossover complexes include unsaturated nitrogen donors.[3] A force field capable of handling more than one ligand type is desirable.

Training Data

Firstly in order to generate a mixed amine imine database training data is required. Following the fact that OPBE has been shown here and by others to be reliable for iron nitrogen systems, OPBE will also be the functional of choice for this study.

A test complex, APEFEH (Figure 5.7), was used to assess basis set effects on our chosen systems. As can be seen in Table 5.5 the geometry of the complex is almost entirely basis set independent with differences of < 0.01 Å in the average of all iron-nitrogen bond lengths. The energetic effects are much starker with the SVP basis set predicting a ΔE_{HL} of 3.05 kcal mol^{-1} whilst TZVP predicts a greater splitting of 7.05 kcal mol^{-1}. The larger TZVP basis set (the RI approximation was utilised and so the def2-TZVP basis set was also needed) is the basis set of choice for the remainder of this study.

Table 5.5: The effect of basis set on the geometry of the low and high spin states of APEFEH with the distances given in Å. The RI approximation was utilised and so the corresponding auxiliary basis sets were also used (def2-SVP/J and def2-TZVP/J as appropriate).

	Low Spin			High Spin		
AVG	def2-SVP	def2-TZVP	Diff	def2-SVP	def2-TZVP	Diff
Fe - N(pyr)	1.938	1.945	-0.007	2.210	2.204	0.006
N(pyr) - C	1.364	1.359	0.004	1.351	1.347	0.004
C - C	1.496	1.493	0.003	1.507	1.504	0.002
C - N	1.468	1.473	-0.005	1.460	1.465	-0.005
Fe - N	2.011	2.010	0.001	2.244	2.236	0.009

Table 5.6: The spin state splitting, ΔE_{HL}, of the training complexes. Note that the calculations on MELLOF07, QOQHEK and WIGPOR were carried out by Professor Robert J. Deeth.

Refcode	ΔE_{HL} / kcal mol^{-1}
APAFEH02[146]	7.1
APAFEM02[147]	5.2
CEYRAA[148]	5.7
FIWGIB[149]	-9.4
KEZPEK[150]	6.1
MELLOF07[151]	4.2
QOQHEK[152]	7.3
WIGPOR[153]	6.1

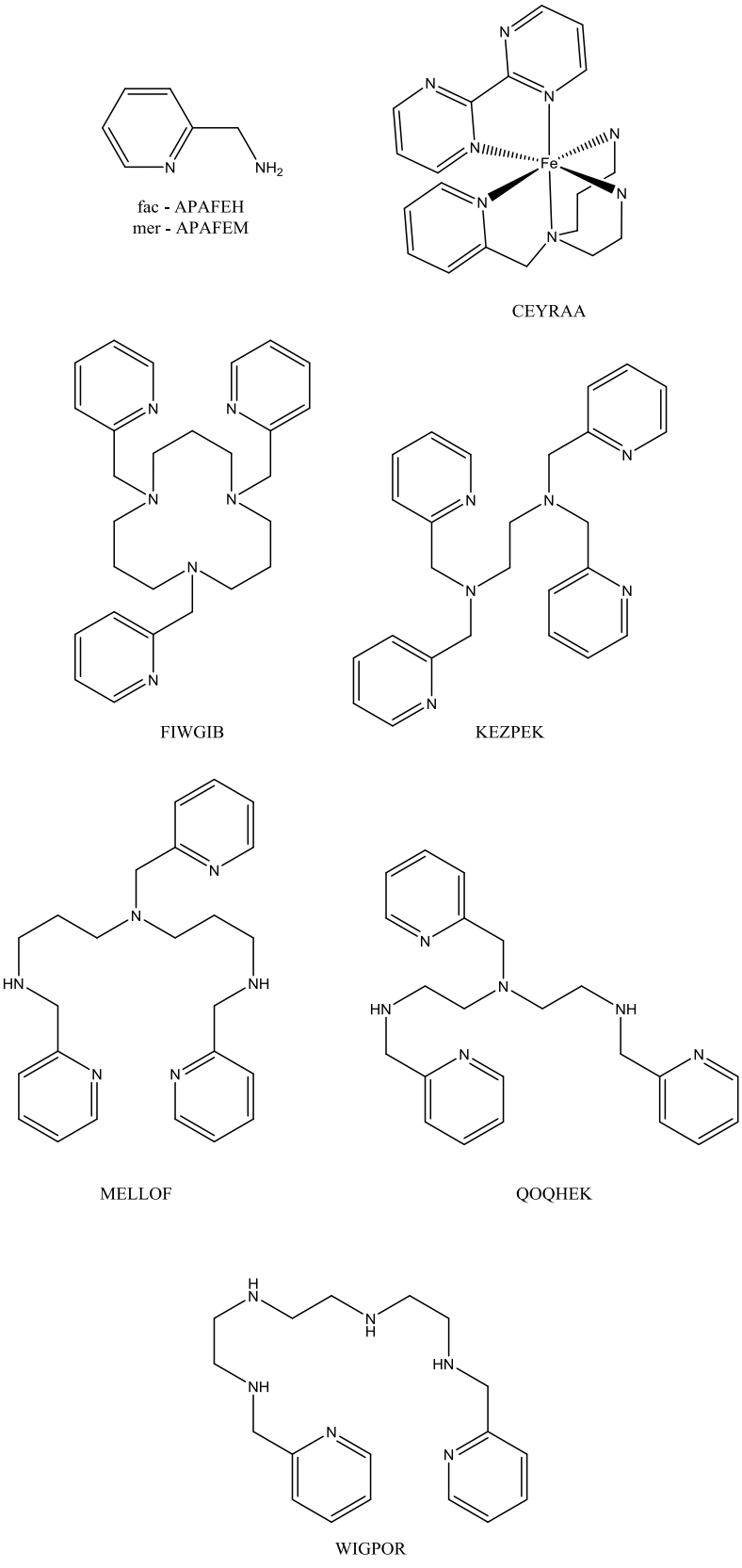

Figure 5.7; The eight pyridine/amine ligands used to form octahedral iron(II) complexes.

The database described in Figure 5.7 and Table 5.6 contains ligands with amine and pyridine donor types, totalling 8 complexes. Initially the amine parameters kept fixed while

all the imine parameters were to be optimised. This assumes that force field terms are additive i.e. the existing amine parameters will be transferable to systems in which other ligand types are present. This mirrors the law of average environment in ligand field theory where ligand field parameters for mixed ligand systems are estimated from adding individual contributions from each ligand. Within fifty generations the parameter sets generated had converged to a single Pareto front, Figure 5.8. While the errors associated with this front are approaching reasonable values (for SCO purposes we deem errors of less than 2 kcal mol^{-1} and 0.06 Å to be sufficient) they are not acceptable.

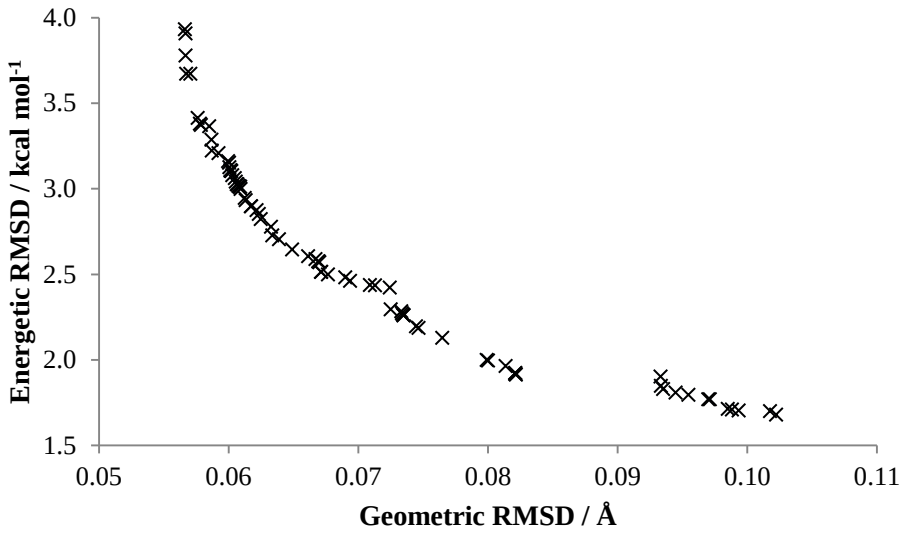

Figure 5.8; A plot of the final Pareto front of a fifty generation parameter optimisation run. The amine parameters were kept fixed while pyridine parameters varied.

To test whether the law of average environments would apply for the LFMM parameters some of the amine parameters were also optimised. Given that mixed ligand force fields generate accurate structures, as demonstrated for copper(II) systems[102] we focus on the transferability of energies for SCO complexes. Since the spin state energetics are directly related to the spin pairing term we decided to only include the pairing energy in the

optimisation. If the law of average environment applies then we would expect the amine spin pairing parameters not to change.

Restarting the optimisation process results in the Pareto front shown in Figure 5.19. While this front is superior to that from the fixed amine example, the spin pairing parameters have changed significantly indicating the law of average environments does not apply.

The performance of the new parameters is also not as accurate as required. This may be related to CEYRAA which is the only complex that contains pyrimidine ligands. Removing this complex and resuming the optimisation process for two 50 generation runs leads to the Pareto front shown in Figure 5.9. Strong energetic accuracy can only be achieved if structural accuracy is sacrificed. Viable force fields can be obtained which show balance in the two objectives, for instance Set 21 (an energetic error of 2.0 kcal mol^{-1} and a structural error of 0.062 Å) and 34 (an energetic error of 1.4 kcal mol^{-1} and a structural error of 0.071 Å) tables 5.7 and 5.8 respectively. These sets were tested (Tables 5.9 and 5.10) and parameter Set 21 is chosen for its balanced treatment of both objectives. If structural accuracy is the only goal – perhaps the generated structures are to be used as starting points for DFT – Set 15 from the preceding run (Table 5.11) displays a geometric RMSD of only 0.05 Å.

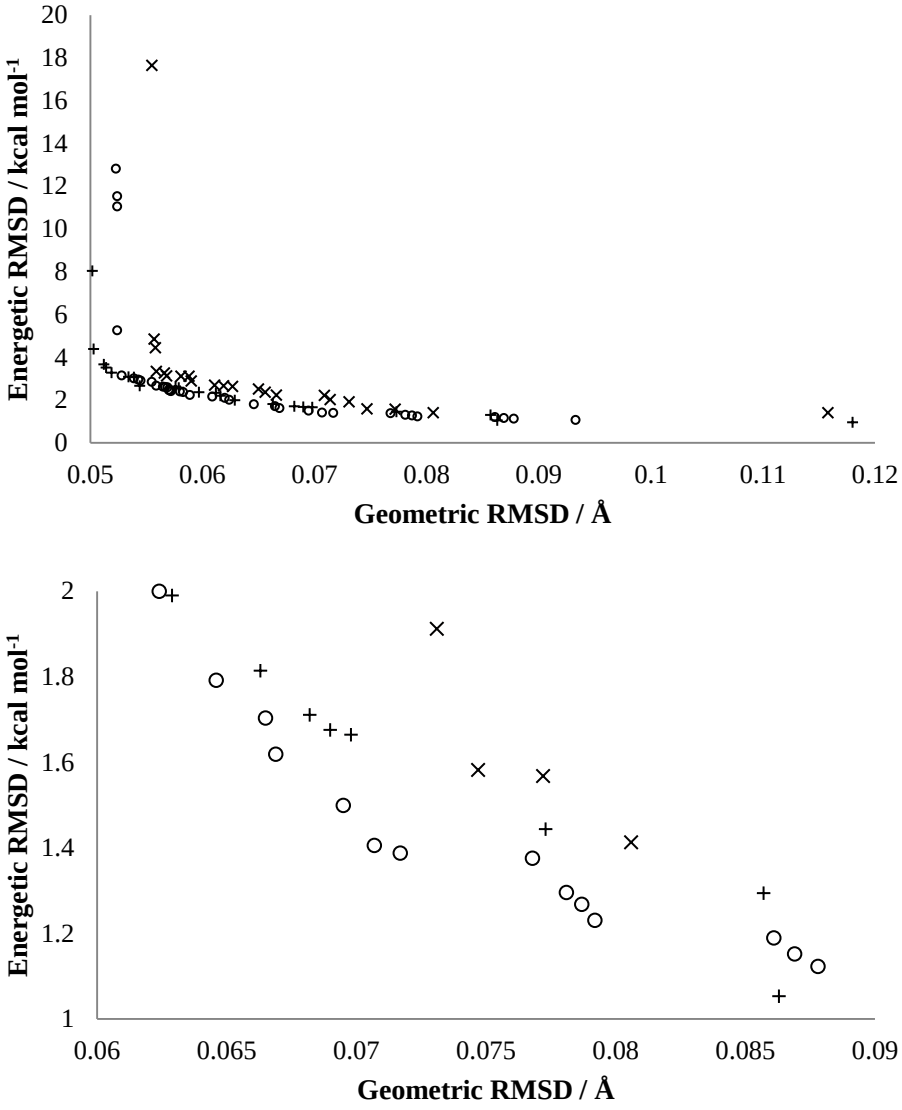

Figure 5.9: Two plots displaying Pareto Front 1 of the 50th Generation of three parameter optimisation runs in which the amine electron pairing parameter was allowed to vary. The first plot is across all values of the penalty functions while the second is across the region of interest. The first optimises pyridine parameters taking the amine parameters as a starting point (X), the second uses the same starting point excluding CEYRAA (+) and the third takes a parameter set from the second run and further optimises it (○).

Table 5.7; Parameter set 21 from the second optimisation run without CEYRAA.

Parameter		Units	N	NPYD
Morse	r_0	Å	2.17	2.06
	D	kcal mol^{-1}	54.9	54.9
	α		1.13	1.54
Ligand-Ligand Repulsion	A_{LL}	kcal mol^{-1} $Å^6$	3,950	4400
AOM	e_σ (a_6)	cm^{-1} $Å^6$	416,000	547,000
	$e_{\pi y}$ (a_6)	cm^{-1} $Å^6$	-	130,000
	e_{ds} (a_6)	cm^{-1} $Å^6$	148,000	149,000
Spin pairing	a_0	kcal mol^{-1}	13.5	14.9
	a_4	kcal mol^{-1} $Å^4$	-61.4	-38.6

Table 5.8; Parameter set 34 from the second optimisation run without CEYRAA.

Parameter		Units	N	NPYD
Morse	r_0	Å	2.17	2.06
	D	kcal mol^{-1}	54.9	54.9
	α		1.13	1.47
Ligand-Ligand Repulsion	A_{LL}	kcal mol^{-1} $Å^6$	3,900	4,200
AOM	e_σ (a_6)	cm^{-1} $Å^6$	416,000	546,000
	$e_{\pi y}$ (a_6)	cm^{-1} $Å^6$	-	227,000
	e_{ds} (a_6)	cm^{-1} $Å^6$	148,000	149,000
Spin pairing	a_0	kcal mol^{-1}	12.6	12.9
	a_4	kcal mol^{-1} $Å^4$	-62.0	-46.6

Table 5.9; The performance of parameter set 21 (2.00 kcal mol^{-1} energetic RMSD and 0.0624 Å structural RMSD) of Run 2 without CEYRAA in the training set.

Name	Spin State	ΔE_{HL} / kcal mol^{-1}		RMSD / Å	
		DFT	LFMM	M-L	Heavy Atom
APAFEH02	LS	0.0	0.0	0.04	0.09
	HS	7.1	10.6	0.04	0.05
APAFEM02	LS	0.0	0.0	0.03	0.15
	HS	5.2	7.0	0.07	0.15
FIWGIB	LS	0.0	0.0	0.08	0.14
	HS	-9.4	-12.7	0.03	0.15
KEZPEK	LS	0.0	0.0	0.07	0.16
	HS	6.1	5.9	0.02	0.31
MELLOF07	LS	0.0	0.0	0.05	0.12
	HS	4.2	4.0	0.05	0.11
QOQHEK	LS	0.0	0.0	0.07	0.09
	HS	7.3	7.0	0.05	0.10
WIGPOR	LS	0.0	0.0	0.03	0.05
	HS	6.1	4.9	0.03	0.04

Table 5.10; The performance of parameter set 34 (1.41 kcal mol^{-1} energetic RMSD and 0.0707 Å structural RMSD) of Run 2 without CEYRAA in the training set.

Name	Spin State	ΔE_{HL} / kcal mol^{-1}		RMSD / Å	
		DFT	LFMM	M-L	Heavy Atom
APAFEH02	LS	0.0	0.0	0.06	0.09
	HS	7.1	10.2	0.04	0.05
APAFEM02	LS	0.0	0.0	0.05	0.15
	HS	5.2	5.4	0.07	0.16
FIWGIB	LS	0.0	0.0	0.10	0.14
	HS	-9.4	-10.9	0.04	0.17
KEZPEK	LS	0.0	0.0	0.09	0.16
	HS	6.1	5.6	0.04	0.31
MELLOF07	LS	0.0	0.0	0.07	0.13
	HS	4.2	4.4	0.05	0.11
QOQHEK	LS	0.0	0.0	0.09	0.10
	HS	7.3	7.0	0.05	0.11
WIGPOR	LS	0.0	0.0	0.05	0.05
	HS	6.1	4.9	0.03	0.04

Table 5.11; Parameter set 15 from the first optimisation run without CEYRAA. This set is recommended for those interested only in geometric accuracy.

Parameter		Units	N	NPYD
Morse	r_0	Å	2.17	2.10
	D	kcal mol^{-1}	54.9	54.9
	α		1.13	1.43
Ligand-Ligand Repulsion	A_{LL}	kcal mol^{-1} $Å^6$	3,950	3,080
AOM	e_σ (a_6)	cm^{-1} $Å^6$	416,000	532,000
	$e_{\pi\gamma}$ (a_6)	cm^{-1} $Å^6$	-	51,700
	e_{ds} (a_6)	cm^{-1} $Å^6$	148,000	133,000
Spin pairing	a_0	kcal mol^{-1}	16.2	17.7
	a_4	kcal mol^{-1} $Å^4$	-44.3	-70.5

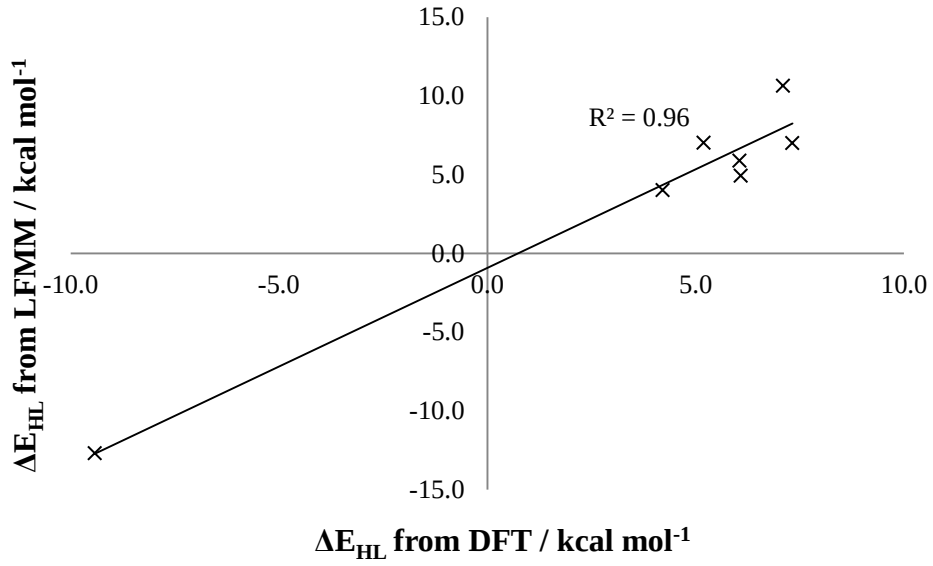

Figure 5.10; A plot of LFMM derived spin state splittings against DFT for parameter set 21.

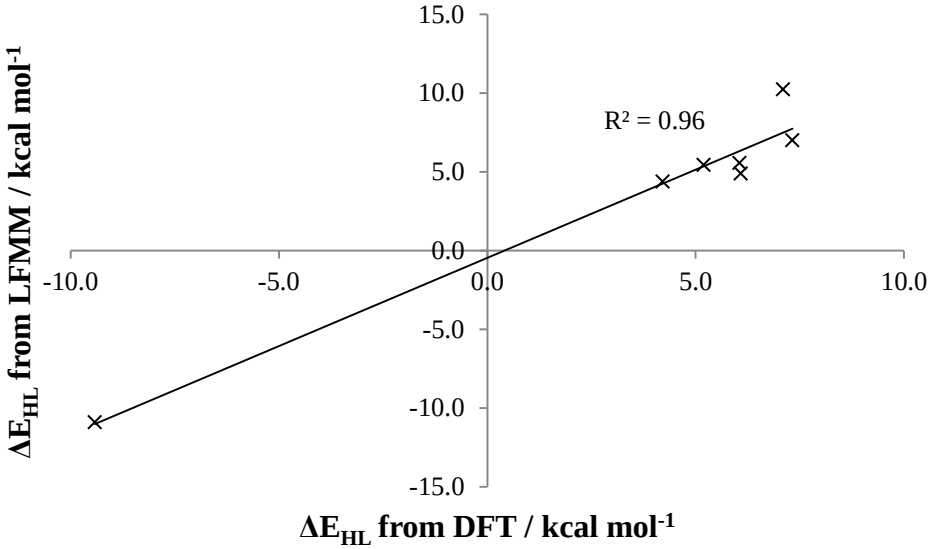

Figure 5.11; A plot of LFMM derived spin state splittings against DFT for parameter set 34.

The relatively poor performance of the parameter optimisation which included CEYRAA was puzzling because the MMFF94 force field assigns the same parameter type to a pyrimidine donor as to a pyridine donor. Hence we did not anticipate any problems. However, the pK_a for pyrimidine is substantially lower than that for pyridine, and while previous studies have satisfactorily used a single set of parameters for ligands with

different pK_as, e.g. primary, secondary and tertiary amines, the difference between pyrimidine and pyridine may imply a significant enough change in metal-ligand bond strength to warrant independent LFMM parameters for the former.

It is also clear from the parameter sets given and a comparison of the Pareto fronts that the law of average environments does not hold true for mixed amine imine systems. Parameter Set 21 for the mixed ligand systems gives a 10.6 kcal mol^{-1} energetic RMSD for the amine training set in Figure 5.1. The behaviour for a small set of pyridine only complexes (Table 5.12) gave a smaller but still significant energetic RMSD of 5 kcal mol^{-1} and a geometric RMSD of 0.09 Å. These results suggest that the law of average environments does not apply especially for spin state energetics. This seems to correlate with the fact that the way the spin pairing energy is handled in LFMM is qualitatively different to the other ligand field contributions. To date the spin pairing energy was treated as being more or less constant across different metal complexes and spin states. This assumption may be invalid and in the future we should explore allowing the spin pairing term to be more strongly geometry and or spin state dependant.

Table 5.12; The four complexes used as a test of the transferability of the mixed force field. Optimised in ORCA with OPBE COSMO(water) RI def2-TZVP def2-TZVP/J

Name	ΔE_{HL} / kcal mol^{-1}
$[Fe(pyr)_6]^{2+}$	-17.09
$[Fe(bipy)_3]^{2+}$	15.84
fac-$[Fe(6\text{-Methyl-2,2'-bipyridine})_3]^{2+}$	1.26
mer-$[Fe(6\text{-Methyl-2,2'-bipyridine})_3]^{2+}$	5.43

In addition the mixed ligand parameter set requires further training data, as discussed in Chapter 6, where it is shown how gaps in the SCO are populated. This should result in an improved force field which is more diverse in its applications.

The use of Hammett sigma values in LFMM

The DFT study in Chapter 4 shows clearly that SCO can be influenced by substituents attached to aromatic rings. It is intriguing to consider how such substituent effects could possibly be incorporated in an LFMM treatment. Hammett's work in assigning values to these effects could prove useful as a means of quantifying variations in spin state energetics.[154] This hypothesis was tested for a series of para substituents on all six of the pyridine rings of iron(II) tris(2,2'-bipyridine).

The DFT data was obtained using a strategy previously shown to work. The structures were optimised using the BP86 functional[70,126] and def2-SVP basis set[127] with the COSMO solvation model[123,155,156] for water within the ORCA DFT package.[129] The RI approximation was used to increase speed and so an auxiliary basis set def2-SVP/J was required. The single point energy calculations were obtained using the OPBE functional,[68,69,74,75] the TZP basis set and COSMO solvation model[157] (water) within ADF 2012.01.[120] The results of these calculations are shown in Table 5.13 and Figure 5.12.

Table 5.13; The spin-state splittings of iron(II) tris(2,2'-bipyridine) substituted on all six para positions.

	BP86 – def2-SVP	OPBE – TZP	
Substituent	ΔE_{HL} / kcal mol^{-1}	ΔE_{HL} / kcal mol^{-1}	Hammett σ value of a para substituent
Dimethylamino	27.15	9.94	-0.83
Amine	25.88	7.96	-0.66
Methoxy	28.08	9.20	-0.27
Ethoxy	27.93	9.17	-0.25
Methyl	30.90	12.58	-0.17
None	31.49	13.13	0.00
Fluoro	28.27	9.32	0.062
Chloro	29.67	10.77	0.227
Bromo	29.94	11.11	0.232
Iodo	30.46	11.63	0.276
Cyano	31.86	12.88	0.66
Nitro	31.73	13.18	0.778

The assumption that DFT computed values of ΔE_{HL} would correlate with Hammett Sigma values does not hold quite as well for these bipyridine complexes as it did for the pytacn complexes (Chapter 4). Figure 5.12 shows the correlation of the relative DFT energetics and the value of the Hammett σ constants. The R^2 for BP86 is substantially higher at 0.68 than for OPBE at 0.48, an interesting result given that OPBE has previously been shown to be reliable for iron(II) amine SCO complexes, as well as the fact that a larger basis set was utilised in the OPBE energetic calculations. However, both R^2 values are somewhat less than obtained for pytacn.

Each pyridine ring has an ortho substituent (the other half of bipyridine) which is also changing. This was not an issue with the pytacn systems[2] studied in Chapter 4. Figure 5.12, also appears to indicate that the unsubstituted and the para substituted methyl system are anomalous. Interestingly H and CH_3 are only inductive while the other substituents are capable of both inductive and mesomeric effects. It is possible that while H and CH_3 could affect metal ligand σ bonding they have little effect on metal ligand π bonding while the other substituents could affect both bonding modes. Removing H and CH_3 from the plot shown in Figure 5.12 substantially improves the R^2 value to 0.91 and 0.74 for BP86 and OPBE respectively. However, given that there are only two inductive substituents perhaps there is insufficient data to draw meaningful conclusions from this.

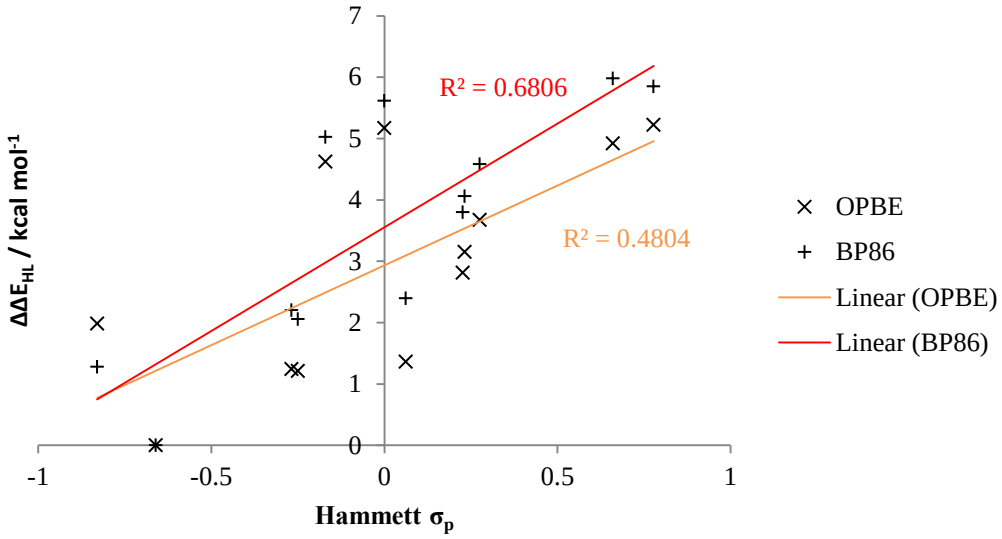

Figure 5.12 – A plot of the OPBE and BP86 spin-state splittings relative to the value for the para-amine species as a function of Hammett sigma values.

Improving the Handley force field

While the parameter set in Table 5.1 is among the best achievable with the training data given, the work of Handley and Deeth is based upon only a limited training set. Two ways of improving upon this proof of concept work are growth of the training set to include more varied N-Fe-N bond angles and Fe-N bond lengths as well as the inclusion of partial charges.

The introduction of charges is vital for solid state applications which are a long term group goal. Mulliken partial charges[158] were chosen, despite their simplistic origins, as this inclusion remains more a proof of concept than a rigorous charge scheme. The calculated Mulliken charges for the four complexes in the Handley and Deeth paper as well as the corresponding free ligands are given in Table 5.14. It is clear that the charges on the iron centre vary significantly between +1.35 and +1.99 dependant on choice of ligand and spin state of the metal centre.

Table 5.14; The calculated Mulliken charges for the four crystallographically characterised complexes in the original Handley and Deeth paper. The coordinated charges are obtained from SPE calculations (OPBE, TZP) on previously optimised structures (BP86, RI approximation, Def2-SVP, Def2-SVP/J auxiliary basis set and COSMO epsilon 80 refractive index 1.33 (water 80.4 and 1.33 respectively)). The uncoordinated charges were calculated solvent free based on single point calculations (OPBE, TZP) on the free ligands based on their LS derived structures.

	Atom	Uncoordinated	HS State	Change in Charge on Coordination	LS State	Change in Charge on Coordination
DETTOL	Fe	2.00	1.57	-0.43	1.82	-0.18
	avg N	-0.25	-0.45	-0.20	-0.42	-0.22
PURYIK	Fe	2.00	1.45	-0.55	1.50	-0.50
	avg N	-0.18	-0.32	-0.14	-0.25	-0.10
PAZXAP	Fe	2.00	1.35	-0.65	1.38	-0.62
	avg N	-0.17	-0.40	-0.24	-0.35	-0.12
Fe399	Fe	2.00	1.57	-0.43	1.99	-0.01
	avg N	-0.20	-0.47	-0.27	-0.44	-0.17

This range of Mulliken charges displayed by the metal show that any model chosen to represent them would be an inherent approximation to the "true" charges. A bond charge increment (bond charge increments are the MMFF94 method of including charges through polarising a bond, reducing the charge on one end and increasing it by the same amount on the other)[98] was chosen to include "Mulliken" charges in a simple manner. This is the first time that charges have been included in an LFMM iron(II) amine force field and so even a simple implementation is progress. Bond charge increments were derived from the iron charges in Table 5.14 in which the average iron charge is +1.58 and so implying an iron-

nitrogen bond charge increment of 0.07 and so the appropriate line in the Merck derived LFMM force field was modified. Figure 5.23 illustrates its effect on atomic charges.

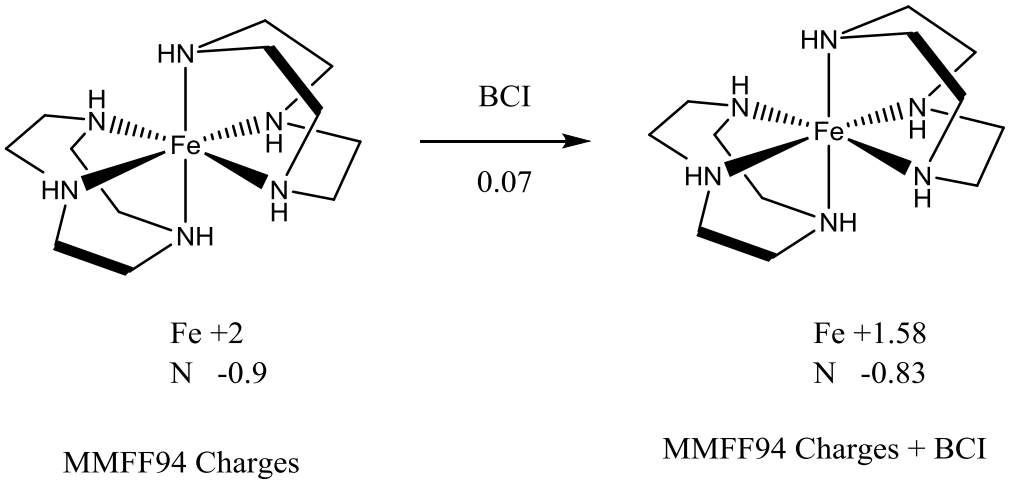

Figure 5.23; The effect of the use of bond charge increments on MMFF94 charges.

This was then subjected to PROTEUS fitting. The parameter file determined as an alternative to the Handley-Deeth parameter set was chosen as a starting point. This leads to the initial introduction of large errors energetic RMSD of 15,836 kcal mol^{-1} and a structural error of 0.39 Å. This rapidly decreases to errors of (for instance) 13 kcal mol^{-1} and 0.1 Å in the initial population. After two 50 generation optimisation runs, the Pareto fronts have converged to a single front. This was taken as a sign that PROTEUS had found the best parameter sets possible within the bounds (and bit string length) specified. However, the energetic error was still too large at over 8 kcal mol^{-1}, Figure 5.24.

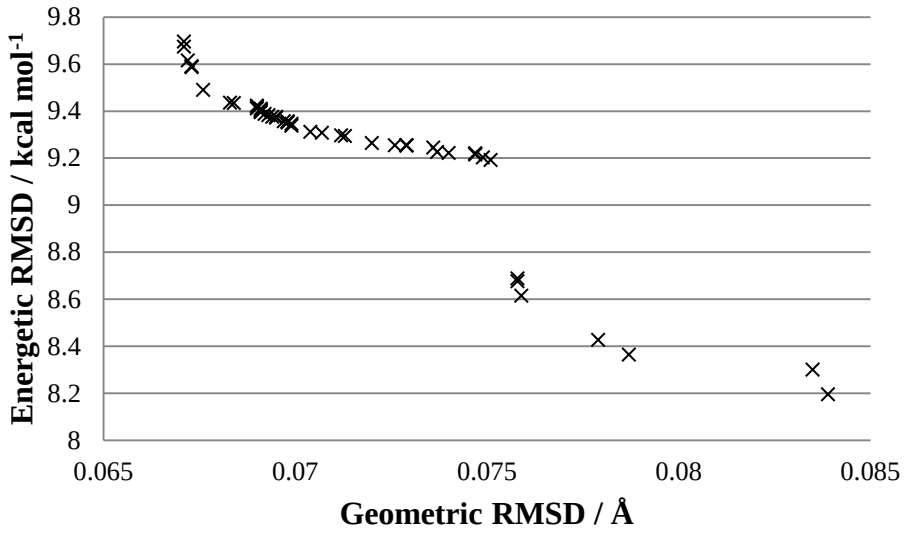

Figure 5.24; A plot of energetic RMSD against geometric RMSD for Pareto front 1 of the 50th generation of the second parameter optimisation of a charged iron(II) amine force field.

An alternative charge scheme lies in Deeth's Proton Scaled Metal Ligand (PSML) charge scheme. This charge protonates the ligand at the site of coordination in order to determine the effect a positive charge has on the partial charges of the ligand by utilising the MMFF94 charge scheme which deals with protonated systems.[159] The charge on the proton is that which is donated to the metal for a given spread of partial charges across the ligand. The user determines the desired charge on the metal (from in this case natural atomic orbital analysis,[160,161] in which atomic orbitals are derived from "the one electron density matrix",[63] Table 5.15). The script determines the metal's proton equivalence and scales the ligand charges appropriately. This charge scheme is superior to the BCI model above in that it achieves the desired charge on the metal in an even manner and not simply depleting electron density from the nitrogen. Natural charges were chosen since relative to Mulliken charges they are more chemically "reasonable" as shown in a study on hexaqua complexes[162] in which the natural charge varied in a consistent fashion as a function of bond length.

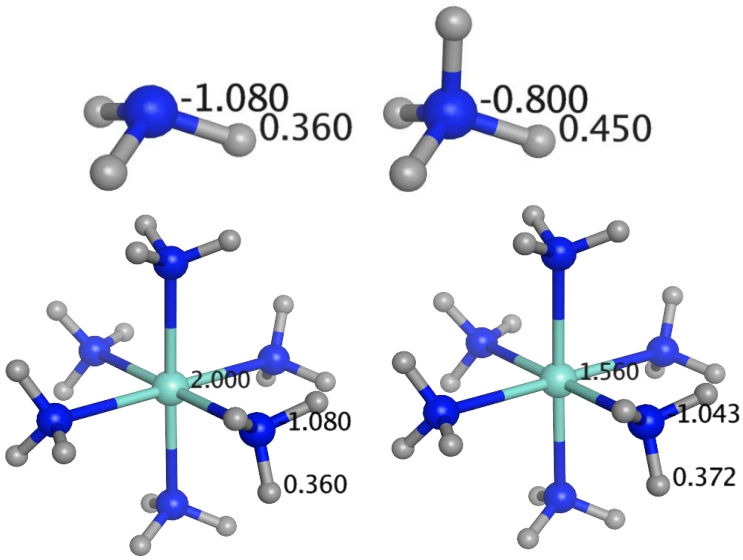

Figure 5.25; Top left are the charges on the nitrogen and hydrogens of ammonia and top right the charges of protonated ammonia, NH_4^+. Bottom left is the charges in the transition metal MMFF94 (without a Fe-N BCI) and right the charges under the PSML routine.

Table 5.15; The Natural Charges[160,161] on iron in a range of iron(II) amine complexes as obtained from Gaussian 03.[163]

	HS	LS
DETTOL	1.57	1.24
Fe399	1.57	1.25
PAZXAP	1.55	1.21
PURYIK	1.55	1.21
Average	1.56	1.23

This charge scheme also allows the user to more easily set spin state dependent charges on the metals. The charge was set to +1.56 in the HS state and +1.23 in the LS state with the ligands partial charges scaled appropriately. The force field was then refitted. The first optimisation run of 50 generations displayed promise and a parameter set from this run with an energetic RMSD of 1.1 kcal mol^{-1} and a geometric RMSD of 0.081 Å was chosen as a starting set for a 100 generation optimisation run. This second run resulted in the Pareto front given in Figure 5.26. Selecting a parameter set (Set 14) with similar geometric accuracy as the uncharged force field results in a 0.2 kcal mol^{-1} increase in the energetic

RMSD from 0.9 to 1.1 kcal mol^{-1}. This increase is deemed acceptable. However, upon further inspection this force field predicts the incorrect spin state for DETTOL. This parameter set predicts it to be HS by <0.1 kcal mol^{-1}. Sets **4** (energetic RMSD of the whole set 1.4 kcal mol^{-1}) and **10** (1.7 kcal mol^{-1}) likewise predict an incorrect high spin ground state for DETTOL by 0.6 and 0.1 kcal mol^{-1} respectively. Set **19** recovers the correct spin state for DETTOL predicting it to be LS by 0.7 kcal mol^{-1}. This parameter set has a geometric RMSD at 0.067 Å and an energetic RMSD of 0.7 kcal mol^{-1}. This geometric RMSD is slightly high. On closer inspection the highest M-L RMS is just 0.073 Å for the HS hexamine complex, Table 5.17. While the highest heavy atom RMSD is that for HS PURYIK, Table 5.17, at 0.18 Å. Superimposing the two complexes with the highest heavy atom RMSD (Figure 5.27) reveals that the structural deviations are acceptable given the high energetic accuracy (an RMSD of 0.7 kcal mol^{-1}) of the force field. Therefore, since the structural RMSD, considering iron-nitrogen and nitrogen-nitrogen distances is less than 0.07 and the structures of the two complexes with the largest heavy atom RMSDs are still qualitatively correct this force field (Parameter Set 19) is the one recommended for use.

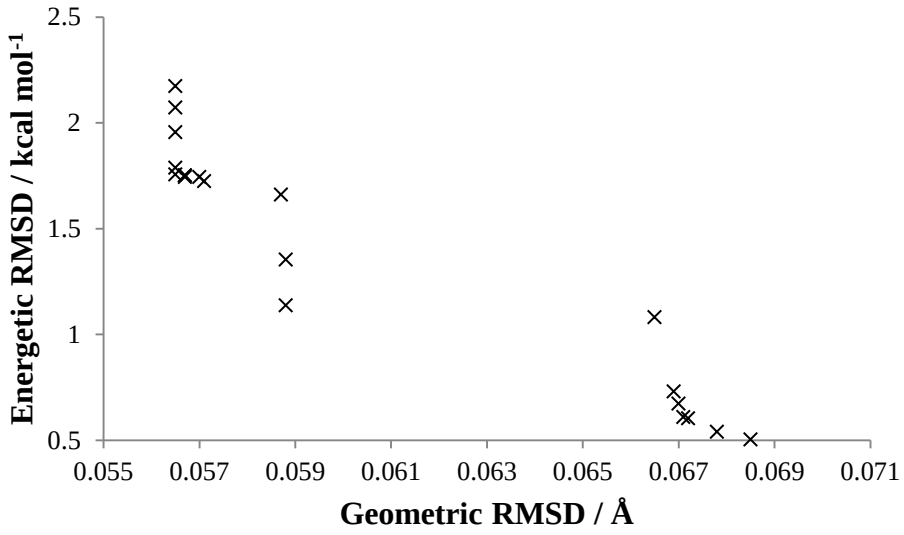

Figure 5.26; A plot of Pareto front 1 from the 100th generation of the second parameter optimisation run.

*Table 5.16; Parameter set **19** from Figure 5.26, with an energetic RMSD of 0.73 kcal mol^{-1} and a geometric RMSD of 0.067 Å.*

Parameter		Units	Value
Morse	r_0	Å	2.22
	D	kcal mol^{-1}	54.9
	α		1.26
Ligand-Ligand Repulsion	A_{LL}	kcal mol^{-1} Å^6	5,200
AOM	e_σ (a_6)	cm^{-1} Å^6	412,000
	e_{ds} (a_6)	cm^{-1} Å^6	118,000
Spin pairing	a_0	kcal mol^{-1}	14.8
	a_4	kcal mol^{-1} Å^4	-80.4

*Table 5.17; The metal-ligand and heavy atom RMSDs for the iron(II) amine training set when using parameter set **19**. Distances in Å.*

Identifier	Spin State	M-L	Heavy Atom
$[Fe(NH_3)_6]^{2+}$	HS	0.07	0.08
$[Fe(NH_3)_6]^{2+}$	LS	0.01	0.01
PURYIK	HS	0.06	0.18
PURYIK	LS	0.03	0.09
DETTOL	HS	0.03	0.07
DETTOL	LS	0.02	0.08
PAZXAP	HS	0.05	0.13
PAZXAP	LS	0.01	0.09
FE399	HS	0.01	0.13
FE399	LS	0.01	0.05

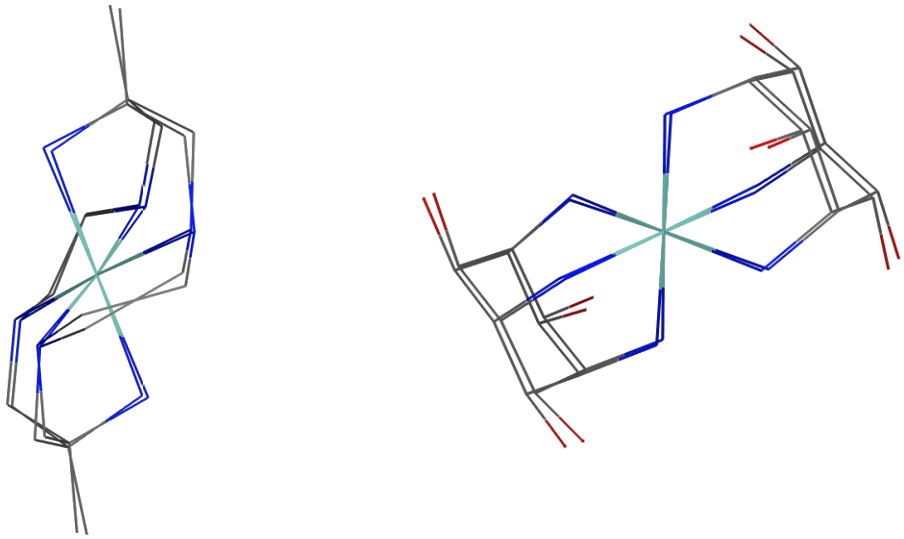

*Figure 5.27; A superposition of the two complexes with the highest heavy atom RMSD for Parameter Set **19**. HS PAZXAP is shown on the left with a heavy atom RMSD of 0.13 Å. Right is HS PURYIK with a heavy atom RMSD of 0.18 Å.*

Generating a charge scheme in MM is both critical and challenging.[164] Utilisation of the normal Coulombic expression to partial atomic charges as in Equation 5.1 introduces long range interactions which would otherwise be screened in real systems.

$$E = \frac{q_i q_i}{\varepsilon r} \qquad \textbf{Equation 5.1}$$

Various methods have been developed to reduce these long range interactions. The distance dependent dielectric, which is utilised here, is based upon a modification of Equation 5.1 to depend on the square of inter atomic distances. While there is no guarantee that partial atomic charges derived from DFT calculations are appropriate for molecular mechanics. It has been shown here that these charges can be included within a force field and the parameters optimised around it. This resulted in a parameter set with similar accuracy to the uncharged force field discussed at the start of the chapter. The use of

Deeth's Proton Scaled Metal Ligand charge scheme could prove invaluable for the inclusion of charges in to systems for which the spin state independent BCI scheme fails.

Addressing the stiff iron-nitrogen-carbon angle term

Within the Handley-Deeth force field the iron(II)-nitrogen-carbon bond angle has a force constant of 200 kcal mol^{-1} deg^{-2} (and a reference angle of 115°) compared to the generic M^{+2}-N-C angle having a force constant of just 30 kcal mol^{-1} deg^{-2}. No reports were made in previous publications as to the reason for this. Using a parameter set (Table 5.18) which reported an energetic RMSD of 0.24 kcal mol^{-1} and a geometric RMSD of 0.065 Å (force constant of 200 kcal mol^{-1} deg^{-2}) as a starting point the force constant was reduced to 30 kcal mol^{-1} deg^{-2}. This reduction in force constant resulted in an energetic RMSD 2.75 kcal mol^{-1} and a geometric RMSD of 0.060 Å. While this adjustment slightly improves upon the geometric term, it is well within the range of those generated in preceding optimisation runs and is not proportionate to the > 2.5 kcal mol^{-1} reduction in the energetic term.

Table 5.18; The parameter set for which an energetic RMSD of 0.24 kcal mol^{-1} and a geometric RMSD of 0.065 Å is obtained using the Fe^{+2}-N-C force constant of 200 kcal mol^{-1} deg^{-2}.

Parameter		Units	Value
Morse	r_0	Å	2.18
	D	kcal mol^{-1}	49.5
	α		1.13
Ligand-Ligand Repulsion	A_{LL}	kcal mol^{-1} Å^6	4,200
AOM	e_σ (a_6)	cm^{-1} Å^6	412,000
	e_{ds} (a_6)	cm^{-1} Å^6	143,000
Spin pairing	a_0	kcal mol^{-1}	14.1
	a_4	kcal mol^{-1} Å^4	-55.5

Table 5.19; The energetic and geometric data obtained after altering the iron(II)-N-C force constant from 200 to 30 kcal mol^{-1} deg^{-2}.

Refcode	Spin State	ΔE_{HL} / kcal mol^{-1}		M-L RMSD / Å	Heavy Atom RMSD / Å
		DFT	LFMM		
$[Fe(NH_3)_6]^{2+}$	HS	-6.7	-6.3	0.060	0.058
	LS			0.025	0.024
PURYIK	HS	-1.6	-1.2	0.029	0.080
	LS			0.038	0.065
DETTOL	HS	1.5	-3.3	0.036	0.092
	LS			0.034	0.050
PAZXAP	HS	14.4	11.0	0.020	0.078
	LS			0.022	0.061
FE399	HS	1.6	3.2	0.032	0.177
	LS			0.001	0.065

As can be seen in Table 5.19 the largest energetic errors correspond to DETTOL and PAZXAP. DETTOL is predicted to have a HS ground state using this parameter set and not the low spin state shown by experiment.

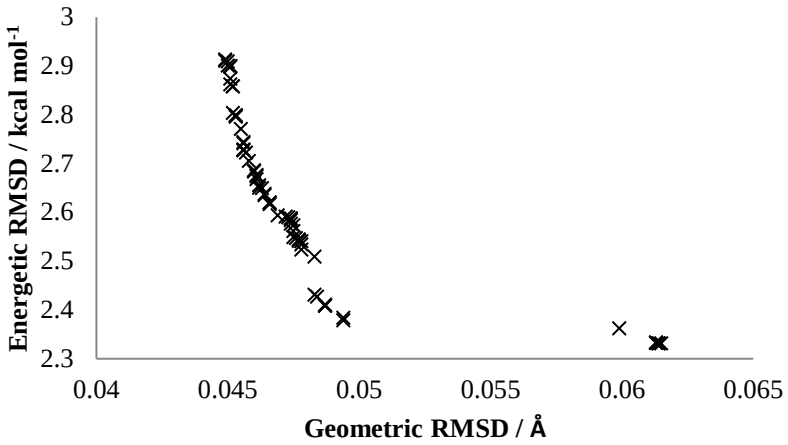

Figure 5.28; The final Pareto front of the fifty generation optimisation run with a reduced bond angle force constant.

After a fifty generation optimisation run the lowest energetic RMSD obtained was 2.33 kcal mol^{-1}, which is substantially larger than the 0.24 kcal mol^{-1} RMSD obtained with the stiffer force constant. In the light of this result it may be worthwhile reviewing previously developed force fields to see whether increasing the angle bend force constants at the donor atom would be beneficial.

Increasing the Transferability

Since the force field was not trained with aromatics in mind (despite their chemical interest) it was deemed prudent to test its transferability before it could be used. The simple tris(1,2-diaminobenzene) iron(II) complex, Figure 5.29, was chosen.[165] This complex displays bending of the benzene rings out of the plane of the Fe-N-C bond angle as shown in Figure 5.29 which shows the HS crystal structure ($\chi_M T_{300K}$ = 3.96 emu K mol^{-1}).[165]

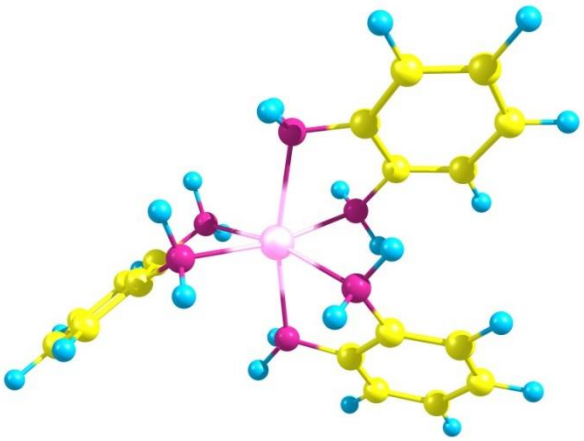

Figure 5.29; The HS crystal structure of tris(1,2-diaminobenzene) iron(II)[165]

DFT corroborates this distortion in the Fe-N-C angle which is more pronounced in the high spin than the low spin state due to the weaker bonds to the metal and reduced steric crowding.

An uncoordinated 1,2-diamino benzene molecule is a conjugated system in which the lone pairs on the nitrogen are involved in bonding with the ring. As a result the geometry at the uncoordinated nitrogen is not a trigonal pyramidal sp^3 hybrid but is instead a trigonal planar sp^2 hybrid with the unpaired electron lying perpendicular to the plane of the nitrogen, Figure 5.30.

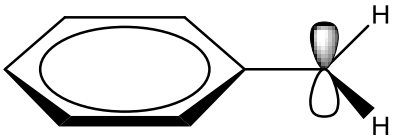

Figure 5.30; The direction of the nitrogen p-orbital containing the lone pair in uncoordinated amino benzene.

In contrast the standard MMFF94 N atom type presumes the nitrogen is tetrahedrally coordinated which means that the Fe-N-C plane and the H-N-H plane are orthogonal and the Fe lies in the plane of the ligand. The true coordination lies between these two extremes. Within MOE as in MMFF94[98] torsions are treated as a Fourier series. This series consists of five cosine functions (MMFF94 uses three terms) Equation 5.2 and through varying the V_n constants the profile of the torsional potential energy surface can be tuned.

$$E_{tors}(\omega) = \frac{1}{2}(V_1(1+\cos(\omega)) - V_2(1-\cos(2\omega)) + V_3(1+\cos(3\omega)) - (V_4(1-\cos(4\omega)) + V_5(1+\cos(5\omega))$$ **Equation 5.2**

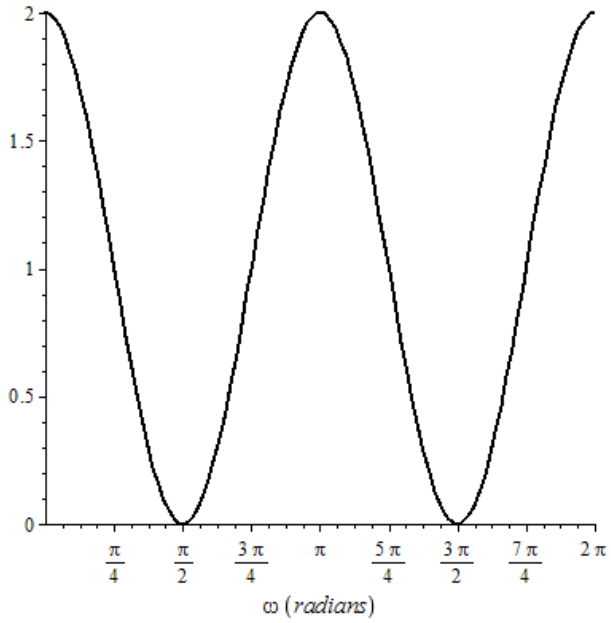

Figure 5.31; A plot of 1+cos(2x) to illustrate the second term scaled by V2/2.

Using a systematic approach the force constant was varied to reproduce the DFT generated structures. Values of the first three $V_n/2$ force constants were varied, Figure 5.32, and it was found that the lowest structural error (heavy atom RMSD) comes from setting V2/2 to 1.75. So this becomes the recommended value for use in LFMM calculations on amino benzenes. Figure 5.33 illustrates the overlap of the crystal[165] and high spin LFMM structures of $[Fe(1,2\text{-diaminobenzene})_3]^{2+}$. While the overlap is not total it is a noticeable improvement on the default value. Should 1,2-diaminobenzene complexes be of interest for SCO applications it is recommended that a force field refitting takes place to achieve the desired energetic accuracy for these systems.

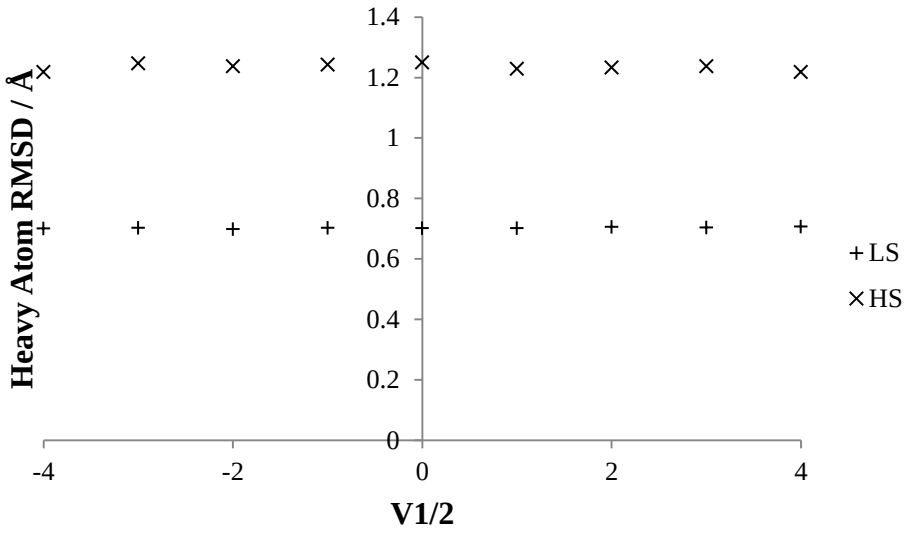

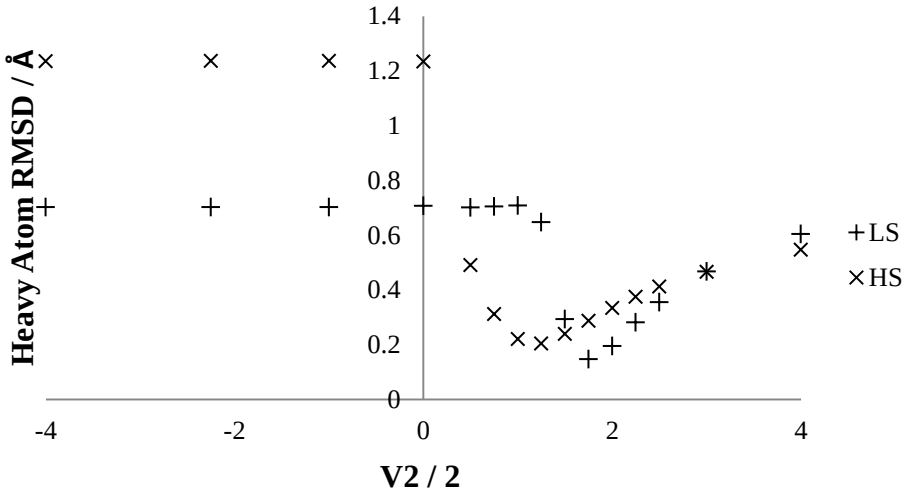

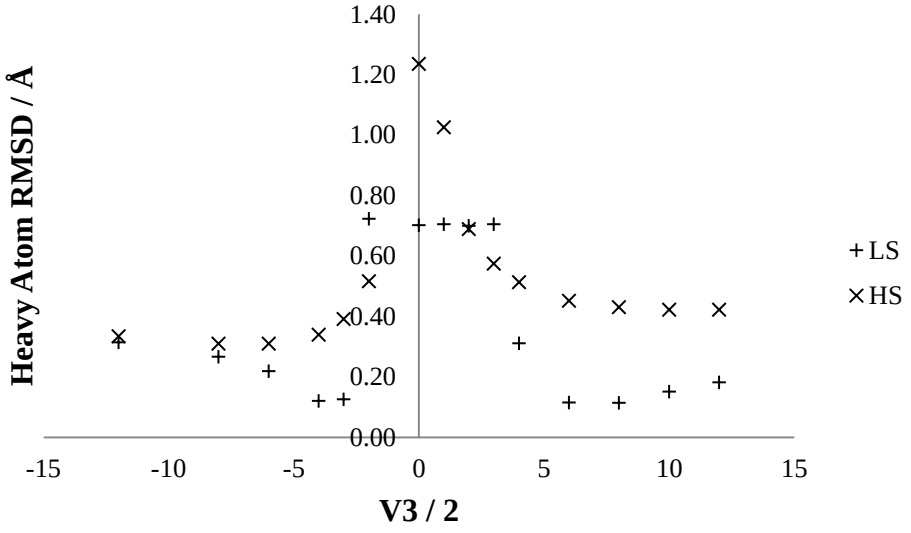

Figure 5.32; Plots of the effect of varying the torsional constants V1/2, V2/2 and V3/2 on the heavy atom RMSD of LFMM structures from the DFT reference structures.

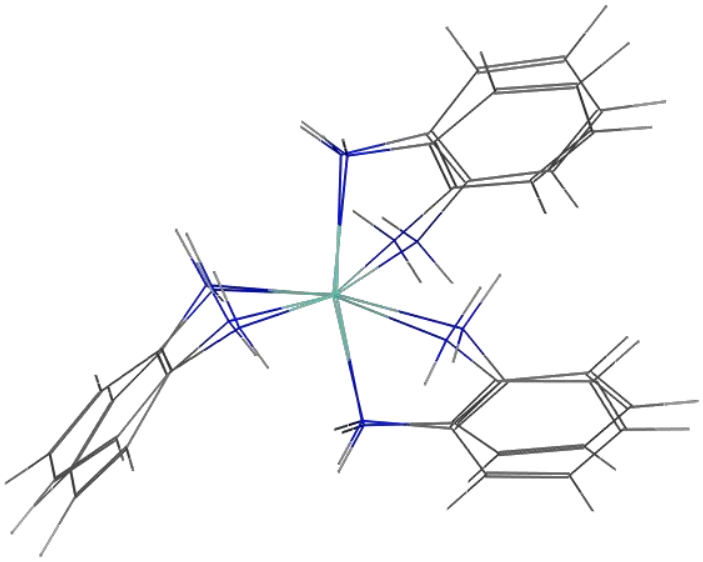

Figure 5.33; The overlap of the crystal structure[165] *and the high spin LFMM structure using the new Fe-N-Car-Car torsional force constant.*

Chapter 6 – The Design of Novel Transition Metal Complexes through Ligand Generation

Despite the volume of iron(II) SCO research published in recent years few groups have pursued the same goal for cobalt(II) systems. Cobalt(II) is d^7 and can therefore adopt either a low (^2E) or high ($^4T_1$) spin form, in octahedral symmetry, involving 1 or 3 unpaired electrons respectively. This is classically illustrated in the form of a Tanabe-Sugano diagram as in Figure 6.1. With studies and reviews in general (see Chapter 1) focussing on unsaturated ligands for six coordinate species[50] no LFMM studies have focussed on cobalt(II) systems either four or six coordinate.

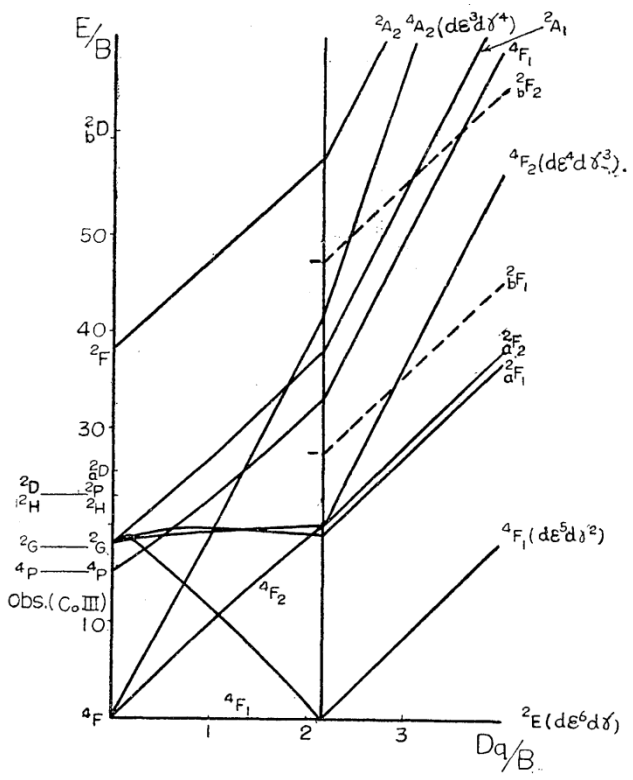

Figure 6.1; The d^7 Tanabe-Sugano diagram.[13] CoIII refers to Co^{2+} and F specifies triply orbitally degenerate octahedral terms. Reproduced with permission from the Physical Society of Japan.

A search of the Cambridge Structural Database reveals that four coordinate cobalt (II) amine complexes do indeed span the spin crossover divide. This is evidenced by the fact that both square planar (LS) and tetrahedral (HS) complexes are contained within the database. The d-orbital splittings for the LS and HS complexes are shown in Figure 6.2.

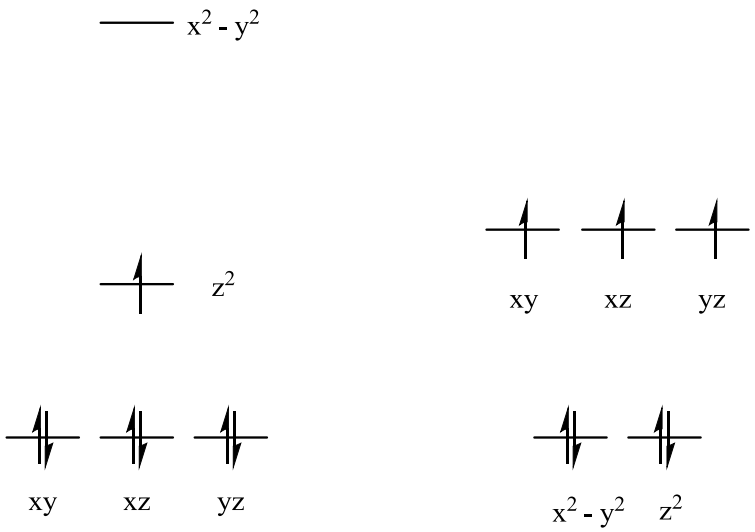

Figure 6.2; The d-orbital splittings of 4-coordinate cobalt(II) amine complexes. The low-spin square planar complex is depicted on the left and the high-spin tetrahedral complex is depicted on the right.

Somewhere between planar and tetrahedral geometries must lie the SCO region. To discover this region an automated procedure will be utilised. Using the drug discovery tools in MOE, ligands can be designed "from scratch". Users input a simple scaffold and from it a range of potential ligands are generated. From these ligands, candidates for SCO are determined and fine tuning of the SCO energy can be carried out. The user can select points of likely substitution and watch as the tools output candidates around the SCO divide (as well as many outside of it). These candidates are then verified by Kohn-Sham density functional theory.

The parameterisation of a robust cobalt(II) force field

The term robust, as used in the title, is of key importance. This force field needs to be capable of handling both the high- and low-spin states as well as tetrahedral and square planar geometries. The subtle balance between the two, which is achieved here, is something molecular mechanics had in the past struggled with; that is, before the inclusion of explicit ligand field effects.

Cobalt(II) amine force fields have long been a goal of our research group. However, the work that had been carried out on these systems by Summer and Masters students had only limited success. The work reported here represents the first utilisable cobalt(II) amine force field.

Computational Details

Structures were optimised using the BP86 functional,[70,126] the RI approximation, the def2-SVP basis set[127] and the COSMO solvation model (water) within the ORCA package. Initially Version 2.9.1 of the ORCA code was used followed by Version 3.0.1.[129] Since no difference is expected in the structures predicted by these implementations distinctions will not be made in the body of the text. Energetics were determined through single point calculations within ADF 2012.01[120] using the OPBE functional,[74,141] TZP basis set,[142] COSMO[123] (water, dielectric constant = 78.39, radius = 1.93 Å) and the SCF sub keys of mixing and level shifting were set to 0.1 and 0.3 respectively. This methodology does not include all of the corrections reported to "improve" calculations including dispersion, zero-point corrections, entropy and relativistic effects as these have been shown in Chapter 4 to reduce agreement with experiment in spite of their notional improved theoretical grounding. Ligand Field Molecular Mechanics calculations were carried using

DommiMOE[101] within Molecular Operating Environment 2010.10[144] and 2011.10.[145]

The PROTEUS automated parameterisation tool,[1] described in Chapters 3 and 5, was employed for all parameters apart from the angular overlap model (AOM) e parameters which were determined, and then fixed, using the following procedure.[1] The AOM parameters are derived by fitting the energies of the predominantly d molecular orbitals from DFT calculations. The DFT orbital populations are averaged to generate an approximate spherical potential to mimic ligand field theory.[166] (ADF single point calculations, OPBE, TZP with small cores and set occupancies of 1.4 in each d-orbital on cobalt(II) bis-ethylenediamine and cobalt(II) tetramine.)

In a square planar geometry, as adopted by LS four coordinate cobalt(II) species, the d-orbitals can be expressed in terms of e_σ and e_π as follows;

$$E(x^2-y^2) = 3e_\sigma$$

$$E(z^2) = e_\sigma - 4e_{ds}$$

$$E(xz, yz) = 2e_\pi$$

$$E(xy) = 4e_\pi$$

Since amines are not π-donors the *xz*, *yz* and xy orbitals are degenerate. Analysis of the d-orbital composition of the LS bis-ethylenediamine complex is given in Table 6.1. (Note that the axis alignment here has the x and y axes bisecting the N-Co-N angle, effectively interchanging the *xy* and x^2-y^2 orbitals). This leads to an e_σ of 9375 cm^{-1} and an e_{ds} of 2074 cm^{-1} for this LS complex.

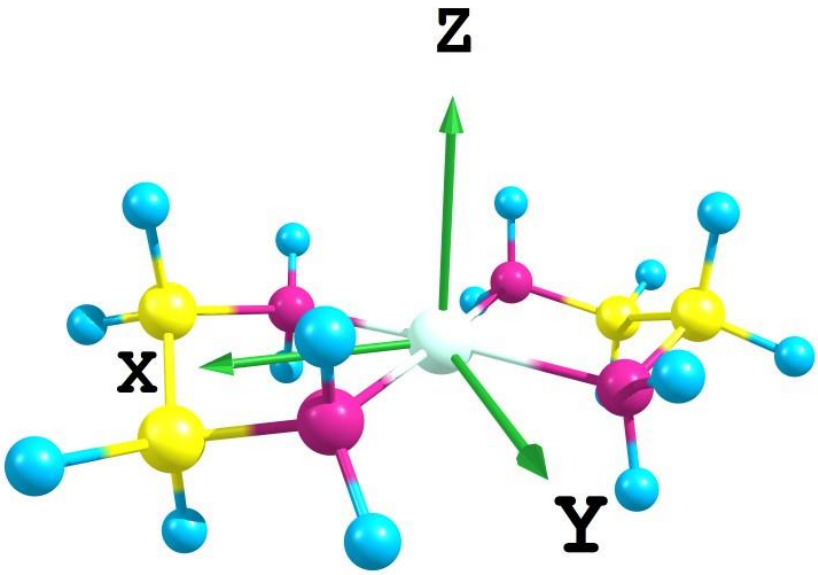

Figure 6.3; Axis frame definition for low spin cobalt(II) bis-ethylenediamine.

Table 6.1; The energies of the LS molecular orbitals of cobalt(II) bis-ethylenediamine and the contributions of the atomic d-orbitals

Orbital Energy /eV	d-orbitals and % contributions to the molecular orbitals		Total % d orbital contribution
-6.656	xz	96%	96%
-6.574	yz	96%	96%
-6.377	z^2 x^2-y^2	60% 27%	87%
-6.303	x^2-y^2 z^2	67% 22%	89%
-3.024	xy	57%	57%

Table 6.2; The energies of the HS molecular orbitals of cobalt(II) bis-ethylenediamine and the contributions of the atomic d-orbitals

Orbital Energy /eV	d-orbitals and % contributions to the molecular orbitals		Total % d orbital contribution
-6.500	x^2-y^2	77%	97%
	yz	10%	
	xy	6%	
	xz	3%	
-6.369	z^2	59%	93%
	xz	18%	
	yz	14%	
	xy	1%	
-5.913	xy	61%	75%
	xz	7%	
	x^2-y^2	5%	
	yz	2%	
-5.238	yz	46%	69%
	z^2	14%	
	xy	6%	
	x^2-y^2	3%	
-5.216	xz	47%	68%
	z^2	10%	
	x^2-y^2	6%	
	yz	3%	
	xy	3%	

The HS orbitals can be described in terms of e parameters as follows;

$$E(xz, yz, x^2 - y^2) = \left(\frac{4}{3}\right) e_\sigma + \left(\frac{8}{9}\right) e_\pi$$

$$E(z^2, xy) = \left(\frac{8}{3}\right) e_\pi$$

This results in an e_σ of 5921 cm^{-1} for the HS bis-ethylenediamine complex. A similar analysis was carried out on the analogous tetramine complex with the e_σ values reported in Table 6.3. The AOM parameters are implemented in DommiMOE as a function of metal

ligand bond length as described in Chapter 3. Assuming a sixth order dependence and reducing the sum of the percentage errors results in an a_6 term of 481,234. This will be rounded to 481,000 for implementation. An a_6 term was utilised as this results in a smaller error than an a_5 term with a mean absolute percentage error of 10 vs 12%. While use of several e_n parameters would allow an exact fit to DFT it will greatly increase the number of parameters and so a compromise was made. Similarly assuming a 6th order dependence of the d-s mixing term on the bond length results in an a_6 of 119,908 which was rounded to 120,000.

Table 6.3; Values of e_σ as derived from DFT calculations and the error through deriving them from an a_6 of 481,234 cm^{-1} Å^{-6}.

	Spin State	Average Co-N Bond Length / Å	DFT Derived e_σ / cm^{-1}	e_σ / cm^{-1} as derived from an a_6 of 481,234/ cm^{-1} Å^6	% Error
Cobalt(II) bis-ethylenediamine	**LS**	1.96	9375	8410	-10.3
	HS	2.05	5921	6505	9.9
Cobalt(II)tetramine	**LS**	1.96	9297	8455	-9.1
	HS	2.04	6045	6620	9.5
				Sum of % errors	0

This force field employs a simple charge model based on the change in Mulliken charges from DFT calculations on high and low spin calculations on the bis-ethylenediamine species to obtain an average iron(II)-N bond charge increment of 0.26 which was subsequently added to the force field file.

Table 6.4; The derivation of the bond charge increment for use in the LFMM force field.

Atom Type	MMFF_tm	Free Ligand	Charge on the HS species	Charge on the LS species	Average Change in Charge
Co	2.00		1.01	0.87	-1.06
N	-0.99	-0.37	-0.33	-0.29	0.06
HN	0.36	0.09	0.15	0.15	0.06
C	0.27	0.39	0.40	0.41	0.01
HC	0.00	-0.10	-0.06	-0.07	0.04

The ligand builder and attachment routines reported here form a novel route to spin-crossover complexes. It allows the user to input simple bidentate ligands, for instance ethylenediamine or propylenediamine, and replace part of the "scaffold" (carbon backbone in these cases) with entries in an R-group library. This is termed Scaffold Replacement within MOE. It is also possible to replace hydrogens on the ligand with entries in this library; this is known as R-group addition. These two strategies allow the generation of thousands of possible ligands. Combinatorial strategies do not claim to sample all ligands. Rather it is hoped instead that a diverse enough subset of all ligands will be sampled in order to assess the viability of a given coordination sphere to display SCO. Examples of the type of ligands generated will be shown in the coming sections.

All candidates were subjected to a rigorous routine of stochastic conformational searching. The stochastic conformational search routine implemented in DommiMOE is based on the work of Ferguson and Ramer.[167] The routine is based upon random perturbations in the ligands torsion angles within pre-set bounds. As a result, the unrestrained metal ligand bond lengths are allowed to vary greatly and therefore sampling is a direct product of torsional perturbations. One spin-state structure needs to be optimised first, the choice of which is arbitrary. This routine optimises the HS state first followed by the LS state as per Figure 6.4. To ensure that as few false negatives are removed as possible candidates with small negative values of ΔE_{HL} needed to pass through the initial cut-offs. This would allow candidates the opportunity to return to the SCO region in subsequent searches.

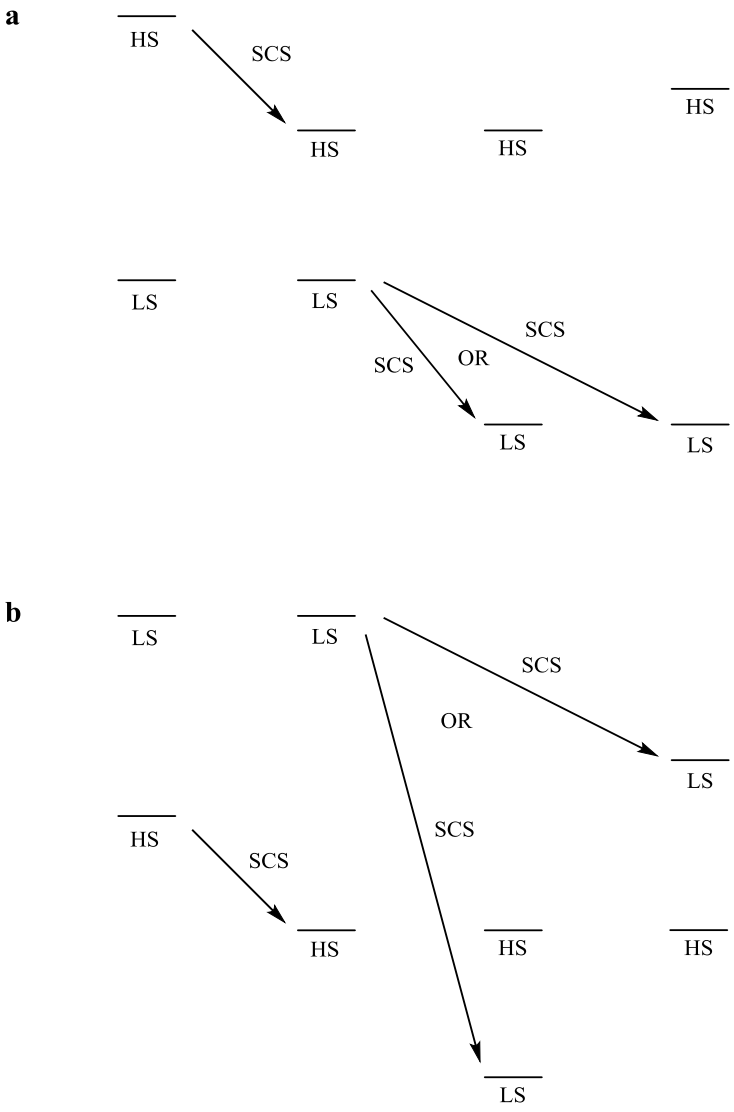

Figure 6.4; Illustrating the effect of the order in which the stochastic searching is carried out and its relationship with "predicted" spin state energetics.

All ligands proposed have been determined to be 100% synthesisable by MOEs internal retrosynthetic analysis tool which breaks down molecules in to their precursors and compares these to a database. If all of the precursors are contained in the database then the molecule is said to be synthesisable as described in the MOE documentation.

Results and Discussion

Five cobalt(II) complexes with tetradentate amine donors based on 14 and 16 membered rings have been synthesised and are reported in the literature. Three of these complexes, NENCEO,[168] RUJSEU[169] and QORPOC[170] (the sixteen membered rings depicted in Figure 6.5) are high spin whilst COANEC[171] and TEXQIW[172] (fourteen membered rings) are low spin. However, no spin crossover systems have been reported. This force field once developed will allow users to populate the SCO window with potential SCO complexes.

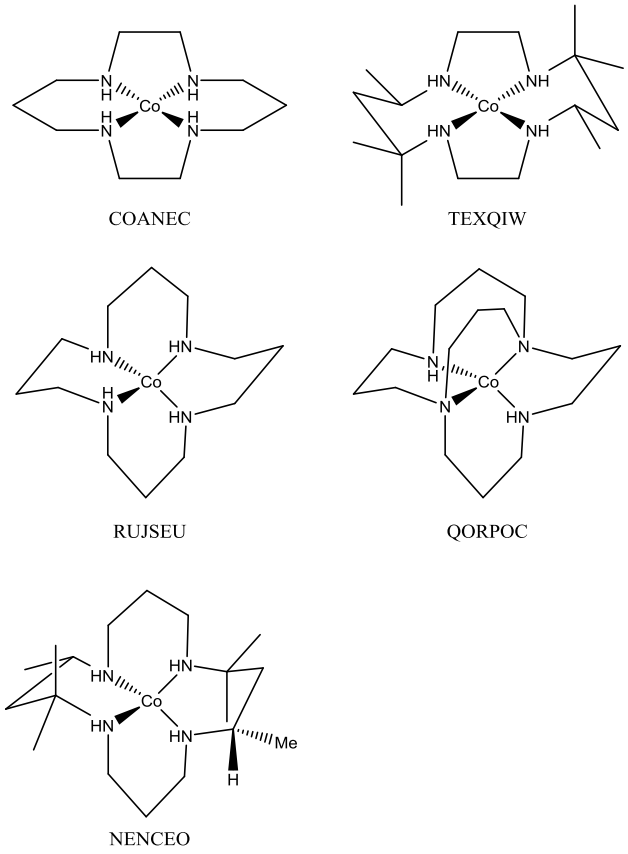

Figure 6.5; The five macrocyclic systems which have been reported in the literature and their Cambridge Structural Database refcodes.

A force field trained on just five complexes is possible. However, it might lack the diversity necessary for the subsequent high throughput screening. More training data are probably required. The DFT methodology (BP86 with solvation for structures and OPBE

with solvation for energetics the standard protocol as described in Chapter 4) was validated against the five macrocyclic complexes (Figure 6.5) for which crystal structures have been reported.

Table 6.5; A comparison of the crystal structures of five cobalt(II) tetramine complexes and the DFT optimised structures.

Refcode	Ground State		Av. Co-N Bond Length / Å	Bond Angle / °					
				1	2	3	4	5	6
COANEC	LS	Expt	1.98	180.0	180.0	94.1	94.1	85.9	85.9
		DFT	1.99	180.0	180.0	93.8	93.8	86.2	86.2
NENCEO	HS	Expt	1.99	130.4	115.8	105.6	104.9	101.2	99.9
		DFT	2.03	129.0	117.1	105.2	105.1	100.9	100.8
QORPOC	HS	Expt	2.02	126.2	107.8	107.2	104.8	104.6	104.3
		DFT	2.02	121.1	107.2	106.8	107.1	106.7	107.2
RUJSEU	HS	Expt	2.01	124.6	122.9	106.0	104.9	101.4	98.9
		DFT	2.03	123.9	123.8	102.8	102.8	102.8	102.8
TEXQIW	LS	Expt	2.01	180.0	180.0	94.2	94.2	85.8	85.8
		DFT	2.00	180.0	180.0	93.8	93.7	86.2	86.2

To provide more training data, calculations on generated complexes were carried out to help fill out the energetic region between the 14 and 16 membered rings, as well as to provide more diverse structures for the training. For the purposes of generating training data, the structures generated need not be global minima only local. The additional complexes are shown in Figure 6.6 as well as cobalt(II) bis-ethylenediamine (**C1**). The energetics of extended training set are given in Table 6.5.

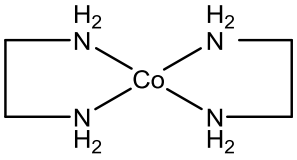

C1

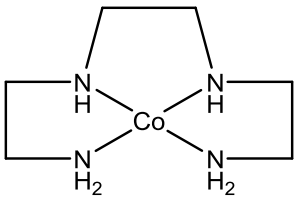

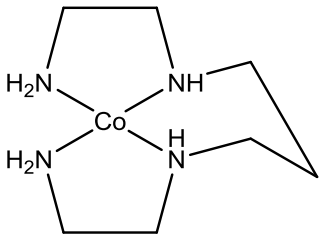

C2 **C3**

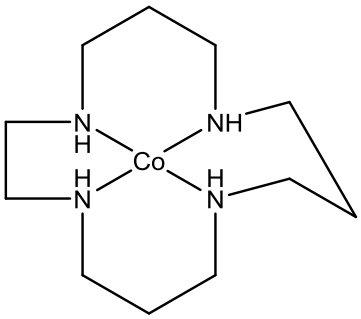

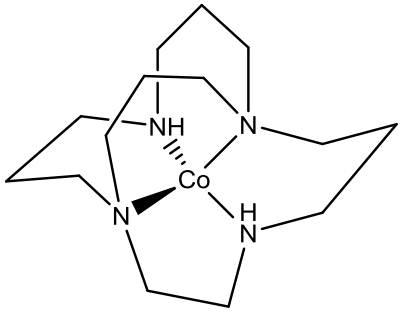

C4 **C5**

*Figure 6.6; The complexes added to the training set in Figure 6.4 to give Training Set 1 (**T1**).*

*Table 6.6; The complexes in training set, **T1**, denoted by their CSD refcodes or designation from Figure 6.5.*

	ΔE_{HL} / kcal mol^{-1}
COANEC	18.54
TEXQIW	17.56
C2	10.70
C1	6.80
C3	2.17
C5	-0.70
C4	-4.80
NENCEO	-11.29
RUJSEU	-12.29
QORPOC	-17.16

A fifty generation parameter optimisation run was carried out allowing all (excluding AOM) parameters to vary. The final Pareto front is shown in Figure 6.7 and the chosen parameter set in Table 6.7 which shows balance in the two objectives. The performance of this parameter set is illustrated in Figure 6.8.

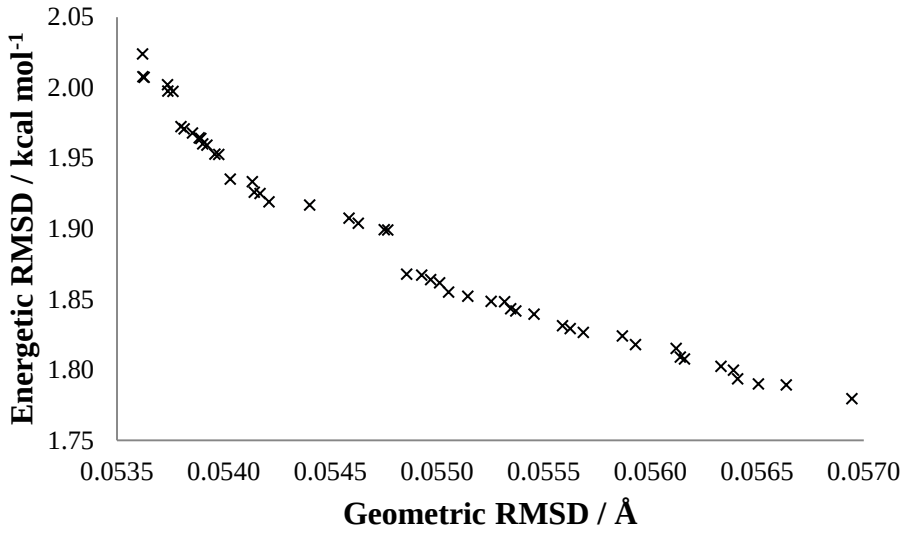

*Figure 6.7; The final Pareto front of the fifty generation parameter optimisation run training set (**T1**).*

*Table 6.7; Parameter set 3 (**P1S3**) from the Pareto front given in Figure 6.7. A parameter set which shows balance in the two objectives for the training set given in figures 6.5 and 6.6.*

Parameter		Units	Value
Morse	r_0	Å	2.09
	D	kcal mol^{-1}	60.0
	α		1.40
Ligand-Ligand Repulsion	A_{LL}	kcal mol^{-1} $Å^6$	4,980
AOM	e_σ (a_6)	cm^{-1} $Å^6$	481,000
	e_{ds} (a_6)	cm^{-1} $Å^6$	120,000
Spin pairing	a_0	kcal mol^{-1}	5.81
	a_6	kcal mol^{-1} $Å^6$	338

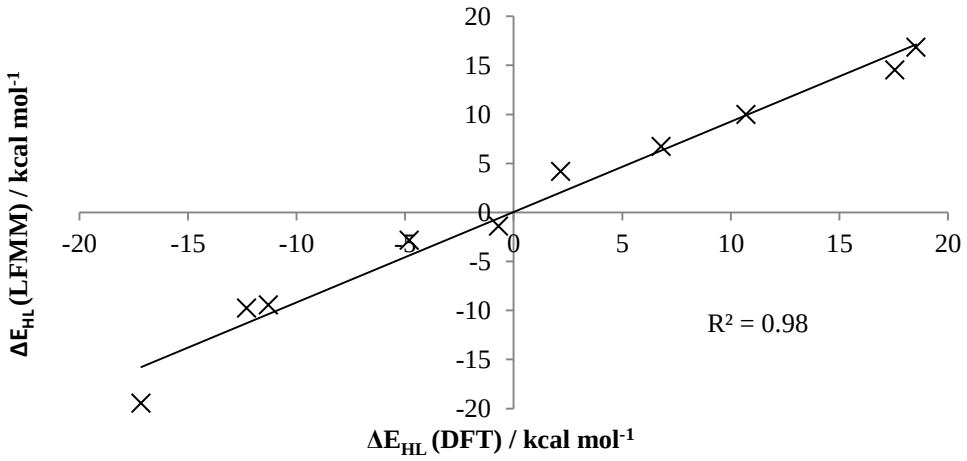

*Figure 6.8; A plot of ΔE_{HL} values obtained from LFMM (**P1S3**) against the DFT target value for training set, **T1**.*

Using the ligand generator routines the CC scaffold of the ethylenediamine ligand was selected for replacement. Of the bis-bidentate complexes generated, 102 lie within our window of interest (ΔE_{HL} 6 to -2 kcal mol^{-1}) based upon LFMM energetics. This simple validation is not yet looking for a global minimum and as such a full conformational search is not required. Of the 102 complexes, 25 were predicted to be synthesisable. Synthesisability was determined using MOE's rsynth tool. An rsynth of 1 (a measure of synthesisability based on retrosynthetic analysis) suggests the molecule is synthesisable while a value of 0 suggests it cannot be made. Values in between indicate varying likelihoods of successful synthesis. Three complexes were chosen to test the current parameter set (Figure 6.9).

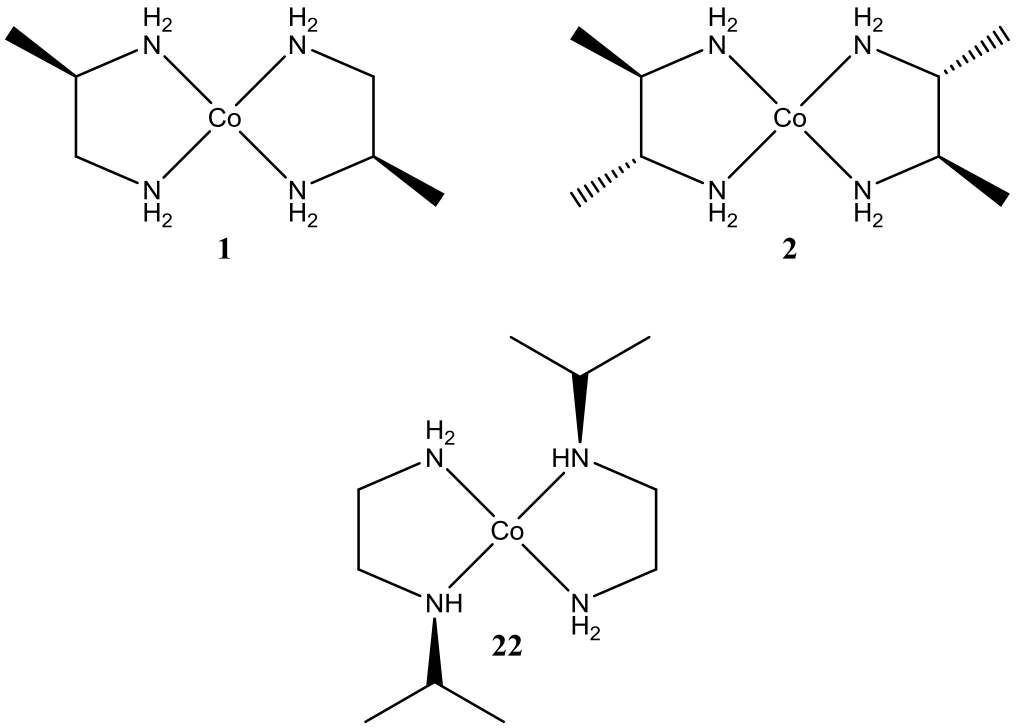

*Figure 6.9 – The three cobalt(II) tetramine complexes with bidentate ligands selected for initial validation of **P1S3**.*

Table 6.8 – The energetics of the small validation set, energies given in kcal mol^{-1}

	LFMM	DFT			
Complex	ΔE_{H-L}	HS	LS	ΔE_{H-L}	Error
1	5.21	-3730.6	-3728.63	5.63	0.42
5	4.42	-4487.17	-4492.65	5.48	1.06
22	2.74	-5222.94	-5225.2	2.26	-0.48

To provide further training data complexes **1** and **5 (22** excluded as error was small) were folded in to the training set to give training set (**T2**). Whilst these complexes are similar to each other, the subtle differences in the coordination environment (the ΔE_{HL} values of **1** and **5** are only 0.15 kcal mol^{-1} different in energy yet LFMM predicted a difference of 0.79 kcal mol^{-1}) provide a further test. Whilst the overall RMSD energetic error fell to 1.7 kcal mol^{-1} the RMSD of the complexes already in the set fell only by 0.04 kcal mol^{-1}; an inconsequential amount. The errors of the new training set fell (by 0.81 kcal mol^{-1} for

complex **5**) showing that their inclusion did improve upon the initial force field. As expected this inclusion offers no improvement for those complexes already in the set.

*Table 6.9; Parameter Set 13 (**P2S13**) from the optimisation on training set, **T2**.*

Parameter		Units	Value
Morse	r_0	Å	2.09
	D	kcal mol^{-1}	60.0
	α		1.47
Ligand-Ligand Repulsion	A_{LL}	kcal mol^{-1} $Å^6$	5,183
AOM	e_σ (a_6)	cm^{-1} $Å^6$	481,000
	e_{ds} (a_6)	cm^{-1} $Å^6$	120,000
Spin pairing	a_0	kcal mol^{-1}	6.24
	a_6	kcal mol^{-1} $Å^6$	304

*Table 6.10: The energetic errors for Par File 13, **P2S13**, from the first optimisation run on Training Set 2, **T2**.*

Identifier	ΔE_{HL} (DFT) / kcal mol^{-1}	ΔE_{HL} (LFMM) / kcal mol^{-1}	Error / kcal mol^{-1}
COANEC	18.54	16.80	-1.74
TEXQIW	17.56	14.57	-2.99
C2	10.70	9.81	-0.89
C1	6.80	6.37	-0.43
1	5.63	6.05	0.42
5	5.48	5.73	0.25
C3	2.17	4.09	1.92
C5	-0.70	-1.39	-0.69
C4	-4.80	-2.99	1.81
NENCEO	-11.29	-9.47	1.82
RUJSEU	-12.29	-9.81	2.48
QORPOC	-17.16	-19.33	-2.17

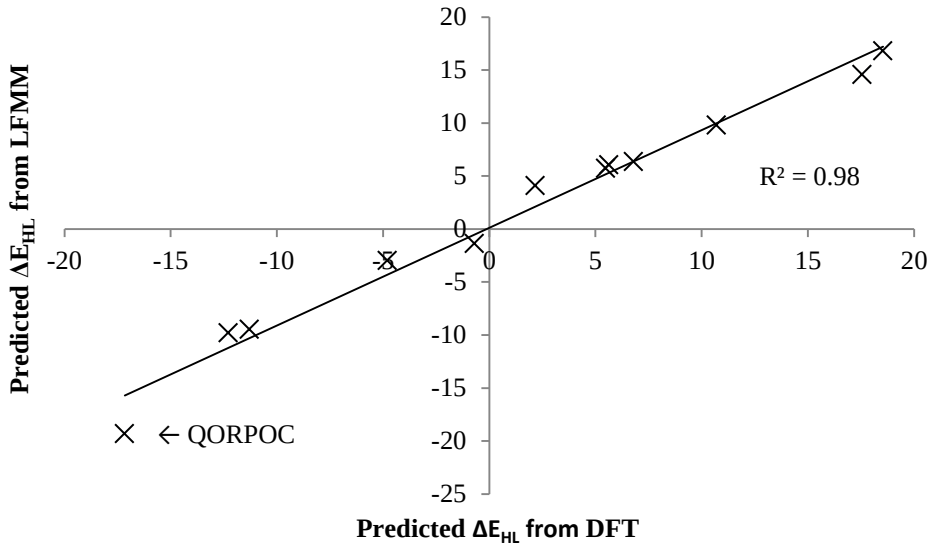

*Figure 6.10; The correlation of DFT and LFMM computed ΔE_{HL} (kcal mol^{-1}) using the parameter set given in Table 6.9 on **T2**.*

It is clear from Table 6.10 that whilst the parameterisation for four coordinate species is sound (R^2 =0.98, Figure 6.10) there is a slight anomaly. Despite the fact that the QOPRPOC error is lower than those of TEXQIW and RUJSEU the sign of the error remains the issue. The error for QORPOC is of the opposite sign to those in the lower left quadrant of Figure 6.10 and experimenting with its removal, leads to a reparametisation which offers lower errors in both objectives, Figure 6.11. While the removal is not reasonable,‡ it did highlight a deficiency in the FF which should be addressed. QORPOC is a sixteen membered chelate with a propane tether connecting two opposite nitrogens. It is comprised entirely of 6 membered rings; these have been shown to be an issue for the iron(II) amine systems studied by Deeth and Handley (2011) as in six membered rings there are two torsion terms involving the Fe-N bonds which are assigned zero force constants.[1] Consequently the chelate ring is unable to adopt all the various conformations found for six membered rings. They solved this problem by explicitly tuning the Fe-N-C-C

‡ A truly diverse force field should be capable of handling all related systems. As such the removal of a structure which has been crystallographically observed is deemed to be unreasonable.

torsion term rather than simply relying on the default generic *-N-C-* (* represents any atom) entry in the MOE force field. The introduction of a similar term here (using the parameters used in the iron example as a starting point) resulted in an improved description of the QORPOC energetics leading to a fall in energetic error from 1.27 kcal mol^{-1} to 0.90 kcal mol^{-1}. This reduction in error comes at a high cost, greatly increasing the errors associated with some of the other systems in the set.

One possible solution is an on the fly identification of six membered rings and thus a different treatment of them w.r.t their five membered counterparts. However it remains unclear as to whether this is the root cause of the issue. Another unique point to note being that both QORPOC and the **C5** species are the only complexes containing tertiary amine donors. Perhaps the use of different parameters for primary, secondary and tertiary amines would improve the fit. These extra levels of complexity are unlikely to prove worthwhile as despite the fact that the **C5** complex shares many of the characteristics of QORPOC (other than one carbon in a chelate ring) the performance of the force field is markedly different with a 1.48 kcal mol^{-1} lower error in the predicted ΔE_{HL} of **C5** than that of QORPOC.

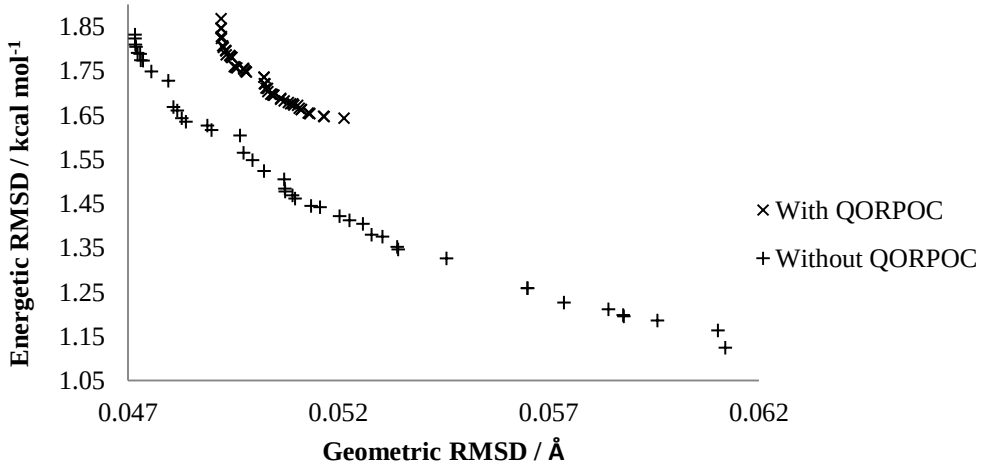

Figure 6.11; Final Pareto fronts with and without QORPOC in the training set.

True high throughput screening

Bidentate Ligands

After running scaffold replacement and R-group addition routines, using the groups given in Figure 6.12, 349 bidentate nitrogen donating ligands were created based upon ethylenediamine and propylenediamine. Of these, 67 entries had an rsynth of 1, this retrosynthetic analysis tool is outlined further in the Computational Details section of this chapter. These 67 ligands were attached to the metal following the procedure outlined in Appendix 2 forming 67 bis-bidentate complexes. These candidates were subjected to rigorous stochastic conformational searching, first for 2000 steps and then for 4000 steps (chiral restraints were used as both enantiomers will be contained in the database for many of the complexes). If both searches result in a best structure with same energy then it is assumed that this is the lowest energy conformation possible for this complex. From this search only one (if any) of the bis-bidentate complexes offers a likely candidate for SCO. This may be an indication of the need to lock potential SCO candidates into a metal geometry between tetrahedral and square planar.

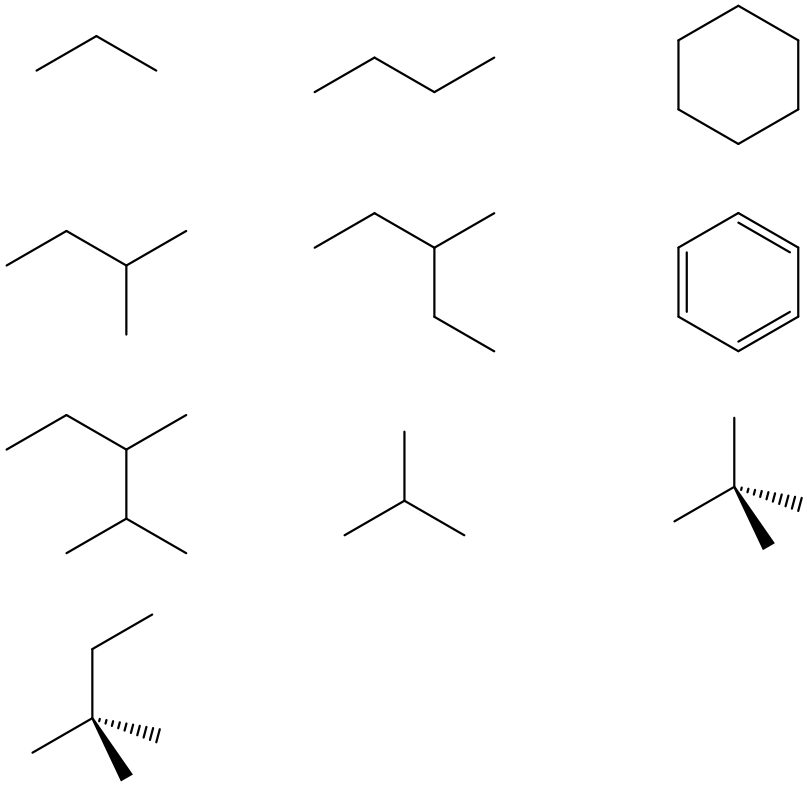

Figure 6.12; The R-groups used for addition and replacement on ethylene diamine and propylene diamine ligands. CH_4 and C_2H_6 were also included in the R-group library however these (most likely due to MOEs internal rules) do not participate in R-group addition.

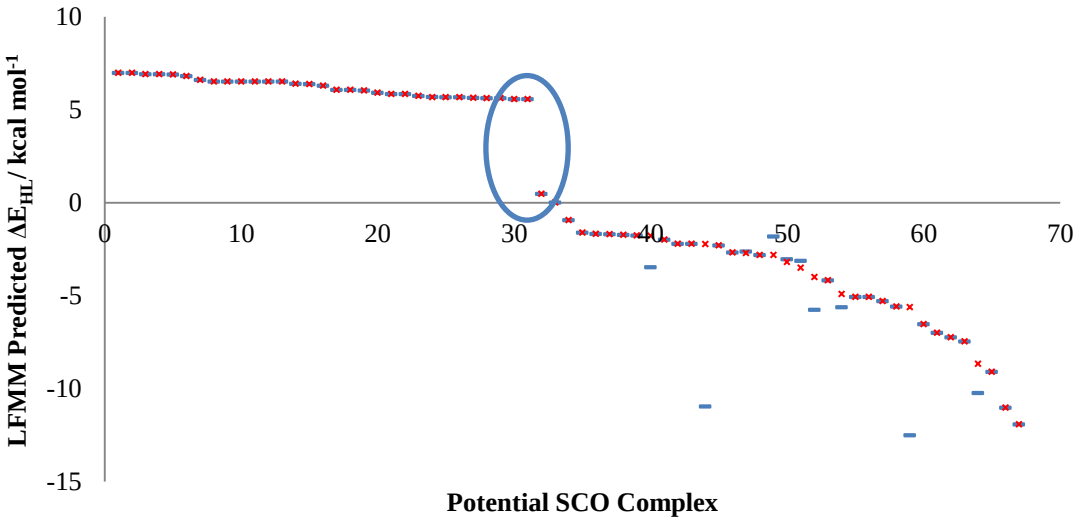

Figure 6.13; The bis-bidentate complexes ordered by ΔE_{HL}. The blue dashes denote the splitting after 2000 steps of stochastic conformational searching (at the HS state) whilst the red crosses denote 4000 steps. The oval indicates the absence of complexes in the SCO region.

It is, in the case of bidentates, too easy for them to fall in to their preferred geometry. It is believed that those complexes with secondary amine donors must adopt a tetrahedral ground state in order to reduce steric interactions between ligand groups, figures 6.13 and 6.14. However, those complexes with only primary amine donors can adopt either a square planar or tetrahedral geometry dependent on the nature of the ligand. For instance the bis-propylenediamine complex and all of its carbon substituted derivatives studied have larger bite angles and are tetrahedral whilst the bis-ethylenediamine complex and its derivatives are low spin consistent with a smaller bite angle and lower steric interactions. This mirrors the relationship between the size of the macrocycle and ground spin state in the literature.

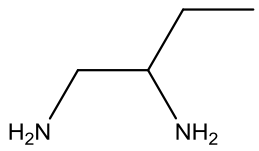

ΔE_{HL}= 6.5 kcal mol^{-1}

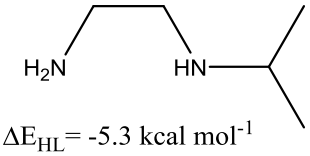

ΔE_{HL}= -5.3 kcal mol^{-1}

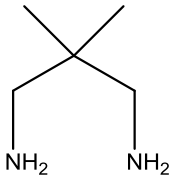

ΔE_{HL}= -2.2 kcal mol^{-1}

*Figure 6.14; Three representative examples of ligands in the bidentate database along with their LFMM predicted (**P2S13**) value of ΔE_{HL}*

Hence with bidentate nitrogen ligands it is difficult, if not impossible, for four-coordinate cobalt(II) to display SCO. The only bidentate complex predicted by LFMM to display SCO is that formed from 1,2-diaminobenzene ligands as in Figure 6.15. However, upon DFT optimisation the structure distorts Figures 6.16 and 6.17 and the DFT predicted spin state splitting is larger than predicted by LFMM at 7 kcal mol^{-1}. As subsequently discovered for iron complexes, and reported in Chapter 5 the aniline type nitrogen is planar when uncoordinated but the force field parameter type enforces a tetrahedral coordination. This problem can be corrected but given that the bidentate systems are not good candidates for SCO this was deemed unnecessary.

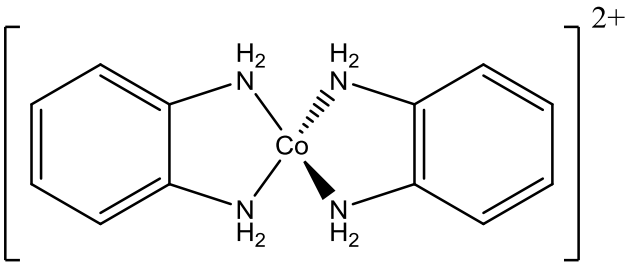

Figure 6.15; The only complex with bidentate ligands predicted to display spin crossover.

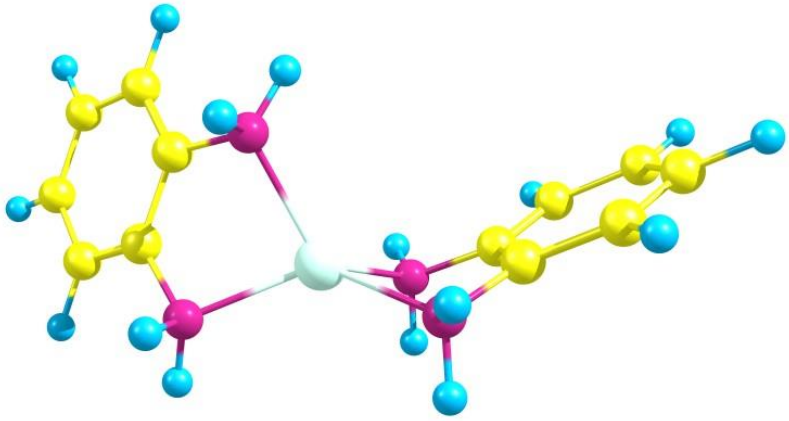

Figure 6.16; The distorted tetrahedral structure obtained upon DFT optimisation of high spin [Co(1,2-diaminobenzene)]$^{2+}$.

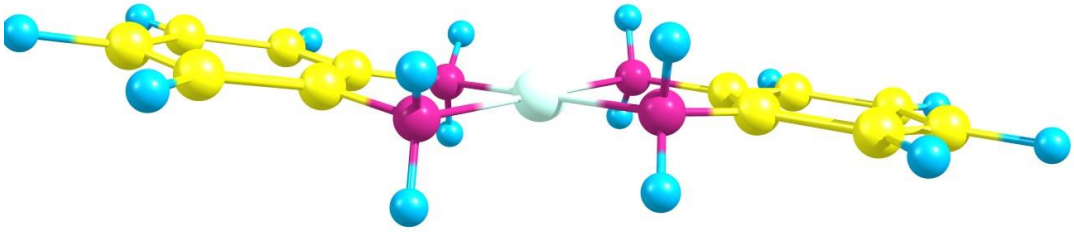

Figure 6.17; The distorted structure obtained upon DFT optimisation of low spin [Co(1,2-diaminobenzene)]$^{2+}$.

Tetradentate Ligands

To form tetradentate complexes, eight of the bidentate ligands previously generated (depicted in Figure 6.18) were used as the starting ligands and the R-group addition tool used upon them to generate tetradentates. This is to say that linking occurred, with the 8 bidentate starting points bonded to the whole database of 349 bidentate ligands. Ligands **L1**-**L5** had all hydrogens selected as points for potential substitution whilst **L6**-**L8** only the hydrogens which are inside the dashed lines in Figure 6.18 could be replaced. Filters were used to remove nitrogen-nitrogen single and double bonds as well as nitrogen-carbon double bonds as such systems fall outside the scope of this study.

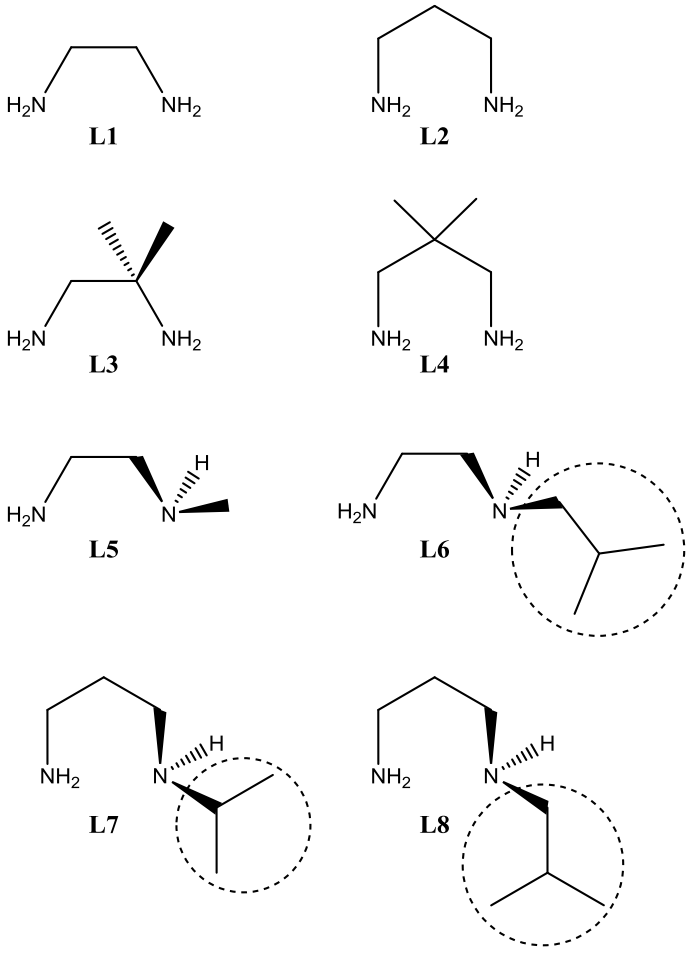

*Figure 6.18; The bidentate ligands chosen for ligand growth. Ligands **L1**-**L5** had all hydrogens selected as points for potential substitution whilst **L6**-**L8** only the selected hydrogens could be replaced.*

The eight ligand starting points were carefully selected. **L1** and **L2** represent simple systems upon which the complexity arises simply from the ligands to which they are bonded. This generated 249 and 8,937 unique ligands respectively. Ligands **L3**-**L8** introduce substituents whose effects may be felt. The reason for the inclusion only of those hydrogens within the dashed line is a pragmatic one. The inclusion of all of the hydrogens of ligands **L6**-**L8** resulted in the program crashing as a result of insufficient memory.

Of the over one hundred thousand (103,944) unique ligands generated, MOE's internal retrosynthetic tool predicted 4,347 of these to be synthesisable. The ligands deemed synthesisable were then attached to the metal using a ligand attachment script. The selection of this much reduced subset greatly reduced the computational cost allowing the subsequent stochastic searching to be carried out on a local machine over the course of days rather than months and increases the chances that predicted SCO complexes have ligands which are synthesisable.

Of these synthesisable candidates generated, 366 potential SCO complexes based on linear or branched tetradentates (excluding those with four membered chelates) have a spin state splitting of between 0 and 5 kcal mol^{-1}. Preliminary stochastic searching (2000 steps representing close to 2 million individual geometry optimisations) on those complexes with values of ΔE_{HL} initially predicted to be between +10 and -5 kcal mol^{-1} (983 complexes) narrowed this number slightly to 349 (322 from entries originally predicted in this range). The candidates for SCO are discussed in depth later as they share characteristics with the macrocyclic systems.

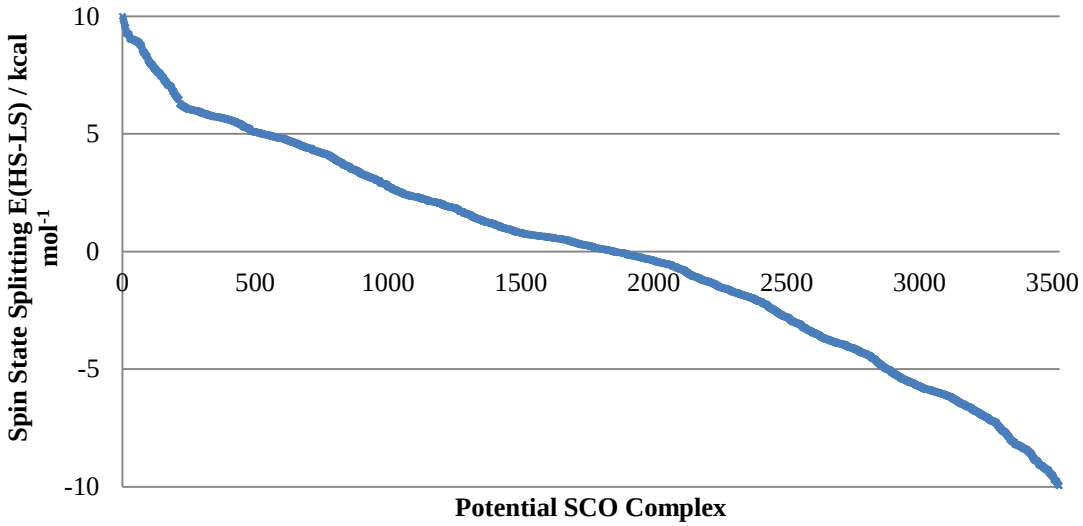

Figure 6.19; A plot of all linear and branched candidates based on raw data i.e. the structures have undergone only a small stochastic search.

Macrocycles

Macrocyclic ligands are generated through a SMARTS[§] match based routine which identifies a chain and subsequently bridges it with either a two or three membered carbon linker, Figure 6.20. These ligands were subjected to a near identical screening process to that used for the tetradentates.

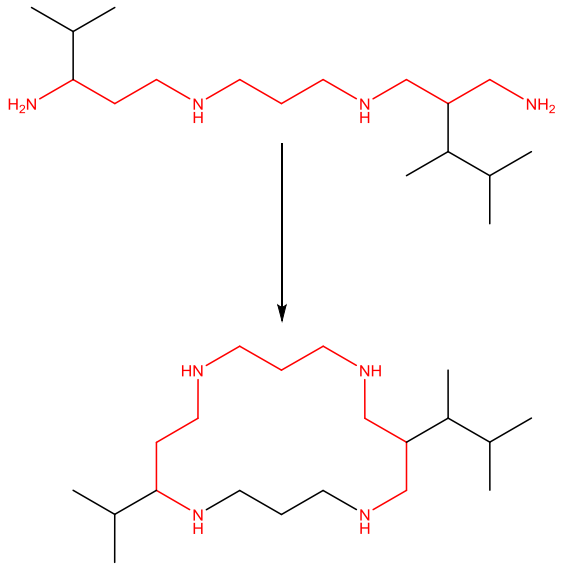

Figure 6.20; An illustration of the identification of a backbone capable of supporting macrocycle formation and the joining to form it.

Unfortunately DFT validation of LFMM energetics resulted in unacceptably large energetic errors (Table 6.11). This prompted a further refitting (generation **P3**) of the parameters including some of the data generated in the "validation" and propylene diamine since many of the ligands include this motif. This resulted in the Pareto front shown in Figure 6.23.

[§] SMiles ARbitrary Target Specification is closely related to the SMILES notation (http://www.daylight.com/dayhtml/doc/theory/). Both tools originate at Daylight Chemical Information Systems. SMILES describes molecules in terms of single line notation, for instance NCCN denotes ethylenediamine. SMARTS is built upon this and allows the detection of a given substructure within a molecule.

*Table 6.11; Validation data for the parameter set (**P2**) given in Table 6.9. Type indicates whether that ligand is bidentate (Bi), a linear or branched tetradentate (L/B) or a macrocycle (M), the ligands are shown in Figures 6.21 and 6.22. Complexes formed from ligand L and propane-1,3-diamine are manual test cases and did not result from the routine. Energies are in kcal mol^{-1}*

Identifier	Type	ΔE_{HL} LFMM / kcal mol^{-1}	ΔE_{HL} DFT / kcal mol^{-1}	Error / kcal mol^{-1}
625	M	9.78	3.28	6.50
339	M	8.24	7.08	1.16
4109	L/B	6.72	9.04	-2.32
62	Bi	5.90	5.64	0.26
4890	L/B	4.70	3.58	1.12
33	M	4.19	-0.09	4.28
L	M	3.54	4.14	-0.60
359	L/B	2.66	-4.72	7.38
3498	L/B	2.17	0.62	1.55
489	M	1.73	1.02	0.71
749	M	0.83	-2.02	2.85
65	Bi	0.46	6.99	-6.53
2681	L/B	0.35	-4.07	4.42
4151	L/B	-0.21	2.77	-2.98
15	Bi	-0.94	-5.86	4.92
Propane-1,3-diamine	Bi	-2.30	-1.89	-0.41
39	Bi	-2.82	-2.42	-0.40
1	Bi	-7.48	-11.71	4.23

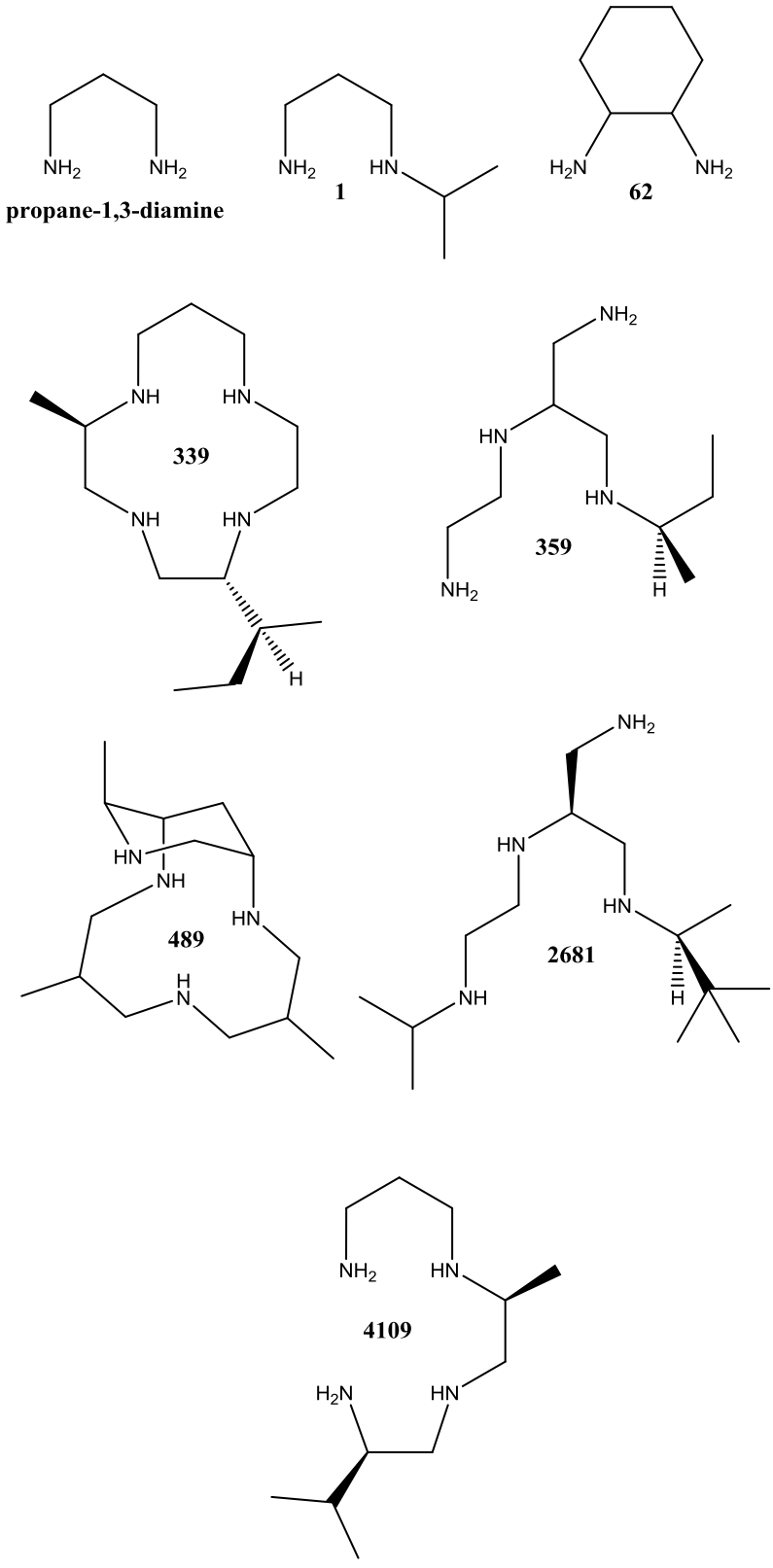

*Figure 6.21; The ligands included in the training set 3 (**T3**).*

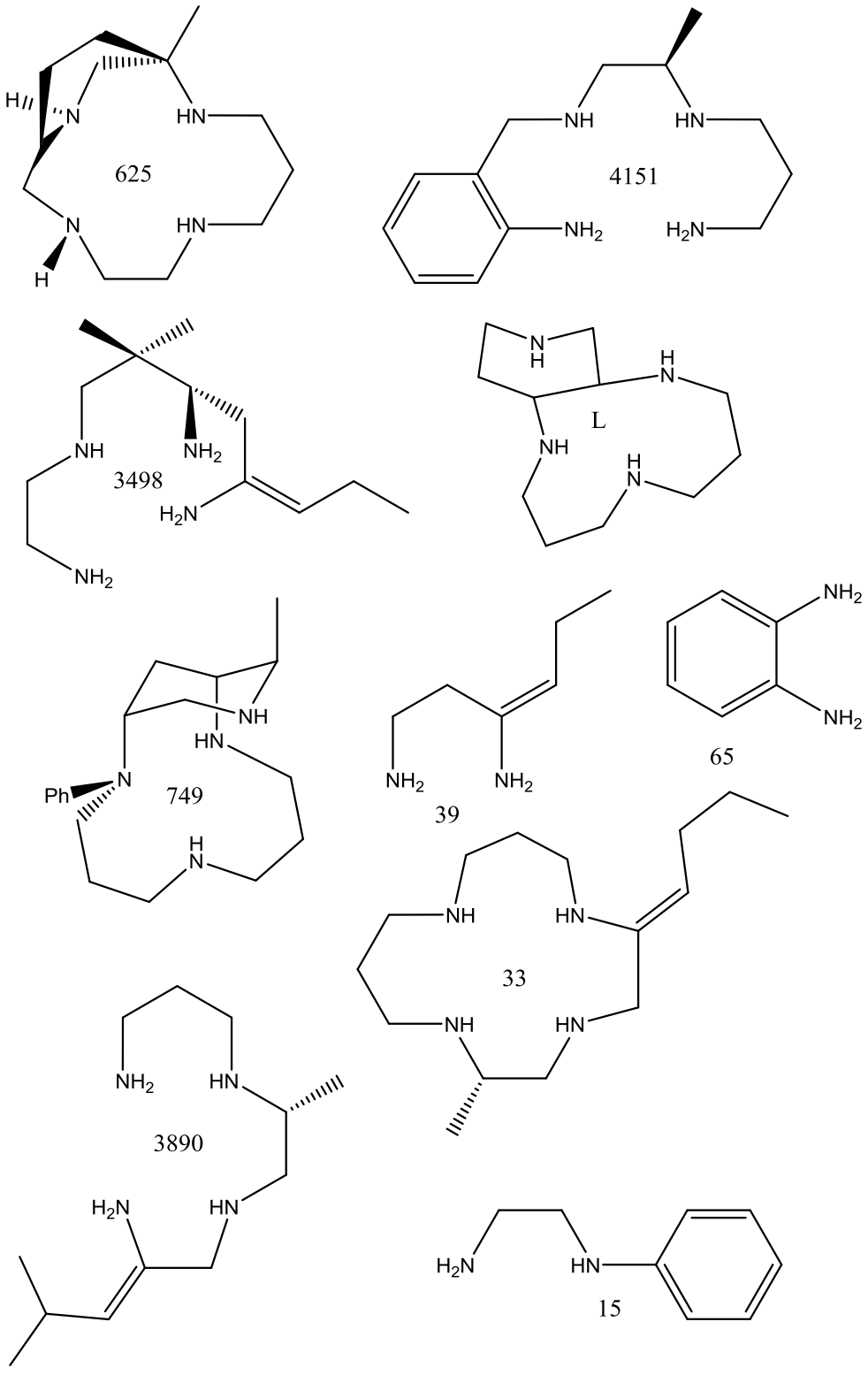

*Figure 6.22; The ligands in the validation set excluded from training set 3 (**T3**). **L** was not part of the set generated but was an experiment in how the force field would handle strained bridging group.*

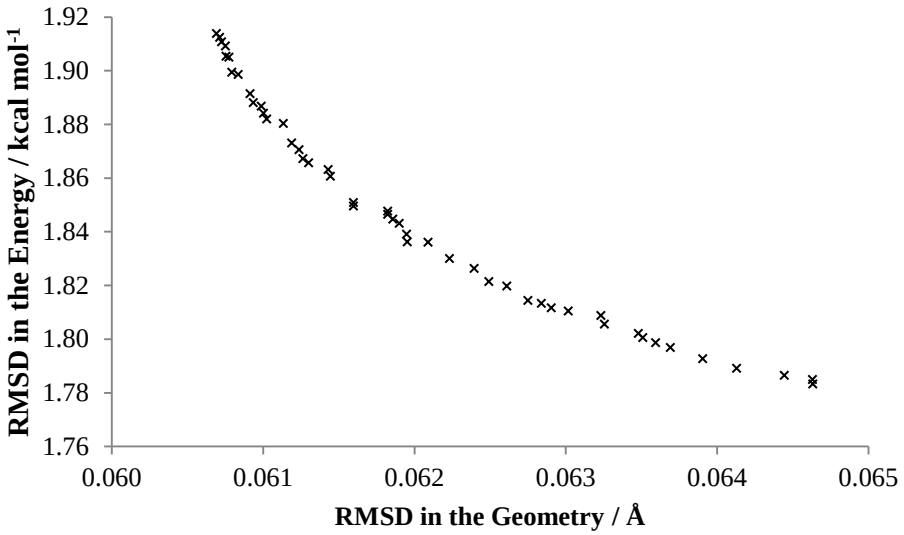

Figure 6.23; The final Pareto front of the third and final generation of force field.

Parameter set 4 of the front (**S4P3**) was selected; it offered a good balance in the energetic and geometric terms with objective errors of 1.83 kcal mol^{-1} and 0.062 Å respectively. A plot of LFMM predicted ΔE_{HL} against that obtained from DFT is shown in Figure 6.24.

*Table 6.12: Parameter set 4 (**S4P3**) used for the final stochastic search runs.*

Parameter		Units	Value
Morse	r_0	Å	2.07
	D	kcal mol^{-1}	60.0
	α		1.61
Ligand-Ligand Repulsion	A_{LL}	kcal mol^{-1} $Å^6$	5,370
AOM	e_σ (a_6)	cm^{-1} $Å^6$	481,000
	e_{ds} (a_6)	cm^{-1} $Å^6$	120,000
Spin pairing	a_0	kcal mol^{-1}	7.17
	a_6	kcal mol^{-1} $Å^6$	244

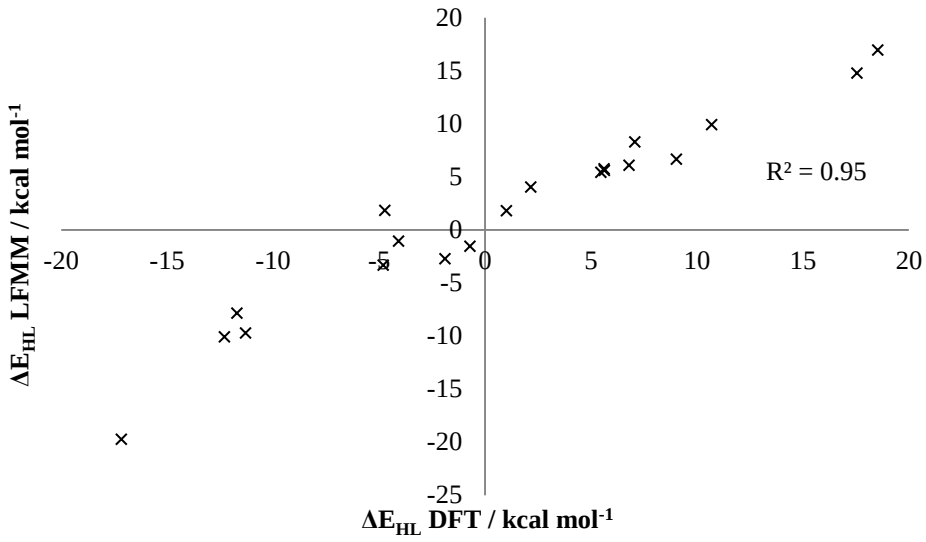

*Figure 6.24; A plot of ΔE_{HL} as predicted by LFMM (**P3**) against those obtained through DFT.*

The Candidates

Some of the structures generated (and included in the validation set) were too strained or esoteric and it was essential that these were removed to avoid wasting CPU time. To address this, the tetradentate database was refined once more removing complexes with elongated Co-N bonds (i.e. > 2.3 Å. Typical Co-N distances do not exceed 2.1 Å) through the use of an SVL script. An example of a complex which would have been removed is given in Figure 6.25.

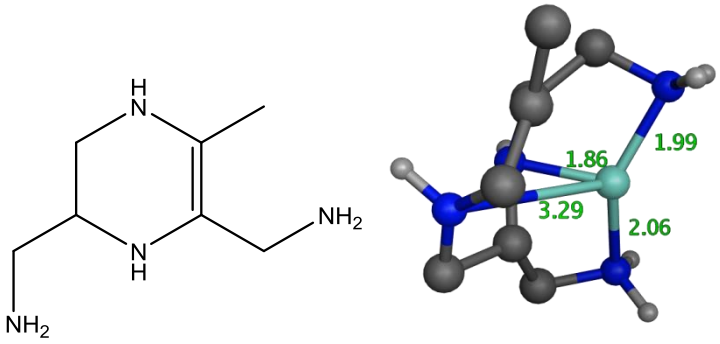

Figure 6.25; An example of a ligand which is strained upon coordination to a cobalt(II) centre. On the left a schematic representation of the ligand and on the right the complex, with bond distances with aliphatic hydrogens removed for clarity.

They were treated with the new force field, **S4P3**. After stochastic searches were carried out on these tetradentate complexes 182 of them are predicted lie between +6 and -2 kcal mol^{-1}. A sample of ten tetradentate species which were predicted by LFMM to occupy the SCO region was chosen for validation, Table 6.13. For eight of the ten complexes both LS and HS DFT optimisations were carried out using the geometries obtained from the 4000 step LFMM searches of their respective spin state. While complexes **455** and **1382** were optimised from the LFMM determined LS geometry only to ensure the DFT and LFMM computed values of ΔE_{HL} were directly comparable i.e. the DFT went to the same structural minima as the LFMM.

Table 6.13; The computed values of ΔE_{HL} from DFT and both of the LFMM stochastic searches. Values in kcal mol^{-1}. DFT optimisations for all complexes for which the low and high spin values of ΔE_{HL} are the same were carried out from LFMM optimised structures at that spin state. Complexes 455 and 1382 were optimised from the LFMM determined LS geometry only to ensure the DFT and LFMM computed values of ΔE_{HL} were directly comparable. Ligands illustrated in Figure 6.26.

Index	LFMM ΔE_{HL} Relative to the HS Structure	LFMM ΔE_{HL} Relative to the LS Structure	HS	LS	ΔE_{HL}
4	1.87	1.87	-4286.99	-4282.4	-4.59
368	1.60	1.60	-5412.74	-5407.67	-5.07
455	-1.70	1.85	-3540.22	-3536.99	-3.23
1173	-1.00	-1.00	-3925.58	-3920.16	-5.42
1217	-1.12	-1.12	-4301.96	-4295.9	-6.06
1285	2.10	2.10	-5043.99	-5039.86	-4.13
1297	2.09	2.09	-5484.67	-5481.86	-2.81
1382	3.23	2.50	-5244.85	-5240.77	-4.08
1947	2.94	2.94	-4879.75	-4886.62	6.87
2637	1.36	1.36	-5792.56	-5789.13	-3.43

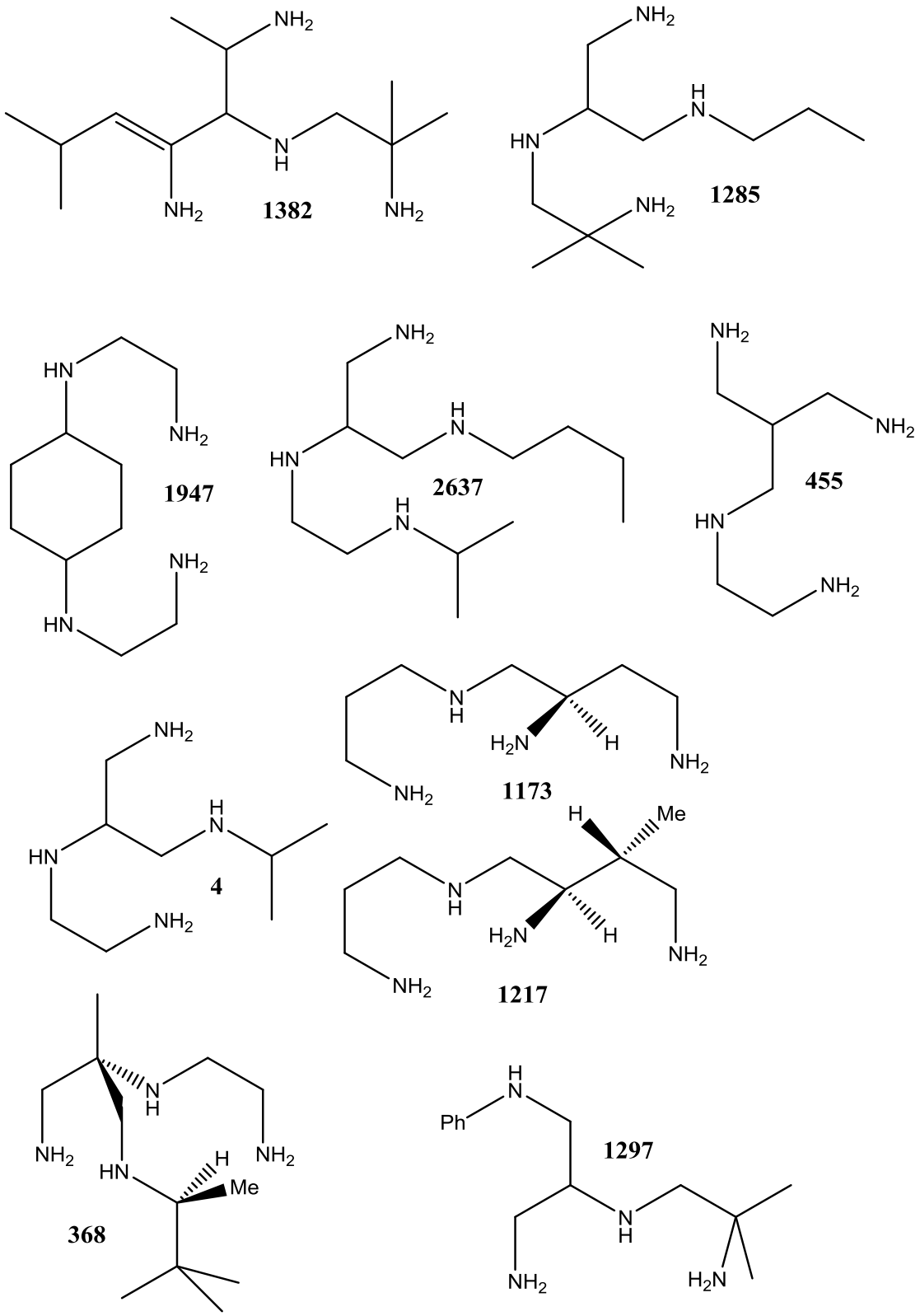

Figure 6.26; The set of ligands from the tetradentate database which LFMM predicted to be SCO. The LFMM and DFT computed spin state splittings of these complexes are given in Table 6.13.

Unexpectedly the correct spin state is only predicted for three out of the ten complexes. Since the generated complex **1285** closely resembles complex **359** in **T3** a comparison of the predicted geometries of the two may give some insight.

A comparison of the LFMM and DFT HS structures is shown in Figure 6.27. Complex **359** is the only complex in the training set for which the reparameterised force field was unable to assign the correct ground state and it is therefore inevitable that the incorrect spin state is predicted for the similar complex **1285**. A comparison of their structures illustrates that while the cobalt coordination spheres from DFT are identical while those from LFMM are both different to the DFT and from each other. The main variations can be seen in the chelate ring which carries the two methyl substituents where one of the Co-N bond lengths is 0.06 shorter than for the corresponding ring without the two methyl groups. Intriguingly both of these complexes are also structurally analogous to complex **2681** for which LFMM predicts the correct ground spin state. However, the structures generated are even less accurate for this complex, Figure 6.28, than for either **359** or **1285**.

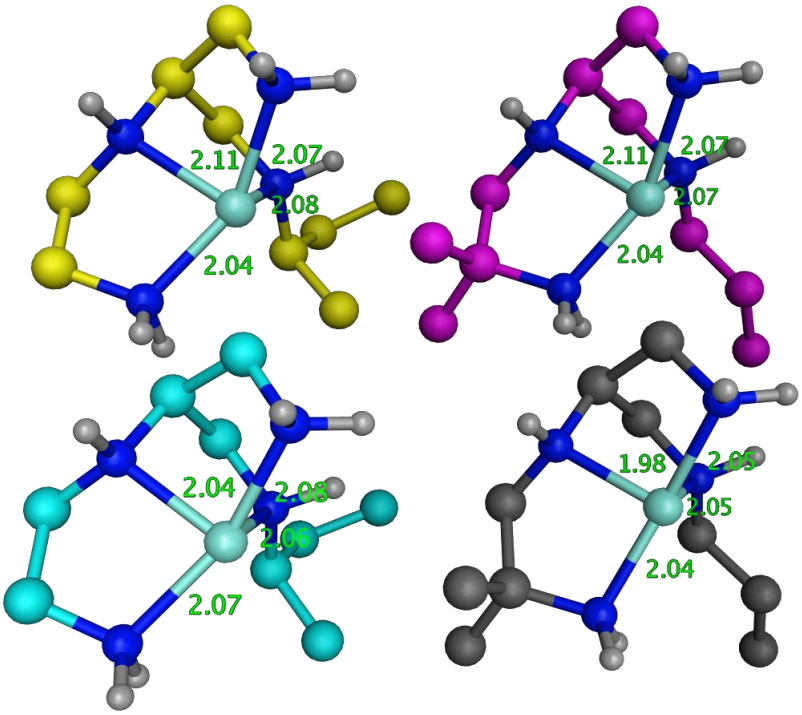

*Figure 6.27; The HS geometries of **359** (left) and **1285** (right). Yellow is the DFT optimised structure of **358** and in blue is the corresponding LFMM structure. Purple is the DFT structure of 1285 and grey is its LFMM structure.*

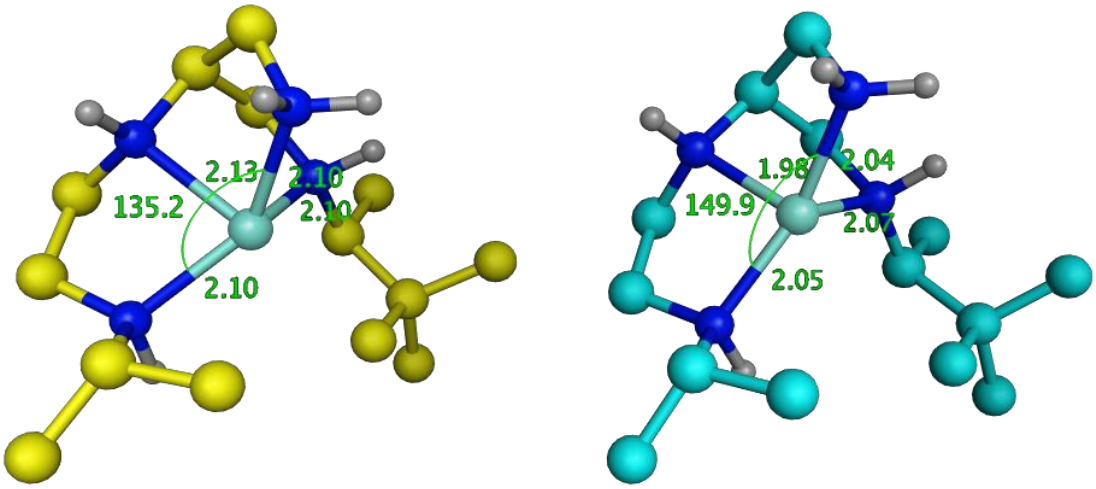

*Figure 6.28; The analogous complex **2681** which was included in the training set. This complex is predicted by the force field to display the correct spin state.*

Moreover the discrepancies between DFT and LFMM are not restricted to these complexes. It is believed that the force field is experiencing a common symptom of force field parameterisation in which a force field is only valid for complexes related to those in its training set. Here we have designed a force field with the aim of studying cobalt(II) macrocycles (and as we will see shortly it performs well for these systems) if the branched acyclic systems are of interest to the group in future these should be included in greater number within the training set. Including increasing numbers of complexes within the training set will result in an increase in parameterisation time and it would be unsurprising if this reduced the accuracy of the macrocyclic systems which are our primary focus of study within this Chapter.

450 macrocycles from the previous searching steps were subjected to 2000 more stochastic search steps using the new force field. From these complexes 290 complexes with ΔE_{HL} between 8 and -4 kcal mol^{-1} were subjected to 4000 step stochastic searches at the HS geometry and then 2000 and 4000 at the low spin geometry. The stochastic searches are judged to have converged if both the two and four thousand step stochastic conformational searches return the same minimum energy structure. DFT validation, optimised from the LFMM generated LS geometry, confirms complexes **172**, **487**, **489**, **491**, **504** and **631,** Figure 6.29, as candidates for SCO with values of ΔE_{HL} in the region of 0-1 kcal mol^{-1}.

Table 6.14; Validation of a selection of the $[CoL]^{2+}$ complexes with macrocyclic ligands in the region of 2-0 kcal mol^{-1}(final LS LFMM stochastic search). Complexes on which DFT was not run are denoted by "---". Both spin states ran from the LS geometry in order to match the LFMM result.

Index	Source of ΔE_{HL} / kcal mol^{-1}			
	4000 Step SCS for the HS State	2000 Step SCS for the LS State	4000 Step SCS for the LS State	DFT
487	1.96	1.96	1.96	0.63
500	1.88	1.88	1.88	-0.15
491	1.84	1.84	1.84	1.03
504	1.78	1.78	1.78	0.03
489	1.77	1.77	1.77	0.98
633	1.74	1.74	1.74	-0.05
631	1.73	1.73	1.73	0.58
168	1.72	1.72	1.72	---
172	1.71	1.75	1.71	0.02
502	1.71	1.71	1.71	-0.09
166	1.71	1.71	1.71	0
170	1.59	1.59	1.59	---
164	1.53	1.23	1.57	---
81	1.89	4.81	1.52	-1.63
89	1.35	1.15	1.15	-2.37
83	1.30	1.06	1.06	-1.97
749	0.79	0.79	0.79	---
107	1.49	0.89	0.78	-1.8
1002	0.85	0.67	0.67	---

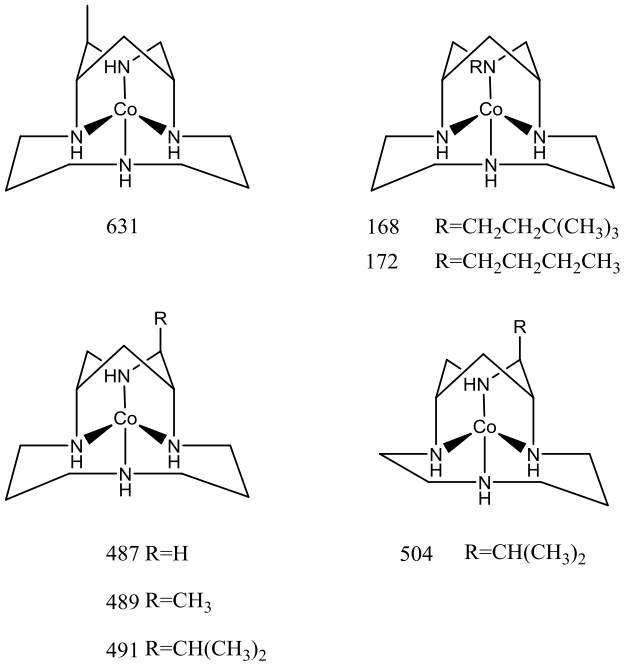

Figure 6.29; A selection of bridged macrocycles which LFMM predicts to display SCO.

The agreement LFMM and DFT spin state energies is satisfactory. Across the considered SCO region of 0-2 kcal mol^{-1} the R^2 correlation is 0.74 (Figure 6.30). Although LFMM often predicts the wrong spin state the energy differences are so small that this is not especially significant. The main issue is that both LFMM and DFT predict small spin state energy differences which vary in more or less the same way for this set of complexes.

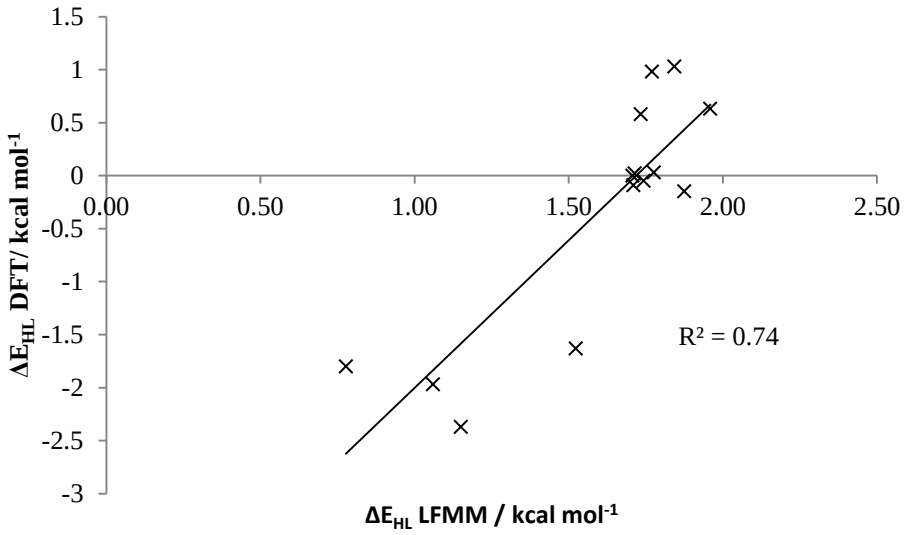

Figure 6.30; The correlation of LFMM and DFT predicted values of ΔE_{HL} for the macrocyclic validation set.

In these SCO candidates based around fused rings (using the simplest, **487**, Figure 6.31, as an example) the DFT optimisation predicts one of the Co-N bonds to be elongated by 0.1 Å in the high spin state consistent with the population of an antibonding orbital predominantly directed towards N1. The difference between the Co-N1 and Co-N2 bonds is larger for DFT than LFMM although the average bond length is the same. It seems that the LFMM potential is somewhat "stiffer" than DFT. The LFMM may lack a little flexibility which may also be a factor for the acyclic tetramines.

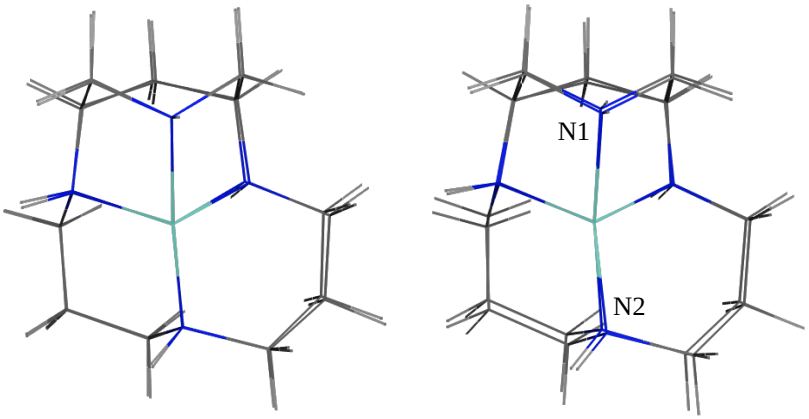

*Figure 6.31; A superposition of the LFMM and DFT structures of complex **487**. The LS form is shown on the left while the HS form is given on the right.*

*Table 6.15; A comparison of the cobalt-axial nitrogen bond lengths for the high spin form of **487.** N1 denotes the axial ligand which forms part of the piperidine ring while N2 is the second axial nitrogen (i.e. the nitrogen trans to that of piperidine).*

	LFMM / Å	DFT / Å
Co-N1	2.07	2.11
Co-N2	2.03	1.99

A point which becomes increasingly clear upon studying the results is the prevalence of the sawhorse/seesaw geometry in the predicted SCO complexes. This geometry resembling an octahedron with two cis ligands removed is counter intuitive considering all reported four coordinate cobalt (II) amines are either square planar or tetrahedral.

The complexes proposed to be sawhorse are locked in this conformation by carbon chains as illustrated in Figure 6.32 which fixes three of the donors on a face of the nominal octahedron and requires the fourth donor to adopt a position trans to one of the other ligands. This gives the effective tetragonal ligand field shown in Figure 6.33.

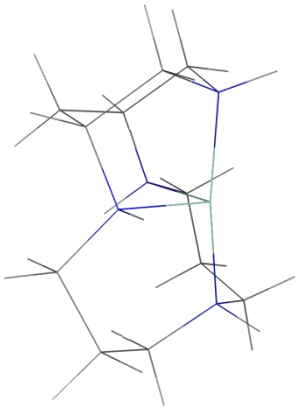

*Figure 6.32; The locked sawhorse geometry of the proposed SCO complex, **487**.*

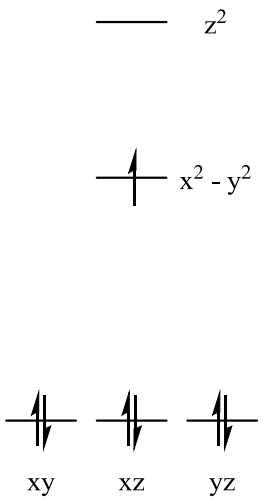

Figure 6.33; The d-orbitals associated with the sawhorse geometry. Axis frame given in Figure 6.34.

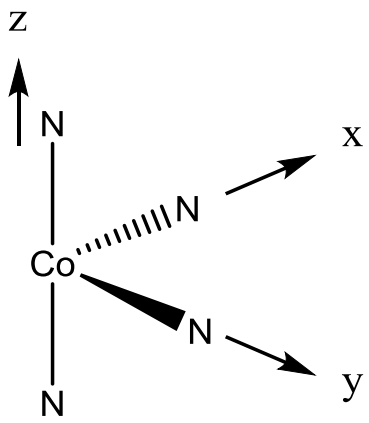

Figure 6.34; The sawhorse geometry which is prevalent in the proposed SCO complexes and the axis frame used in discussion of its orbitals.

If the promotion of an electron from one of the three degenerate orbitals of the LS sawhorse to the d(z^2) orbital is similar to the d-d repulsion energy then SCO is possible. The constraining of the fourth ligand appears to enable this for the sawhorse geometry.

It is important to note that one major issue with force field based approaches is the poor treatment of complexes for which a bond is unstable as is the case for ligand dissociation. This is apparent for complex **767** (Figure 6.35) for which one of the Co-N bond lengths in the HS state is predicted by DFT to be 2.19 Å.

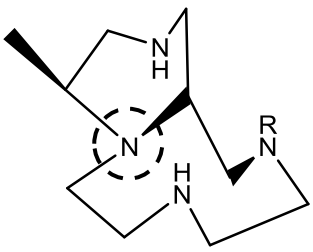

767 R=$CH_2C(CH_3)_3$

*Figure 6.35; The macrocyclic complex (**767**) which DFT predicts the ligands to dissociate at the highlighted tertiary amine donor.*

The sawhorse geometry requires two empty coordination sites which presents challenges for synthesis. Bulky groups which shield these sites or the use of weakly coordinating anions may facilitate the realisation of the sawhorse motif in the design of novel cobalt SCO complexes. Among the most commonly utilised weakly coordinating anion is $[B(CH_3(CF_3)_2)_3]^-$ with this property attributed to steric effects.[173] However, the most appropriate weakly coordinating anion for a given application must be determined experimentally.[173]

While this sawhorse geometry has yet to be achieved in cobalt(II) systems. The copper(I) tetramine GUGWEK (Cambridge Structural Database REFCODE) depicted in Figure 6.36[174] does adopt this geometry. This ligand is a 14-membered ring bridged by an ethylene group with benzyl substituents on opposing nitrogens.[174] The authors rationalise this structure by stating "the pendant benzyl groups appear to block the approach of ligands to" the vacant coordination sites.[174] The cobalt(II) analogue is predicted by LFMM (after stochastic searching) to be slightly HS by 0.8 kcal mol^{-1}. This was confirmed by DFT which predicts a ΔE_{HL} of -0.74 kcal mol^{-1} in good agreement with the LFMM prediction. Whilst this complex is not predicted to be SCO it could be utilised as a potential scaffold for ligand generation in the future.

Hubin's thesis[175] describes a related cobalt(II) complex (in which the benzyl groups are replaced by methyl substituents and the cobalt is bent away from the macrocyclic ligand). In this complex a pseudo octahedral geometry is adopted with the "empty" sites are occupied with chloride ligands.

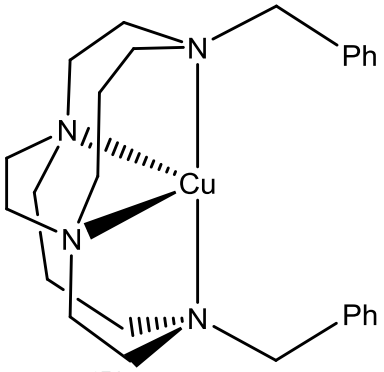

Figure 6.36; The copper(I) complex[174] which is structurally analogous to the proposed cobalt(II) species.

Conclusions

This chapter has shown it is possible to develop an LFMM force field which can predict novel four-coordinate Co(II) amine complexes with the potential to display spin crossover.

Force field fitting is inherently interpolative so it is up to the user to ensure that the training set covers the required diversity of systems. It is believed that the issue with the tetradentate ligands is a result of this behaviour. There will always be a trade-off between the breadth of applications and accuracy. The design of a force field for the exploration of macrocyclic SCO complexes may result in one which is not transferable to acyclic systems.

We have proposed macrocyclic spin crossover complexes with fused rings which facilitate a sawhorse geometry at the cobalt(II) centre. This sawhorse geometry is intriguing and its occurrence in the CSD (albeit not for cobalt(II) amines) is encouraging. Perhaps this research will inspire an experimentalist to try to synthesise such a complex.

In future, the tools and approach explored here could allow chemists to explore new metal-ligand combinations which have not so far been considered as capable of supporting SCO. But of course, the final proof of the methodology will come from experiment and it is hoped that this and future studies by the group will encourage synthetic chemists.

Chapter 7 – Conclusion

This aim of the work presented in this thesis was to explore computational approaches to the modelling and discovery of spin crossover transition metal complexes. We considered both 'ab initio' methods, based mainly on DFT, and empirical force fields based on ligand field molecular mechanics. It has been shown in Chapter 4 that a user can choose a functional and basis set combination through validation to experimental data which will yield accurate results for a series of related systems. However, it would be naive to assume that the specific protocols that emerge from this approach would be suitable in all cases. For instance the methodology adopted here of OPBE and a triple-ζ basis set plus polarisation has been shown to work well for iron(II) but proves less satisfactory for manganese systems. It should not be assumed that addition of all of the corrections known (e.g. solvation, dispersion and ZPE) will yield the most accurate result. The success of OPBE for iron(II) systems lies in the cancellation of errors and not in its theoretical grounding. Other protocols such as the BP86/def2-SVP basis/COSMO combination used in the study of the R,R' Pytacn complexes of Prat et al[2] yield promising results despite their simplicity. Changing the substituents on the pyridine ring was shown by Prat et al to directly influence the reported magnetic moment.[2] Here it has been shown that these remote effects on a metals spin state are reflected in the computed values of ΔE_{HL}. It is recommended that the OPBE/TZP/COSMO approach be utilised for iron-nitrogen systems. This functional choice is in line with the recommendations of Swart et al.[59]

Given the developments in coupled cluster calculations it is hoped that in the near future a wealth of training data for force field fitting will become available to take us, in principle into areas where there are no experimental data.

In chapter 5, attention turned to developing empirical force fields for modelling SCO efficiently. Empirical force fields are vitally important as even if the perfect functional existed, it would take too long to do the millions of calculations necessary for high throughput screening.

However, force fields are only as good as their parameters. Given that optimising parameters for complex force fields is challenging there was a clear need for more automated procedures. The PROTEUS tool is a crucial was proven by Deeth and Handley to offer a straight forward way to obtain new parameters.[1] On closer inspection we found bugs which hindered its application to new and interesting systems. The PROTEUS parameter optimisation routine has been debugged and will produce after successive generations a series of parameter sets which are optimal. While LFMM works reasonably well at reproducing DFT some error remains. It is possible that varying all the LFMM parameters is not enough and it is presumed that some of the 'conventional' FF parameters also need to be optimised. The work of the Norrby group on Q2MM illustrates that results from quantum mechanics can be reproduced exactly if you're prepared to optimise all relevant force field parameters as seen for their work on rhodium catalysis.[176] However, to implement this in LFMM would require a rebuilding of the scripts both for LFMM and the PROTEUS optimisation routine and represents a major undertaking.

Iron(II) amines have been shown by others to display spin crossover.[3] In our exploration of amine donors we found that LFMM failed to reproduce the structural distortion of $[Fe(1,2\text{-diaminobenzene})_3]^{2+}$, which is reported in the literature and confirmed by DFT. This was corrected in Chapter 5 and it was found that a V2/2 parameter of 1.75 is suitable for $[Fe(1,2\text{-diaminobenzene})_3]^{2+}$.

Within the custom force field (derived from MMFF94) the force constant for the Fe-N-C

bond was set to 200 kcal mol^{-1} deg^{-2}, considerably stiffer than the default value for an M-N-C bond of 30 kcal mol^{-1} deg^{-2}. While no evidence was reported in any of the literature for this, some justification has now been established in that a reduction in the force constant leads to a decrease in energetic accuracy.

Different approaches to the treatment of electrostatic interactions have been considered including the bond charge increments and the PSML approach. Both techniques require a pre-existing knowledge of the metal charge for reference cases usually obtained from DFT calculations. Mulliken derived bond charge increments proved easy to include in the case of the four coordinate cobalt(II) amine force field through the BCI scheme but were more problematic for the six coordinate iron(II) amine force field. Using the Proton Scaled Metal Ligand charge scheme natural charges have been successfully incorporated in to an iron(II) amine force field. It has also been shown that a mixed ligand force field can be generated. However, these force fields remain highly specialised in their applications. It should therefore remain a goal of the group to explore how more transferable parameters may be generated. It remains possible that limited transferability is the inescapable cost of good structural accuracy and energetic accuracy from the limited number of parameters optimised.

Once a force field has been generated, it can and should be utilised. In Chapter 6 the topic of high throughput screening was considered. Potential spin crossover candidates have been proposed. These complexes, which adopt sawhorse geometries, could prove to be interesting synthetic targets. The occurrence of the copper(I) complex GUGWEK complex in the literature inspires confidence. While the substitution of the copper for cobalt(II) results in a slightly HS complex (as predicted by LFMM and DFT) it could be utilised as a scaffold for future searching.

Hopefully this work has illustrated the many exciting possibilities LFMM provides in the field transition metal computational chemistry allowing for theory to lead experiment rather than follow. There are still some bugs in the methodology and it hoped that future research in the group will help to clarify this.

References:

(1) Handley, C.; Deeth, R. J. *J. Chem. Theory Comput.* **2011**.

(2) Prat, I.; Company, A.; Corona, T.; Parella, T.; Ribas, X.; Costas, M. *Inorg. Chem.* **2013**, *52*, 9229.

(3) Halcrow, M. A. *Polyhedron* **2007**, *26*, 3523.

(4) Letard, J. F.; Guionneau, P.; Nguyen, O.; Costa, J. S.; Marcen, S.; Chastanet, G.; Marchivie, M.; Goux-Capes, L. *Chem.-Eur. J.* **2005**, *11*, 4582.

(5) Bousseksou, A.; Vieu, C.; Letard, J. F.; Demont, P.; Tuchagues, J. P.; Malaquin, L.; Menegotto, J.; Salmon, L.; Google Patents: 2003.

(6) Ni, Z.; Shores, M. P. *J. Am. Chem. Soc.* **2009**, *131*, 32.

(7) Ni, Z.; Shores, M. P. *Inorg. Chem.* **2010**, *49*, 10727.

(8) Young, M. C.; Liew, E.; Ashby, J.; McCoy, K. E.; Hooley, R. J. *Chem. Commun.* **2013**, *49*, 6331.

(9) Young, M. C.; Liew, E.; Hooley, R. J. *Chem. Commun.* **2014**, *50*, 5043.

(10) Gutlich, P.; Garcia, Y.; Goodwin, H. A. *Chem Soc Rev* **2000**, *29*, 419.

(11) Baker JR, W. A.; Bobonich, H. M. *Inorg. Chem.* **1964**, *3*, 1184.

(12) König, E.; Madeja, K. *Inorg. Chem.* **1967**, *6*, 48.

(13) Tanabe, Y.; Sugano, S. *J. Phys. Soc. Jpn.* **1954**, *9*, 766.

(14) Paulsen, H.; Schünemann, V.; Wolny, J. A. *Eur. J. Inorg. Chem.* **2013**, *2013*, 628.

(15) Halcrow, M. A. In *Spin-Crossover Materials*; John Wiley & Sons Ltd: 2013, p 147.

(16) Real, J. A.; Gaspar, A. B.; Niel, V.; Muñoz, M. C. *Coord. Chem. Rev.* **2003**, *236*, 121.

(17) Diebold, A.; Hagen, K. S. *Inorg. Chem.* **1998**, *37*, 215.

(18) Turner, J. W.; Schultz, F. A. *Inorg. Chem.* **1999**, *38*, 358.

(19) Turner, J. W.; Schultz, F. A. *Inorg. Chem.* **2001**, *40*, 5296.

(20) Bradley, G. M., V.; Nelson, S. M. *J. Chem. Soc.* **1978**, 522.

(21) Spiering, H.; Kohlhaas, T.; Romstedt, H.; Hauser, A.; Bruns-Yilmaz, C.; Kusz, J.; Gütlich, P. *Coord. Chem. Rev.* **1999**, *190–192*, 629.

(22) Hauser, A.; Jeftić, J.; Romstedt, H.; Hinek, R.; Spiering, H. *Coord. Chem. Rev.* **1999**, *190–192*, 471.

(23) Zhu, D.; Xu, Y.; Yu, Z.; Guo, Z.; Sang, H.; Liu, T.; You, X. *Chem. Mater.* **2002**, *14*, 838.

(24) Jin Zhong, Z.; Tao, J.-Q.; Yu, Z.; Dun, C.-Y.; Liu, Y.-J.; You, X.-Z. *J. Chem. Soc., Dalton Trans.* **1998**, 327.

(25) Bushuev, M. B.; Daletsky, V. A.; Pishchur, D. P.; Gatilov, Y. V.; Korolkov, I. V.; Nikolaenkova, E. B.; Krivopalov, V. P. *Dalton Trans.* **2014**, *43*, 3906.

(26) Halcrow, M. A. *Chem. Lett.* **2014**, *43*, 1178.

(27) Müller, B. R.; Leibeling, G.; Jäger, E.-G. *Chem. Phys. Lett.* **2000**, *319*, 368.

(28) Weber, B.; Bauer, W.; Obel, J. *Angew. Chem. Int. Ed.* **2008**, *47*, 10098.

(29) Weber, B. In *Spin-Crossover Materials*; John Wiley & Sons Ltd: 2013, p 55.

(30) Petrouleas, V.; Tuchagues, J. P. *Chem. Phys. Lett.* **1987**, *137*, 21.

(31) Boinnard, D.; Bousseksou, A.; Dworkin, A.; Savariault, J. M.; Varret, F.; Tuchagues, J. P. *Inorg. Chem.* **1994**, *33*, 271.

(32) Burnett, M. G.; McKee, V.; Nelson, S. M. *J. Chem. Soc., Dalton Trans.* **1981**, 1492.

(33) Amendola, V.; Boiocchi, M.; Colasson, B.; Fabbrizzi, L.; Rodriguez Douton, M.-J.; Ugozzoli, F. *Angew. Chem. Int. Ed.* **2006**, *45*, 6920.

(34) Barrett, S. A.; Kilner, C. A.; Halcrow, M. A. *Dalton Trans.* **2011**, *40*, 12021.

(35) Halcrow, M. A. *Chem Soc Rev* **2011**, *40*, 4119.

(36) Li, B.; Wei, R.-J.; Tao, J.; Huang, R.-B.; Zheng, L.-S.; Zheng, Z. *J. Am. Chem. Soc.* **2010**, *132*, 1558.

(37) Real, A.; Zarembowitch, J.; Kahn, O.; Solans, X. *Inorg. Chem.* **1987**, *26*, 2939.

(38) Ruben, M.; Breuning, E.; Lehn, J.-M.; Ksenofontov, V.; Renz, F.; Gütlich, P.; Vaughan, G. B. M. *Chemistry – A European Journal* **2003**, *9*, 4422.

(39) Shatruk, M.; Dragulescu-Andrasi, A.; Chambers, K. E.; Stoian, S. A.; Bominaar, E. L.; Achim, C.; Dunbar, K. R. *J. Am. Chem. Soc.* **2007**, *129*, 6104.

(40) Duriska, M. B.; Neville, S. M.; Moubaraki, B.; Cashion, J. D.; Halder, G. J.; Chapman, K. W.; Balde, C.; Létard, J.-F.; Murray, K. S.; Kepert, C. J.; Batten, S. R. *Angew. Chem. Int. Ed.* **2009**, *48*, 2549.

(41) Carmen Muñoz, M.; Antonio Real, J. In *Spin-Crossover Materials*; John Wiley & Sons Ltd: 2013, p 121.

(42) Sim, P. G.; Sinn, E. *J. Am. Chem. Soc.* **1981**, *103*, 241.

(43) Garcia, Y.; Gütlich, P. In *Spin Crossover in Transition Metal Compounds II*; Springer Berlin Heidelberg: 2004; Vol. 234, p 49.

(44) Morgan, G. G.; Murnaghan, K. D.; Müller-Bunz, H.; McKee, V.; Harding, C. J. *Angew. Chem. Int. Ed.* **2006**, *45*, 7192.

(45) Nihei, M.; Shiga, T.; Maeda, Y.; Oshio, H. *Coord. Chem. Rev.* **2007**, *251*, 2606.

(46) Cambi, L.; Szegö, L. *Berichte der deutschen chemischen Gesellschaft (A and B Series)* **1931**, *64*, 2591.

(47) Cambi, L.; Szegö, L. *Berichte der deutschen chemischen Gesellschaft (A and B Series)* **1933**, *66*, 656.

(48) Mukherjee, S.; Weyhermüller, T.; Bill, E.; Wieghardt, K.; Chaudhuri, P. *Inorg. Chem.* **2005**, *44*, 7099.

(49) Jørgensen, C. K. *Coord. Chem. Rev.* **1966**, *1*, 164.

(50) Krivokapic, I.; Zerara, M.; Daku, M. L.; Vargas, A.; Enachescu, C.; Ambrus, C.; Tregenna-Piggott, P.; Amstutz, N.; Krausz, E.; Hauser, A. *Coord. Chem. Rev.* **2007**, *251*, 364.

(51) Hayami, S.; Komatsu, Y.; Shimizu, T.; Kamihata, H.; Lee, Y. H. *Coord. Chem. Rev.* **2011**, *255*, 1981.

(52) Stoufer, R. C.; Busch, D. H.; Hadley, W. B. *J. Am. Chem. Soc.* **1961**, *83*, 3732.

(53) Mizuno, K.; Lunsford, J. H. *Inorg. Chem.* **1983**, *22*, 3484.

(54) Tiwary, S. K.; Vasudevan, S. *Chem. Phys. Lett.* **1997**, *277*, 84.

(55) Tiwary, S. K.; Vasudevan, S. *Inorg. Chem.* **1998**, *37*, 5239.

(56) Venkataramani, S.; Jana, U.; Dommaschk, M.; Sönnichsen, F. D.; Tuczek, F.; Herges, R. *Science* **2011**, *331*, 445.

(57) Swart, M.; Groenhof, A. R.; Ehlers, A. W.; Lammertsma, K. *J. Phys. Chem. A* **2004**, *108*, 5479.

(58) Guell, M.; Luis, J. M.; Sola, M.; Swart, M. *J. Phys. Chem. A* **2008**, *112*, 6384.

(59) Swart, M. *J. Chem. Theory Comput.* **2008**, *4*, 2057.

(60) Swart, M.; Guell, M.; Sola, M. *Phys. Chem. Chem. Phys.* **2011**, *13*, 10449.

(61) Ye, S. F.; Neese, F. *Inorg. Chem.* **2010**, *49*, 772.

(62) Pierloot, K.; Vancoillie, S. *J. Chem. Phys.* **2006**, *125*.

(63) Jensen, F. *Introduction to Computational Chemistry*; 2nd edn. ed.; John Wiley & Sons Ltd: Chichester, 2007.

(64) Neese, F. *J. Biol. Inorg. Chem.* **2006**, *11*, 702.

(65) Koch, W.; Holthausen, M. C. *A Chemist's Guide to Density Functional Theory*; Wiley-VCH: Weinheim, 2000.

(66) Hohenberg, P.; Kohn, W. *Physical Review* **1964**, *136*, B864.

(67) Vosko, S. H.; Wilk, L.; Nusair, M. *Can. J. Phys.* **1980**, *58*, 1200.

(68) Perdew, J. P.; Burke, K.; Ernzerhof, M. *Phys. Rev. Lett.* **1996**, *77*, 3865.

(69) Perdew, J. P.; Burke, K.; Ernzerhof, M. *Phys. Rev. Lett.* **1997**, *78*, 1396.

(70) Becke, A. D. *Phys. Rev. A* **1988**, *38*, 3098.

(71) Harvey, J. N. *Struct. Bond.* **2004**, *112*, 151.

(72) Daku, L. M. L.; Vargas, A.; Hauser, A.; Fouqueau, A.; Casida, M. E. *ChemPhysChem* **2005**, *6*, 1393.

(73) Deeth, R. J.; Fey, N. *J. Comput. Chem.* **2004**, *25*, 1840.

(74) Handy, N. C.; Cohen, A. J. *Molecular Physics* **2001**, *99*, 403.

(75) Hoe, W.-M.; Cohen, A. J.; Handy, N. C. *Chem. Phys. Lett.* **2001**, *341*, 319.

(76) Becke, A. D. *J. Chem. Phys.* **1986**, *84*, 4524.

(77) Swart, M.; Solà, M.; Bickelhaupt, F. M. *J. Chem. Phys.* **2009**, *131*.

(78) Sellmann, D.; Soglowek, W.; Knoch, F.; Ritter, G.; Dengler, J. *Inorg. Chem.* **1992**, *31*, 3711.

(79) Becke, A. D. *J. Chem. Phys.* **1993**, *98*, 5648.

(80) Reiher, M.; Salomon, O.; Hess, B. A. *Theor. Chem. Acc.* **2001**, *107*, 48.

(81) Respondek, I.; Bressel, L.; Saalfrank, P.; Kampf, H.; Grohmann, A. *Chem. Phys.* **2008**, *347*, 514.

(82) Jensen, K. P.; Cirera, J. *J. Phys. Chem. A* **2009**, *113*, 10033.

(83) Andersson, K.; Malmqvist, P. A.; Roos, B. O. *J. Chem. Phys.* **1992**, *96*, 1218.

(84) Jensen, F. *Introduction to computational chemistry*; 2nd ed. ed.; Wiley: Chichester, 2007.

(85) Fouqueau, A.; Mer, S.; Casida, M. E.; Daku, L. M. L.; Hauser, A.; Mineva, T.; Neese, F. *J. Chem. Phys.* **2004**, *120*, 9473.

(86) Kepp, K. P. *Coord. Chem. Rev.* **2013**, *257*, 196.

(87) Neese, F.; Liakos, D.; Ye, S. *JBIC Journal of Biological Inorganic Chemistry* **2011**, *16*, 821.

(88) Enachescu, C.; Nishino, M.; Miyashita, S. In *Spin-Crossover Materials*; John Wiley & Sons Ltd: 2013, p 455.

(89) Stoleriu, L.; Chakraborty, P.; Hauser, A.; Stancu, A.; Enachescu, C. *Phys. Rev. B* **2011**, *84*, 134102.

(90) Enachescu, C.; Stoleriu, L.; Stancu, A.; Hauser, A. *Phys. Rev. Lett.* **2009**, *102*, 257204.

(91) Deeth, R. J. *Adv. Inorg. Chem.* **2010**, *62*, 1.

(92) Burton, V. J.; Deeth, R. J.; Kemp, C. M.; Gilbert, P. J. *J. Am. Chem. Soc.* **1995**,

117, 8407.

(93) Burton, V. J.; Deeth, R. J. *J. Chem. Soc., Chem. Commun.* **1995**, 573.

(94) Deeth, R. J.; Anastasi, A. E.; Wilcockson, M. J. *J. Am. Chem. Soc.* **2010**, *132*, 6876.

(95) Deeth, R. J. *Inorg. Chem.* **2007**, *46*, 4492.

(96) Deeth, R. J.; Fey, N.; Williams-Hubbard, B. *J. Comput. Chem.* **2005**, *26*, 123.

(97) Deeth, R. J.; Anastasi, A.; Diedrich, C.; Randell, K. *Coord. Chem. Rev.* **2009**, *253*, 795.

(98) Halgren, T. A. *J. Comput. Chem.* **1996**, *17*, 490.

(99) Schäffer, C. E.; Jørgensen, C. K. *Mol. Phys.* **1965**, *9*, 401.

(100) Figgis, B. N.; Hitchman, M. A. *Ligand Field Theory and Its Applications*; Wiley-VCH: New York, 2000.

(101) Deeth, R. J.; Fey, N.; Williams–Hubbard, B. *J. Comput. Chem.* **2005**, *26*, 123.

(102) Deeth, R. J.; Hearnshaw, L. J. A. *Dalton Trans.* **2006**, 1092.

(103) Brodbeck, R.; Deeth, R. J. *Dalton Trans.* **2011**, *40*, 11147.

(104) Warshel, A.; Lifson, S. *J. Chem. Phys.* **1970**, *53*, 582.

(105) Allinger, N. L.; Yuh, Y. H.; Lii, J. H. *J. Am. Chem. Soc.* **1989**, *111*, 8551.

(106) Maple, J. R.; Hwang, M. J.; Stockfisch, T. P.; Dinur, U.; Waldman, M.; Ewig, C. S.; Hagler, A. T. *J. Comput. Chem.* **1994**, *15*, 162.

(107) Norrby, P.-O.; Liljefors, T. *J. Comput. Chem.* **1998**, *19*, 1146.

(108) Mostaghim, S.; Hoffmann, M.; Konig, P. H.; Frauenheim, T.; Teich, J. In *Evolutionary Computation, 2004. CEC2004. Congress on* 2004; Vol. 1, p 212.

(109) Zitzler, E.; Thiele, L. *Evolutionary Computation, IEEE Transactions on* **1999**, *3*, 257.

(110) Deb, K.; Pratap, A.; Agarwal, S.; Meyarivan, T. *Evolutionary Computation, IEEE Transactions on* **2002**, *6*, 182.

(111) Root, D. M.; Landis, C. R.; Cleveland, T. *J. Am. Chem. Soc.* **1993**, *115*, 4201.

(112) Cleveland, T.; Landis, C. R. *J. Am. Chem. Soc.* **1996**, *118*, 6020.

(113) Landis, C. R.; Cleveland, T.; Firman, T. K. *J. Am. Chem. Soc.* **1998**, *120*, 2641.

(114) Firman, T. K.; Landis, C. R. *J. Am. Chem. Soc.* **2001**, *123*, 11728.

(115) Tubert-Brohman, I.; Schmid, M.; Meuwly, M. *J. Chem. Theory Comput.* **2009**, *5*, 530.

(116) Comba, P.; Hambley, T. W.; Martin, B. *Molecular Modeling of Inorganic Compounds*; Third Edition ed.; Wiley-VCH: Weinheim, 2009.

(117) Carlsson, A. E.; Zapata, S. *Biophys. J.* **2001**, *81*, 1.

(118) Xiang, J. Y.; Ponder, J. W. *J. Comput. Chem.* **2013**, *34*, 739.

(119) Cirera, J.; Babin, V.; Paesani, F. *Inorg. Chem.* **2014**, *53*, 11020.

(120) E.J. Baerends, T. Z., J. Autschbach, D. Bashford, A. Bérces, F.M. Bickelhaupt, C. Bo, P.M. Boerrigter, L. Cavallo, D.P. Chong, L. Deng, R.M. Dickson, D.E. Ellis, M. van Faassen, L. Fan, T.H. Fischer, C. Fonseca Guerra, A. Ghysels, A. Giammona, S.J.A. van Gisbergen, A.W. Götz, J.A. Groeneveld, O.V. Gritsenko, M. Grüning, S. Gusarov, F.E. Harris, P. van den Hoek, C.R. Jacob, H. Jacobsen, L. Jensen, J.W. Kaminski, G. van Kessel, F. Kootstra, A. Kovalenko, M.V. Krykunov, E. van Lenthe, D.A. McCormack, A. Michalak, M. Mitoraj, J. Neugebauer, V.P. Nicu, L. Noodleman, V.P. Osinga, S. Patchkovskii, P.H.T. Philipsen, D. Post, C.C. Pye, W. Ravenek, J.I. Rodríguez, P. Ros, P.R.T. Schipper, G. Schreckenbach, J.S. Seldenthuis, M. Seth, J.G. Snijders, M. Solà, M. Swart, D. Swerhone, G. te Velde, P. Vernooijs, L. Versluis, L. Visscher, O. Visser, F. Wang, T.A. Wesolowski, E.M. van Wezenbeek, G. Wiesenekker, S.K. Wolff, T.K. Woo, A.L. Yakovlev, ADF2012.01, SCM, Theoretical Chemistry, Vrije Universiteit, Amsterdam, The Netherlands, 2012.

(121) Boeyens, J. C. A.; Forbes, A.; Hancock, R. D.; Wieghardt, K. *Inorg. Chem.* **1985**, *24*, 2926.

(122) Ammeter, J. H.; Bucher, R.; Oswald, N. *J. Am. Chem. Soc.* **1974**, *96*, 7833.

(123) Klamt, A.; Schuurmann, G. *J. Chem. Soc. Perk. Trans. 2* **1993**, 799.

(124) Hocking, R. K.; Deeth, R. J.; Hambley, T. W. *Inorg. Chem.* **2007**, *46*, 8238.

(125) Kepp, K. P. *Journal of Inorganic Biochemistry* **2011**, *105*, 1286.

(126) Perdew, J. P. *Phys. Rev. B* **1986**, *33*, 8822.

(127) Schäfer, A.; Horn, H.; Ahlrichs, R. *J. Chem. Phys.* **1992**, *97*, 2571.

(128) Baerends, E. J.; Ellis, D. E.; Ros, P. *Chem. Phys.* **1973**, *2*, 41.

(129) Neese, F. *Wiley Interdisciplinary Reviews: Computational Molecular Science* **2012**, *2*, 73.

(130) Börzel, H.; Comba, P.; Pritzkow, H.; Sickmüller, A. F. *Inorg. Chem.* **1998**, *37*, 3853.

(131) Ghisletta, M.; Hausherr-Primo, L.; Gajda-Schrantz, K.; Machula, G.; Nagy, L.; Schmalle, H. W.; Rihs, G.; Endres, F.; Hegetschweiler, K. *Inorg. Chem.* **1998**, *37*, 997.

(132) König, E.; Watson, K. J. *Chem. Phys. Lett.* **1970**, *6*, 457.

(133) Konno, M.; Mikami-Kido, M. *Bull. Chem. Soc. Jpn.* **1991**, *64*, 339.

(134) Martin, L. L.; Hagen, K. S.; Hauser, A.; Martin, R. L.; Sargeson, A. M. *J. Chem. Soc., Chem. Commun.* **1988**, *0*, 1313.

(135) Jensen, K. P.; Roos, B. O.; Ryde, U. *J. Chem. Phys.* **2007**, *126*, 014103.

(136) Grimme, S. *J. Comput. Chem.* **2004**, *25*, 1463.

(137) Grimme, S. *J. Comput. Chem.* **2006**, *27*, 1787.

(138) Jurecka, P.; Sponer, J.; Cerny, J.; Hobza, P. *Phys. Chem. Chem. Phys.* **2006**, *8*, 1985.

(139) Grimme, S.; Antony, J.; Ehrlich, S.; Krieg, H. *J. Chem. Phys.* **2010**, *132*, 154104.

(140) Hansch, C.; Leo, A.; Taft, R. W. *Chemical Reviews* **1991**, *91*, 165.

(141) Hoe, W. M.; Cohen, A. J.; Handy, N. C. *Chem. Phys. Lett.* **2001**, *341*, 319.

(142) Van Lenthe, E.; Baerends, E. J. *J. Comput. Chem.* **2003**, *24*, 1142.

(143) Baerends, E. J.; Ellis, D. E.; Ros, P. *Theor. Chim. Acta* **1972**, *27*, 339.

(144) Molecular Operating Environment (MOE), C. C. G. I., 1010 Sherbooke St. West, Suite #910, Montreal, QC, Canada, H3A 2R7, **2010**.

(145) *Molecular Operating Environment (MOE), 2011.10; Chemical Computing Group Inc., 1010 Sherbooke St. West, Suite #910, Montreal, QC, Canada, H3A 2R7, 2011.*

(146) Katz, B. A.; Strouse, C. E. *Inorg. Chem.* **1980**, *19*, 658.

(147) Katz, B. A.; Strouse, C. E. *J. Am. Chem. Soc.* **1979**, *101*, 6214.

(148) Bushuev, M. B.; Jeanneau, E.; Luneau, D.; Matouzenko, G. S. *Inorg. Chim. Acta* **2007**, *360*, 1639.

(149) Alcock, N. W.; Zhang, D.; Busch, D. H. *Acta Crystallographica Section C* **1999**, *55*, 886.

(150) Chang, H. R.; McCusker, J. K.; Toftlund, H.; Wilson, S. R.; Trautwein, A. X.; Winkler, H.; Hendrickson, D. N. *J. Am. Chem. Soc.* **1990**, *112*, 6814.

(151) Buron-Le Cointe, M.; Ould Moussa, N.; Trzop, E.; Moréac, A.; Molnar, G.; Toupet, L.; Bousseksou, A.; Létard, J. F.; Matouzenko, G. S. *Phys. Rev. B* **2010**, *82*, 214106.

(152) Matouzenko, G. S.; Borshch, S. A.; Jeanneau, E.; Bushuev, M. B. *Chemistry – A European Journal* **2009**, *15*, 1252.

(153) Arulsamy, N.; Glerup, J.; Hodgson, D. J. *Inorg. Chem.* **1994**, *33*, 3043.

(154) Hammett, L. P. *J. Am. Chem. Soc.* **1937**, *59*, 96.

(155) Klamt, A. *J. Phys. Chem.* **1995**, *99*, 2224.

(156) Klamt, A.; Jonas, V. *J. Chem. Phys.* **1996**, *105*, 9972.

(157) Pye, C. C.; Ziegler, T. *Theor. Chem. Acc.* **1999**, *101*, 396.

(158) Mulliken, R. S. *J. Chem. Phys.* **1955**, *23*, 1833.

(159) Halgren, T. A. *J. Comput. Chem.* **1996**, *17*, 520.

(160) Reed, A. E.; Weinhold, F. *J. Chem. Phys.* **1983**, *78*, 4066.

(161) Reed, A. E.; Weinstock, R. B.; Weinhold, F. *J. Chem. Phys.* **1985**, *83*, 735.

(162) Deeth, R. J.; Randell, K. *Inorg. Chem.* **2008**, *47*, 7377.

(163) Frisch, M. J.; Trucks, G. W.; Schlegel, H. B.; Scuseria, G. E.; Robb, M. A.; Cheeseman, J. R.; J. A. Montgomery, J.; Vreven, T.; Kudin, K. N.; Burant, J. C.; Millam,

J. M.; Iyengar, S. S.; Tomasi, J.; Barone, V.; Mennucci, B.; Cossi, M.; Scalmani, G.; Rega, N.; Petersson, G. A.; Nakatsuji, H.; Hada, M.; Ehara, M.; Toyota, K.; Fukuda, R.; Hasegawa, J.; Ishida, M.; Nakajima, T.; Honda, Y.; Kitao, O.; Nakai, H.; Klene, M.; Li, X.; Knox, J. E.; Hratchian, H. P.; Cross, J. B.; Bakken, V.; Adamo, C.; Jaramillo, J.; Gomperts, R.; Stratmann, R. E.; Yazyev, O.; Austin, A. J.; Cammi, R.; Pomelli, C.; Ochterski, J. W.; Ayala, P. Y.; Morokuma, K.; Voth, G. A.; Salvador, P.; Dannenberg, J. J.; Zakrzewski, V. G.; Dapprich, S.; Daniels, A. D.; Strain, M. C.; Farkas, O.; Malick, D. K.; Rabuck, A. D.; Raghavachari, K.; Foresman, J. B.; Ortiz, J. V.; Cui, Q.; Baboul, A. G.; Clifford, S.; Cioslowski, J.; Stefanov, B. B.; Liu, G.; Liashenko, A.; Piskorz, P.; Komaromi, I.; Martin, R. L.; Fox, D. J.; Keith, T.; Al-Laham, M. A.; Peng, C. Y.; Nanayakkara, A.; Challacombe, M.; Gill, P. M. W.; Johnson, B.; Chen, W.; Wong, M. W.; Gonzalez, C.; Pople, J. A.; Gaussian 03 Revision D.01, Gaussian Inc., Wallingford CT,: 2004.

(164) Norrby, P.-O.; Brandt, P. *Coord. Chem. Rev.* **2001**, *212*, 79.

(165) Matsumoto, T.; Chang, H.-C.; Wakizaka, M.; Ueno, S.; Kobayashi, A.; Nakayama, A.; Taketsugu, T.; Kato, M. *J. Am. Chem. Soc.* **2013**, *135*, 8646.

(166) Deeth, R. J. *J. Chem. Soc., Dalton Trans.* **2001**, 664.

(167) Ferguson, D. M.; Raber, D. J. *J. Am. Chem. Soc.* **1989**, *111*, 4371.

(168) Curtis, N. F.; Gladkikh, O. P. *Aust. J. Chem.* **2000**, *53*, 727.

(169) Chen, L.; Cotton, F. A. *Inorg. Chim. Acta* **1997**, *263*, 9.

(170) Broge, L.; Pretzmann, U.; Jensen, N.; Søtofte, I.; Olsen, C. E.; Springborg, J. *Inorg. Chem.* **2001**, *40*, 2323.

(171) Endicott, J. F.; Lilie, J.; Kuszaj, J. M.; Ramaswamy, B. S.; Schmonsees, W. G.; Simic, M. G.; Glick, M. D.; Rillema, D. P. *J. Am. Chem. Soc.* **1977**, *99*, 429.

(172) Knoch, F.; Thaler, F.; Schindler, S. *Z. Kristall.* **1996**, *211*, 717.

(173) Krossing, I.; Raabe, I. *Angew. Chem. Int. Ed.* **2004**, *43*, 2066.

(174) Hubin, T. J.; Alcock, N. W.; Busch, D. H. *Acta Crystallographica Section C* **2000**,

56, 37.

(175) Hubin, T. J., University of Kansas, 1999.

(176) Donoghue, P. J.; Helquist, P.; Norrby, P.-O.; Wiest, O. *J. Chem. Theory Comput.* **2008**, *4*, 1313.

Appendix 1 – ADFs Functionals (called by the METAGGA and HARTREEFOCK Keywords) and their References as extracted from an ADF output.

KCIS-modified	[1]	M06-L	[39]
KCIS-original	[2]	BLYP-D	[40]
PKZB	[3]	BP86-D	[41]
VS98	[4]	PBE-D	[42]
LDA(VWN)	[5]	TPSS-D	[43]
PW91	[6]	B97-D	[44]
BLYP	[7]	revTPSS	[45]
BP	[8]	PBEsol	[46]
PBE	[9]	RGE2	[47]
RPBE	[10]	SSB-D	[48]
revPBE	[11]	SOGGA	[49]
OLYP	[12]	SOGGA11	[50]
FT97	[13]	TPSSh	[51]
BLAP3	[14]	B3LYP(VWN5)	[52]
HCTH/93	[15]	O3LYP(VWN5)	[53]
HCTH/120	[16]	KMLYP(VWN5)	[54]
HCTH/147	[17]	PBE0	[55]
HCTH/407	[18]	B3LYP*(VWN5)	[56]
BmTau1	[19]	BHandH	[57]
BOP	[20]	BHandHLYP	[58]
PKZBx-KCIScor	[21]	B97	[59]
VS98-x(xc)	[22]	B97-1	[60]
VS98-x-only	[23]	B97-2	[61]
Becke00	[24]	mPBE0KCIS	[62]
Becke00x(xc)	[25]	mPBE1KCIS	[63]
Becke00-x-only	[26]	B1LYP(VWN5)	[64]
Becke88x+BR89c	[27]	B1PW91(VWN5)	[65]
OLAP3	[28]	mPW1PW	[66]
TPSS	[29]	mPW1K	[67]
mPBE	[30]	tau-HCTH-hybrid	[68]
OPBE	[31]	X3LYP(VWN5)	[69]
OPerdew	[32]	OPBE0	[70]
mPBEKCIS	[33]	M05	[71]
mPW	[34]	M05-2X	[72]
tau-HCTH	[35]	M06	[73]
XLYP	[36]	M06-2X	[74]
KT1	[37]	B3LYP-D	[75]
KT2	[38]		

[1] J.B. Krieger, J. Chen, G.J. Iafrate, and S. Kurth

modified Krieger-Chen-Iafrate-Savin functional, unpublished

[2] original Krieger-Chen-Iafrate-Savin functional

J.B. Krieger, J. Chen, G.J. Iafrate, and A. Savin

In: Electron Correlations and Materials Properties

Editors: A. Gonis and N. Kioussis (Plenum, New York, 1999)

[3] J.P. Perdew, S. Kurth, A. Zupan, and P. Blaha

Phys. Rev. Lett. 82 (1999) 2544, Ibid. E 82 (1999) 5179

[4] T. van Voorhis and G.E. Scuseria, J. Chem. Phys. 109 (1998) 400

[5] S.H. Vosko, L. Wilk, and M. Nusair, Can. J. Phys. 58 (1980) 1200

[6] J.P. Perdew in: Electronic Structure of Solids 1991

Ed. P. Ziesche and H. Eschrig (Akademie, Berlin, 1991) p. 11

and

J.P. Perdew, J.A. Chevary, S.H. Vosko, K.A. Jackson, M.R. Pederson

D.J. Singh, and C. Fiolhais, Phys. Rev. B46 (1992) 6671

Ibid. E 48 (1993) 4978

[7] A.D. Becke, Phys. Rev. A38 (1988) 3098

and

C. Lee, W. Yang, and R.G. Parr, Phys. Rev. B37 (1988) 785

[8] A.D. Becke, Phys. Rev. A38 (1988) 3098

and

J.P. Perdew, Phys. Rev. B33 (1986) 8822

Erratum: J.P. Perdew, Phys. Rev. B34 (1986) 7406

[9] J.P. Perdew, K. Burke, and M. Ernzerhof, Phys. Rev. Lett. 77 (1996) 3865, Ibid. E 78 (1997) 1396

[10] B. Hammer, L.B. Hansen, J.K. Norskov, Phys. Rev. B59 (1999) 7413

[11] Y. Zhang and W. Yang, Phys. Rev. Lett. 80 (1998) 890

[12] N.C. Handy, and A.J. Cohen Mol.Phys.99 (2001) 403

and

C. Lee, W. Yang, and R.G. Parr, Phys. Rev. B37 (1988) 785

[13] M. Filatov and W. Thiel, Mol. Phys. 91 (1997) 847

[14] E.I. Proynov, S. Sirois, and D.R. Salahub, Int. J. Quant. Chem. 64 (1997) 427

[15] F.A. Hamprecht, A.J. Cohen, D.J. Tozer, and N.C. Handy, J. Chem. Phys. 109 (1998) 6264

[16] A.D. Boese, N.L. Doltsinis, N.C. Handy, and M. Sprik, J. Chem. Phys. 112 (2000), 1670

[17] A.D. Boese, N.L. Doltsinis, N.C. Handy, and M. Sprik, J. Chem. Phys. 112 (2000), 1670

[18] A.D. Boese and N.C. Handy, J. Chem. Phys. 114, (2001) 5497

[19] E.I. Proynov, H. Chermette, and D.R. Salahub, J. Chem. Phys. 113, (2000) 10013

[20] A.D. Becke, Phys. Rev. A38 (1988) 3098

and

T. Tsuneda, T. Suzumura, and K. Hirao, J. Chem. Phys. 110 (1999) 10664

[21] PKZB exchange, KCIS correlation as in

S. Kurth, J.P. Perdew, and P. Blaha, Int. J. Quant. Chem. 75 (1999) 889

[24] A.D. Becke, J. Chem. Phys. 112 (2000) 4020

[25] A.D. Becke, J. Chem. Phys. 112 (2000) 4020

[26] A.D. Becke, J. Chem. Phys. 112 (2000) 4020

[27] A.D. Becke and M.R. Roussel, Phys. Rev. A39 (1989) 3761

A.D. Becke, J. Chem. Phys. 88 (1988) 1053

A.D. Becke, Int. J. Quant. Chem. (Symp.) 28 (1994) 625

[28] N.C. Handy, and A.J. Cohen Mol.Phys.99 (2001) 403

and

E.I. Proynov, S. Sirois, and D.R. Salahub, Int. J. Quant. Chem. 64 (1997) 427

[29] J. Tao, J.P. Perdew, V.N. Staroverov and G.E. Scuseria, Phys. Rev. Lett. 91 (2003) 146401

V.N. Staroverov, G.E. Scuseria, J. Tao and J.P. Perdew, J. Chem. Phys. 119(23) (2003) 12129-12137

[30] C. Adamo, V. Barone, J. Chem. Phys. 116 (2002) 5933

[31] M. Swart, A.W. Ehlers, K. Lammertsma, Mol. Phys. 102 (2004) 2467

see also:

N.C. Handy, and A.J. Cohen Mol.Phys.99 (2001) 403

J.P. Perdew, K. Burke, and M. Ernzerhof, Phys. Rev. Lett. 77 (1996) 3865, 78 (1997) 1396

[32] N.C. Handy, and A.J. Cohen Mol.Phys.99 (2001) 403

and

J.P. Perdew, Phys. Rev. B33 (1986) 8822

Erratum: J.P. Perdew, Phys. Rev. B34 (1986) 7406

[33] J. Toulouse and C. Adamo, Chem. Phys. Lett. 362 (2002) 72

[34] C. Adamo and V. Barone, J. Chem. Phys. 108 (1998) 664

[35] A.D. Boese and N.C. Handy, J. Chem. Phys. 116 (2002) 9559

[36] X. Xu and W.A. Goddard III, PNAS 101 (2004) 2673

[37] T.W. Keal and D.J. Tozer, J. Chem. Phys. 119 (2003) 3015

[38] T.W. Keal and D.J. Tozer, J. Chem. Phys. 119 (2003) 3015

[39] Y. Zhao and D.G. Truhlar, J. Chem. Phys. 125 (2006) 194101

[40] S. Grimme, J. Comput. Chem. 27 (2006) 1787

[41] S. Grimme, J. Comput. Chem. 27 (2006) 1787

[42] S. Grimme, J. Comput. Chem. 27 (2006) 1787

[43] S. Grimme, J. Comput. Chem. 27 (2006) 1787

[44] S. Grimme, J. Comput. Chem. 27 (2006) 1787

[45] J.P. Perdew, A. Ruzsinszky, G.I. Csonka, L.A. Constantin, and J. Sun,

Phys. Rev. Lett. 103, 026403 (2009)

[46] J.P. Perdew, A. Ruzsinszky, G.I. Csonka, O.A. Vydrov, G.E. Scuseria, L.A. Constantin, X. Zhou, and K. Burke, Phys. Rev. Lett. 100, 136406 (2008)

[47] A. Ruzsinszky, G.I. Csonka, and G.E. Scuseria, J. Chem. Theory Comput. 5, 763 (2009)

[48] M. Swart, M. Sola and F.M. Bickelhaupt, J. Chem. Phys. 2009, 131, 094103

See also: J. Comp. Meth. Sci. Engin. 2009, 9, 69

Contains portions of :

Disp.Correction: S. Grimme, J. Comput. Chem. 27 (2006) 1787

KT1: T.W. Keal and D.J. Tozer, J. Chem. Phys. 119 (2003) 3015

[49] Zhao, Y.; Truhlar, D. G., J. Chem. Phys. 128, 184109 (2008)

[50] R. Peverati, Zhao, Y.; Truhlar, D. G., J. Phys. Chem. Lett. 2, 1991 (2011)

[51] J. Tao, J.P. Perdew, V.N. Staroverov and G.E. Scuseria, Phys. Rev. Lett. 91 (2003) 146401

V.N. Staroverov, G.E. Scuseria, J. Tao and J.P. Perdew, J. Chem. Phys. 119(23) (2003) 12129-12137

Exact exchange based on: M.A. Watson et al., J. Chem. Phys. 119(13) (2003) 6475-6481

[52] P.J. Stephens, F.J. Devlin, C.F. Chabalowski and M.J. Frisch, J. Phys. Chem. 98 (1994) 11623-11627

Exact exchange based on: M.A. Watson et al. J. Chem. Phys. 119(13) (2003) 6475-6481

VWN1/VWN5 see:

R.H. Hertwig, W. Koch, Chem. Phys. Lett. 268 (1997) 345-351

[53] A.J. Cohen and N.C. Handy, Mol. Phys., 99(7) (2001) 607-615

Exact exchange based on: M.A. Watson et al., J. Chem. Phys. 119(13) (2003) 6475-6481

[54] J.K. Kang and C.B. Musgrave, J. Chem. Phys. 115(24) (2001) 11040-11051

Exact exchange based on:

M.A. Watson et al., J. Chem. Phys. 119(13) (2003) 6475-6481

[55] J.P. Perdew, M. Ernzerhof and K. Burke, J. Chem. Phys. 105 (1996) 9982

M. Ernzerhof and G. Scuseria, J. Chem. Phys. 110 (1999) 5029

C. Adamo and V. Barone, J. Chem. Phys. 110 (1999) 6158

Exact exchange based on:

M.A. Watson et al., J. Chem. Phys. 119(13) (2003) 6475-6481

[56] M. Reiher, O. Salomon and B.A. Hess, Theor. Chem. Acc., 107 (2001) 48

Exact exchange based on:

M.A. Watson et al., J. Chem. Phys. 119(13) (2003) 6475-6481

VWN1/VWN5 see:

R.H. Hertwig, W. Koch, Chem. Phys. Lett. 268 (1997) 345-351

[57] 50% exact exchange and 50% LDA exchange, plus LYP correlation

Exact exchange based on:

M.A. Watson et al., J. Chem. Phys. 119(13) (2003) 6475-6481

C. Lee, W. Yang, and R.G. Parr, Phys. Rev. B37 (1988) 785

[58] 50% exact exchange and 50% Becke88 exchange, plus LYP correlation

Exact exchange based on: M.A. Watson et al.

J. Chem. Phys. 119(13) (2003) 6475-6481

C. Lee, W. Yang, and R.G. Parr, Phys. Rev. B37 (1988) 785

[59] A.D. Becke, J. Chem. Phys. 107(20) (1997) 8554

Exact exchange based on:

M.A. Watson et al., J. Chem. Phys. 119(13) (2003) 6475-6481

[60] F.A. Hamprecht, A.J. Cohen, D.J. Tozer and N.C. Handy, J. Chem. Phys. 109(15) (1998) 6264

Exact exchange based on:

M.A. Watson et al., J. Chem. Phys. 119(13) (2003) 6475-6481

[61] P.J. Wilson, T.J. Bradley and D.J. Tozer, J. Chem. Phys. 115(20) (2001) 9233

Exact exchange based on:

M.A. Watson et al., J. Chem. Phys. 119(13) (2003) 6475-6481

[62] J. Toulouse and C. Adamo, Chem. Phys. Lett. 362 (2002) 72

Exact exchange based on:

M.A. Watson et al., J. Chem. Phys. 119(13) (2003) 6475-6481

[63] J. Toulouse and C. Adamo, Chem. Phys. Lett. 362 (2002) 72

Exact exchange based on:

M.A. Watson et al., J. Chem. Phys. 119(13) (2003) 6475-6481

[64] C. Adamo and V. Barone, Chem. Phys. Lett. 274 (1997) 242

Exact exchange based on:

M.A. Watson et al., J. Chem. Phys. 119(13) (2003) 6475-6481

VWN1/VWN5 see: R.H. Hertwig, W. Koch, Chem. Phys. Lett. 268 (1997) 345-351

[65] C. Adamo and V. Barone, Chem. Phys. Lett. 274 (1997) 242

Exact exchange based on:

M.A. Watson et al., J. Chem. Phys. 119(13) (2003) 6475-6481

VWN1/VWN5 see:

R.H. Hertwig, W. Koch, Chem. Phys. Lett. 268 (1997) 345-351

[66] C. Adamo and V. Barone, J. Chem. Phys. 108 (1998) 664

Exact exchange based on:

M.A. Watson et al., J. Chem. Phys. 119(13) (2003) 6475-6481

[67] B.J. Lynch, P.L. Fast, M. Harris and D.G. Truhlar, J. Phys. Chem. A, 104 (2000) 4811

Exact exchange based on:

M.A. Watson et al. J. Chem. Phys. 119(13) (2003) 6475-6481

[68] A.D. Boese and N.C. Handy, J. Chem. Phys. 116 (2002) 9559

Exact exchange based on:

M.A. Watson et al. J. Chem. Phys. 119(13) (2003) 6475-6481

[69] X. Xu and W.A. Goddard III, PNAS 101 (2004) 2673

[70] OPBE mixed with 25% exact exchange

M. Swart, A.W. Ehlers, K. Lammertsma, Mol. Phys. 102 (2004) 2467

see also:

N.C. Handy, and A.J. Cohen Mol.Phys.99 (2001) 403

J.P. Perdew, K. Burke, and M. Ernzerhof, Phys. Rev. Lett. 77 (1996) 3865,

78 (1997) 1396

[71] Y. Zhao, N. E. Schultz and D.G. Truhlar, J. Chem. Phys. 123 (2005) 161103

[72] Y. Zhao, N. E. Schultz and D.G. Truhlar, J. Chem. Theory Comput. 2 (2006) 364

[73] Y. Zhao and D.G. Truhlar, Theor. Chem. Acc. 120 (2008) 215.

[74] Y. Zhao and D.G. Truhlar, Theor. Chem. Acc. 120 (2008) 215.

[75] S. Grimme, J. Comput. Chem. 27 (2006) 1787

Appendix 2 - The Use of DommiMOE as a Ligand Generation Tool

Using ethylenediamine as an example we will explore the generation of large numbers of unique bi-, tri-, tetra-, penta- and hexadentate ligands for coordination to metal centres. Within MOE (using the 2011 version for illustration) there are several drug discovery tools which can be used for this purpose; the most useful of these are Add Group to Ligand (R-Group addition), scaffold replacement and the combinatorial builder.

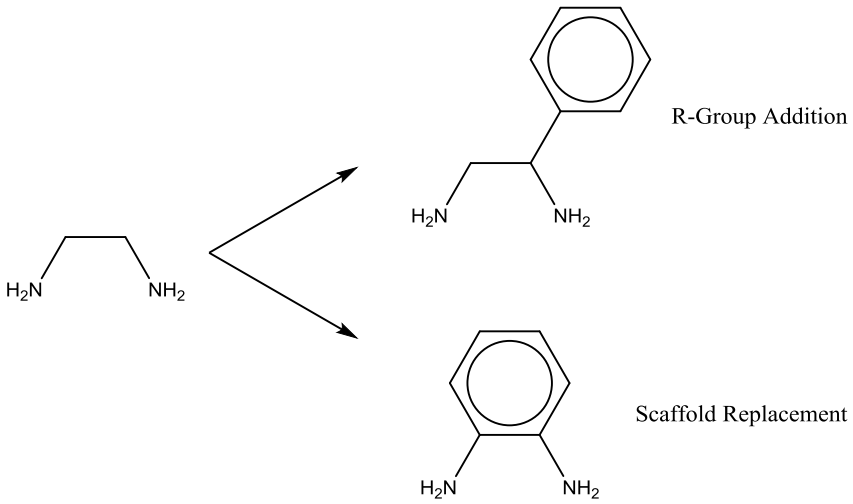

Figure A2.1; A pictorial depiction of R-Group Addition and scaffold replacement.

Bidentates

Bidentates are the simplest ligands to modify. Ethylenediamine has two carbons and eight hydrogens and these are all eligible to be switched or changed. Consider for instance the hydrogens; these form ideal addition points to grow the ligand through substituting them with R-groups from an R-group library, this leaves three unique possibilities for mono substitution.[**] To do this add R-groups to an R-group library, you can call this anything,

[**] Monosubstitution forms the default for this tool. The simplest way to get bis-substitution is to either run successive additions or to obtain them as a by-product of scaffold replacement, see next section.

then open the tool via Compute→Fragments→Add Group to Ligand and select it as the linker database. The default filter is aimed at drug discovery, insert in its place a filter specific for your problem or leave it blank to generate all options, this will be further explored later.

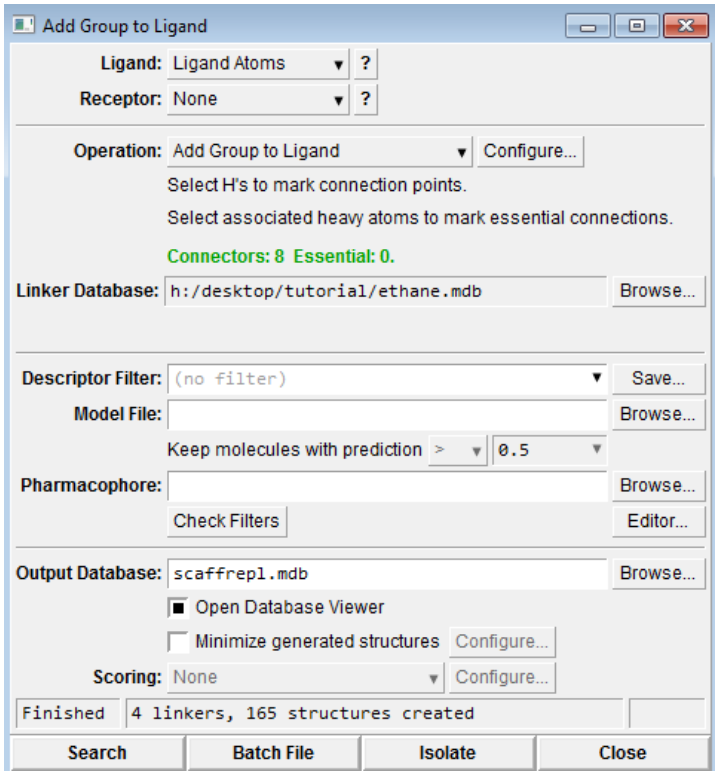

Figure A2.2; The window to access the Add Group to Ligand tool.

Imagine substituting one or more of the hydrogens with the carbons in a single propane.[††] The result of this is the sixteen unique ligands depicted in Figure 3. Figure 3 does not include all possible combinations as those which defy the internal rules are not generated. This is a key point to note with regard to this technique. Not all possible conformations are generated; the hope being that enough will be to understand substituent effects.

[††] Methane will not replace hydrogens in ethylenediamine, nor will it add ethane. However, once we reach propane additions can take place. This is a result of the underlying rules over which we have no control without altering MOEs internal code this is possible but by no means is it entry level.

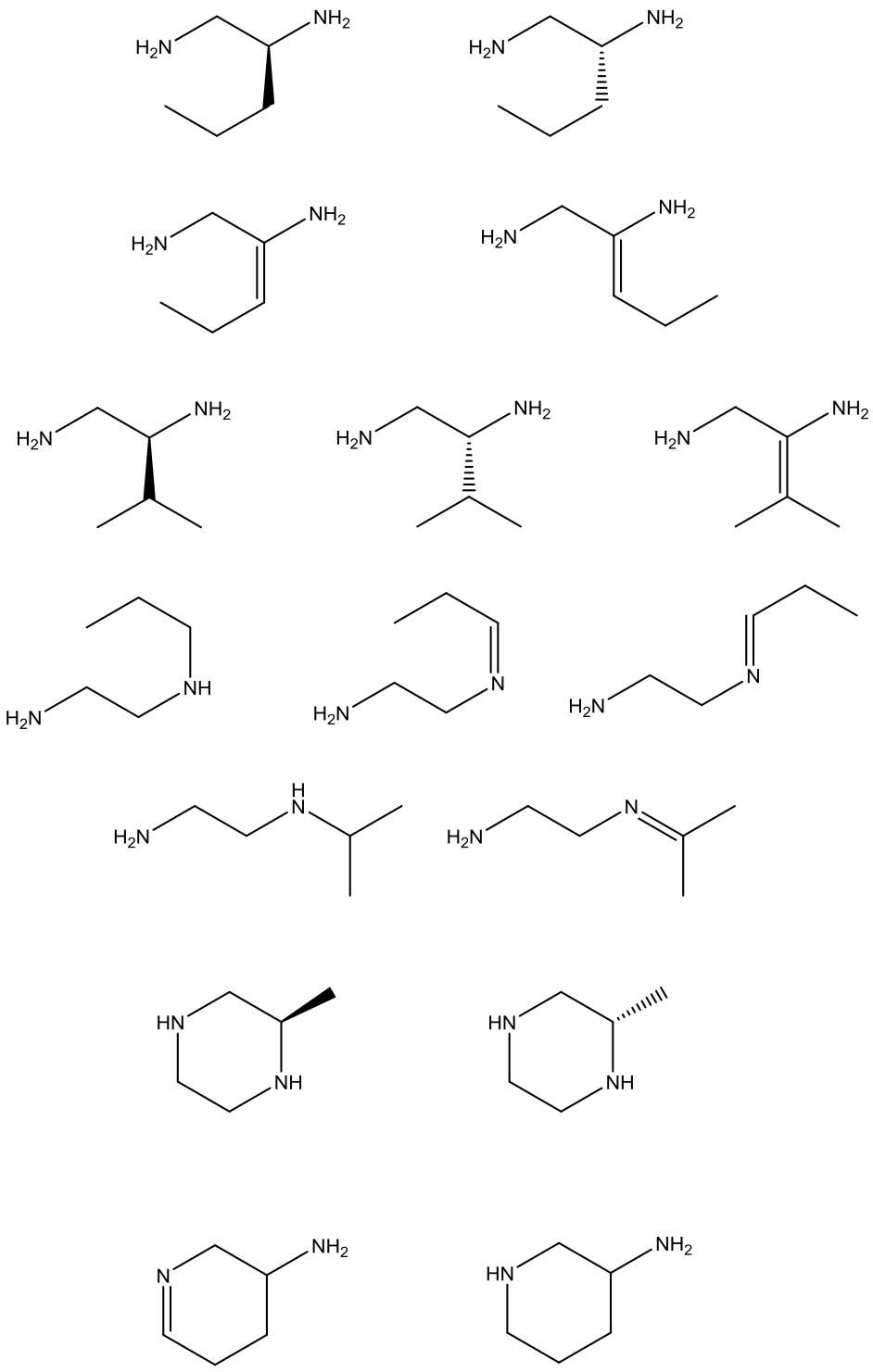

Figure A2.3; The sixteen ligands which result from the use of the R-Group addition tool with ethylenediamine as the ligand and propane as the R-Group.

One of substitution options is simple growth resulting in a nitrogen-carbon bond. If both hydrogens are replaced it would result in a double bond. The parameters to handle unsaturated ligand systems may not exist or the user simply may not be interested in them.

It’s simple to filter these out, in the filter line type “N=C”<1.

The second option for ligand growth is replacement and in the case of ethylenediamine the two carbon backbone form ideal points for replacement. MOE terms this the scaffold. It holds the groups at fixed positions but they do not necessarily care about the form and/or would like to try other options. What if these two carbons are replaced by aromatic carbons? The result of such a switch is also shown in Figure A2.1.

Now we understand what it does, how do we do it? It’s accessed from the same window as before (just change the operation). The window can be seen in Figure A2.4 below.

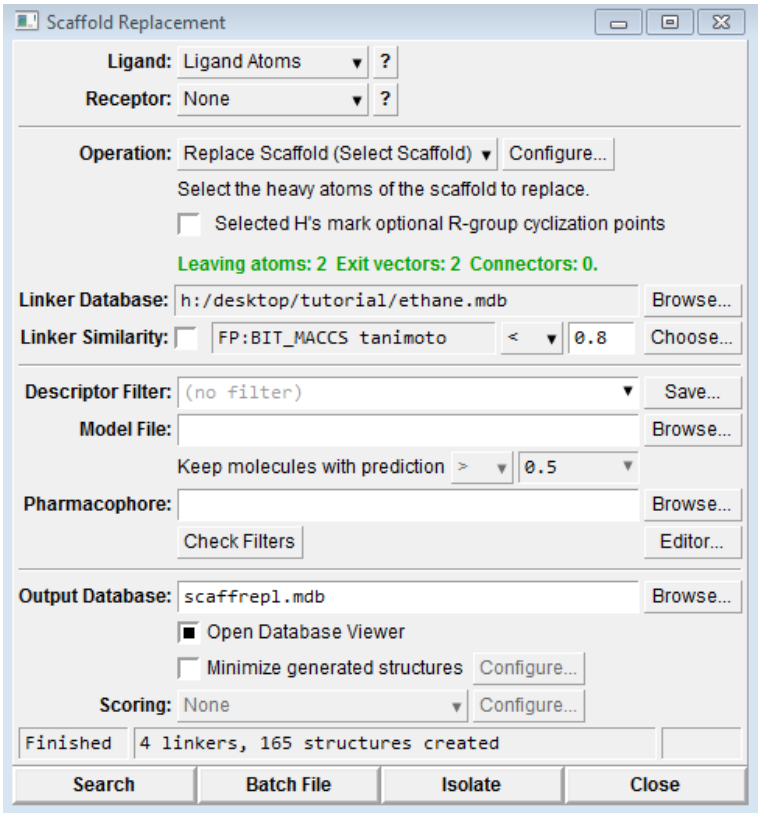

Figure A2.4; The window to access the Scaffold Replacement tool

Select in the ligand the scaffold, in ethylenediamine this is simply done by selecting the carbon-carbon bond. The exit vectors will be automatically defined.

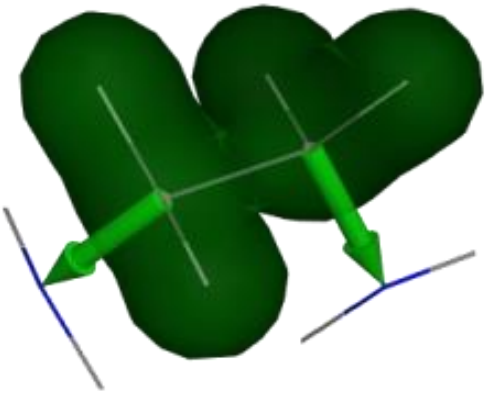

Figure A2.5; The scaffold of ethylenediamine selected for replacement with the green arrows indicating the exit vectors.

"Selected H's mark optional R-group cyclization points" is a self-explanatory tool which will introduce rings into the ligand. Neglect the Linker Similarity option, model file and pharmacophore options. Adding a filter if needed to remove unwanted ligands.

Growing the R-group library will result in near exponential growth of the number of generated ligands. Many of the ligands generated will be duplicates. The simplest way to remove these is to follow this procedure;

Duplicate the mol field →Convert to smiles → Select unique → Invert selection → Delete Selected entries

Now we have a database of unique bidentate ligands based upon ethylenediamine, the procedure could be duplicated for other ligands. Propylenediamine for instance. In the absence of suitable scaffold replacements few results will be generated so in this example selecting just two carbons for replacement may be prudent.

Tridentate Ligands

These can be built by addition from a chosen bidentate ligand and an R-Group library of "monodentates" or conversely from a monodentate using the previously generated bidentate ligand library as the R-groups. Either is a valid approach. The writer prefers using the latter approach several times on different monodentates.

Tetradentates

These can be formed by selecting a series of bidentates and coupling them to the bidentate library. More useful results may be found by selecting ligands with useful linking substituents (or adding them manually). This is not necessarily needed for all bidentates as the library should include them.

Tetradentate Macrocyclic Rings

Tetradentate macrocycles are prominent ligands in the literature. It is therefore useful to incorporate them in to any ligand search. MOE allows the writing of scripts which will carry out many molecular transformations. The easiest way it was found to form these rings was to identify within the tetradentate database backbones which could support a ring and to bridge them using a few different alkanes (the script written for this is included as an appendix and can be run easily within MOE.

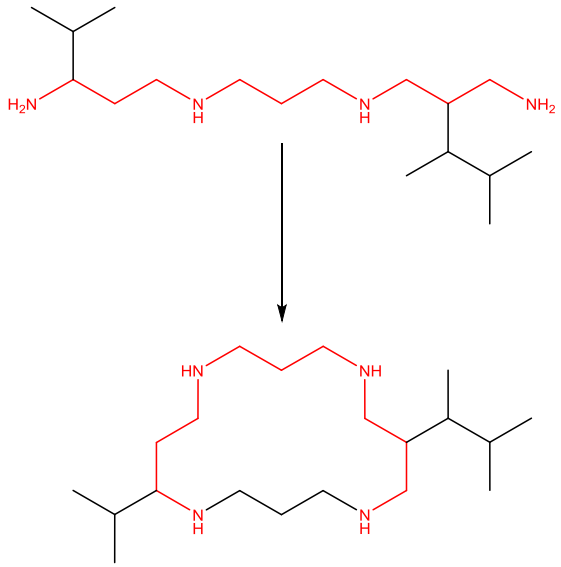

Figure A2.5; A depiction of the result of running a cyclisation routine.

Penta and Hexadentates

These can be formed in a similar manner to those above.

Addition to a Metal Centre

Use a script to identify the number of donors within a ligand, how many ligands are needed to reach a given coordination number and attach them to the metal centre. This may on occasion result in threading of the ligand through the coordination ring. This is usually removed by a short stochastic search. The ligands conformation should now be reasonable. However, a thorough stochastic search is required to ensure the conformation is the global minimum and not just a local.

Other Approaches

If the reader has a ligand in mind which they wish to vary, the above tools are capable of this. If for instance the user wishes to study substituent effects on the value ΔE_{HL} for a given complex, running the scaffold through the addition process should allow for this.